GROWTH AND PROPERTIES OF TUNGSTENBRONZE FERROELECTRIC CRYSTALS AND FILMS(Dissertation_全文)

AUTHOR(S):

Adachi, Masatoshi

GROWTH AND PROPERTIES OF TUNGSTEN-BRONZE FERROELECTRIC CRYSTALS AND FILMS

BY

MASATOSHI ADACHI

MAY 1982

DEPARTMENT OF ELECTRONICS

KYOTO UNIVERSITY

KYOTO, JAPAN

GROWTH AND PROPERTIES OF TUNGSTEN-BRONZE FERROELECTRIC CRYSTALS AND FILMS

by

MASATOSHI ADACHI

MAY 1982

DEPARTMENT OF ELECTRONICS

KYOTO UNIVERSITY

KYOTO, JAPAN

ABSTRACT

$K_3Li_2Nb_5O_{15}$ (KLN) is a typical compound ferroelectric material of completely filled tungsten-bronze structure and belongs to a tetragonal crystallographic system with a point group symmetry of 4mm. It is well known that the KLN is one of the most interesting materials for various applications because of the excellent electro-optic, nonlinear-optic and piezoelectric properties. In this thesis, growth and properties of tungsten-bronze crystals and films, belonging to the KLN family, are studied and discussed from an applicational point of view. The thesis contains the following studies.

(1) The KLN crystals have been grown from a melt with excess K_2O and Li_2O, using a KLN or $K_2BiNb_5O_{15}$ (KBN) crystal as a seed. Pale-yellow single crystals up to about 8-10 mm in diameter and 30 mm in length are obtained. The composition of the grown-crystals is analyzed to be $K_{2.89}Li_{1.55}Nb_{5.11}O_{15}$. X-ray, dielectric and chemical etching measurements have been carried out. The lattice constants a and c are determined as 12.58 and 4.01 Å, respectively, and the dielectric constants $\varepsilon_{11}^T/\varepsilon_0$ and $\varepsilon_{33}^T/\varepsilon_0$ at room temperature are 306 and 115, respectively.

(2) All the elastic and piezoelectric constants of KLN have been measured from room temperature to about 120°C by observing resonant and antiresonant frequencies. The electro-mechanical coupling factors k_{15}, k_{31}, k_{33} and k_t are 0.34, 0.18, 0.52 and 0.53, respectively. The temperature coefficients of elastic compliances Ts_{33}^E, Ts_{44}^E and Ts_{66}^E are considerably small and are -0.98, -1.2 and 0.075 x 10^{-4}/°C, respectively. The above results suggest that

the KLN crystal can be a suitable material for bulk transducers as well as for surface acoustic wave (SAW) devices.

(3) Crystals of $K_{3(1-x)}Na_{3x}Li_2Nb_5O_{15}$(KNLN) have been grown by the Czochralski method. The attempted values for x are 0, 0.1, 0.2, 0.25 and 0.3. The analyses on the crystallographic and dielectric properties show that the structural phase change from the tungsten-bronze to the perovskite structures occurs at x between 0.2 and 0.25. The electro-mechanical, linear electro-optic and nonlinear-optic properties of KNLN (x=0 and 0.1) are measured to examine the influence of the Na doped in KLN. It is found that the electro-optical halfwave voltage (v_π) relating to the electro-optic coefficient r_c for KNLN can be reduced to such an extent as much smaller than that for KLN, by adjusting the Na concentration to x=0.1. On the other hand, one of the nonlinear-optic coefficients, d_{31}, of KNLN (x=0.1) is somewhat larger than that of KLN (x=0) and is determined as $d_{31}^{KNLN(x=0.1)} = 1.6\ d_{31}^{KLN}$. It is therefore concluded that although piezoelectricity in KNLN crystals becomes weaker as the Na concentration increases, the addition of small amount of the Na to KLN as a whole results in more preferable linear-optic and nonlinear-optic behaviors than pure KLN.

(4) Tungsten-bronze KBN crystals have been grown by the rf heating Czochralski method. Large-size pale-yellow crystals up to about 35 mmϕ x 40 mm are easily grown. X-ray, dielectric, chemical etching, conoscopic and thermal expansion measurements are carried out in order to assess fundamental properties of KBN. It is found that KBN is a ferroelectric material with the polar axis parallel

to the [001] axis. The lattice constants a, b and c are determined as 17.878, 17.888 and 7.853 Å, respectively. Furthermore, all the elastic constants and four of the twelve independent photoelastic tensor elements are also determined for applications to acousto-optic devices.

(5) KLN single-crystal films have been successfully grown with good epitaxy on KBN substrates by the "epitaxial growth by melting" (EGM). For the substrates, KBN single crystals are used because of the following reasons: The crystal structures of KLN and KBN are the same tungsten-bronze type; the melting point of KBN is higher than that of KLN by about 250°C; and the lattice mismatch between the KLN film and the KBN substrate is about 0.32 and 2.3 % for the a and c axes in the KLN coordinate system. The KLN films obtained are transparent, but their surfaces are relatively rough. The analyses on these KLN films by X-ray, reflection electron diffraction (RED) and scanning electron microscopy (SEM) methods indicate that the films are single crystals of high quality.

(6) KLN single crystal films have been sputtered on the KBN substrates. The KLN target is prepared by sintering pressed powder with potassium and lithium enriched composition. Optimum growth conditions for the high quality single-crystal KLN films are Ar (50%) + O_2 (50%) atmosphere, 9 x 10^{-2} Torr, rf power input below 150 W, and substrate temperatures of 580 to 630 °C. The crystallographic identifications of the KLN films are made by X-ray, RED and SEM measurements. It is found that single-crystal films of KLN have been epitaxially grown on KBN substrates. The lattice constants a and c of the KLN films

are 12.7 and 3.96 Å, respectively. Preliminary measurements on the optical waveguides are carried out. The ordinary refractive index n_o in the KLN film is determined as 2.27.

(7) RF diode sputtering is used to fabricate KLN thin films. The optimum growth conditions are Ar (50%) + O_2 (50%) atmosphere, 9.0×10^{-2} Torr, about 140 W rf power and 600 to 650 °C substrate temperature. The X-ray and electron diffraction results show that an (001) KLN single-crystal films is epitaxially grown on an $(01\bar{1}2)$ sapphire substrate at substrate temperatures above 600 °C by rf sputtering, and also that the obtained KLN film is of a single crystal with considerably good quality. On the other hand, an (001)- oriented KLN film sputtered on an (0001) sapphire substrate is seen to be polycrystalline. The TE_0 mode optical propagation loss in the KLN film is relatively small as 7.8 dB/cm, and the KLN film is a suitable material for optical waveguides.

(8) Finally, characteristics of surface acoustic wave (SAW) properties of tungsten-bronze layered structures of (KLN film)/(substrate) and ($Pb_2KNb_5O_{15}$ (PKN))/(substrate) combinations have been calculated. The maximum attainable value of the 1st peak for the electro-mechanical coupling factor $\Delta v/v$ is 0.045 at KH (wave number times film thickness) = 0.9 in the case of the layered structure of (PKN)/(sapphire). This value is about twice as large as that of Y-cut, Z-prop., $LiNbO_3$. The preliminary experiment on SAW properties of the layered structure of (KLN)/(sapphire) is carried out. The SAW propagation on the KLN film has been successfully observed. The above results

suggest the potential usefulness of the layered structures of (KLN)/(substrate) and (PKN)/(substrate) combinations for SAW applications.

ACKNOWLEDGMENTS

The author wishes to express his sincere gratitude and appreciation to Professor Akira Kawabata for his continuing guidance, invaluable advice and encouragement throughout this work. The author deeply acknowledges the invaluable guidance and advice of Professor Tadashi Shiosaki. The author wishes to thank Professor Toshinori Takagi for his continuous encouragement, stimulating discussion and criticism on the manuscript. The author is grateful to Professor Akio Sasaki for his useful suggestions and criticism on the manuscript.

Appreciations are due to former Professor Tetsuro Tanaka for his genial guidance and encouragement, and to Dr. Susumu Fukuda for his fruitful discussion and experimental facilities. Appreciations are also due to Professors Hiroyuki Matsunami, Shigeo Fujita and Junji Saraie for their helpful advices, discussion and experimental facilities.

Grateful thanks are due to the present and former members of Professor Kawabata's research group, Drs. Shinzo Ohnishi and Takashi Yamamoto, Messrs. Takashi Sakata, Masayasu Miyake, Minoru Hori, Akira Kawakatsu and Masahiko Nozaki, for their valuable participations in the work. Thanks are also due to Mitsumasa Oku, Tetsuji Sekiya, Masanobu Miyasato, Toshihiko Tanioka, Fumio Takei, Masanobu Yanagiya, Katsuhiko Kumagawa and Shoichi Mochizuki, for their help in the experiments and calculations as senior students.

The author wishes to express his thank to Mr. Eiji Ieki and Mr. Satoru Fujishima, of Murata Mfg. Co. Ltd., for supplying KLN targets and many valuable discussions.

Part of this work was financially supported by the Grant-in-Aid for Scientific Research from the Ministry of Education, Science and Culture (No. 742025, No 875158, No. 375160, No. 420525 and No. 56420037), the Research Grant of the TAKEDA Science Foundation and the KURATA Research Grant of the KURATA Foundation.

CONTENTS

CHAPTER 1 INTRODUCTION

Sixty years have elapsed since Valasek's discovery of the peculiar dielectric phenomenon, known today under the name of ferroelectricity, of Rochelle salt in 1921 [1]. After this discovery, it intrigued and stimulated a great deal of research. In about 1935, a new series of ferroelectric crystals, potassium dihydrogen phosphate (KDP) and related isomorphous compounds, was produced by Busch and Scherrer [2] in Zurich. Prior to about 1940 only two types of ferroelectrics were known, RS and some closely related tartrates, and KDP and its isomorphs described above. The anomalous dielectric properties of a new ferroelectrics, barium titanate ($BaTiO_3$), were discovered on ceramic specimens independently by Wainer and Salomon [3] in 1942, by Ogawa [4] in 1944, and by Wul [5] in 1945. The ferroelectric activity of this $BaTiO_3$ was reported independently by Von Hippel and co-workers [6] in 1944 and by Wul [7] in 1946. After this discovery of $BaTiO_3$, $BaTiO_3$ and similar structures have turned out to be the most useful and interesting ferroelectrics. So far a large number of ferroelectric materials have been grown and have attracted considerable interest in their applications to practical uses. Total number of ferroelectrics discovered from 1921 till about June, 1978 are about 150 (including only pure compounds.)[8].

Among various ferroelectric materials, a number of ferroelectric niobates having tetragonal or related orthorhombic tungsten-bronze structure have especially attracted much attention for electro-optic, nonlinear optic, bulk wave and surface acoustic wave (SAW) applications. The term "tungsten-bronze" derives from the metalic potassium tungsten oxide,

K_xWO_3 (x=0.5), which was first found by Magneli [9].
The tungsten-bronze structure is characterized by a framework of BO_6 octahedra sharing the corners with each other, and is represented by general chemical formula $(A_1)_2(A_2)_4C_4(B_1)_2(B_2)_8O_{30}$ corresponding to the contents of a unit cell with an approximate dimension of 12.5 x 12.5 x 4.0 Å.

The tungsten-bronze ferroelectrics, $Pb_5Nb_{10}O_{30} = PbNb_2O_6$ was first discovered by Goodman[10] in 1953. However, it was not until 1958 that Francombe and Lewis[11] realized that it had the same structure as K_xWO_3. After the discovery of $PbNb_2O_6$ a great deal of work on related materials took place for applications in the quantum electronics field at a number of laboratories throughout the world. In 1967, at IBM and at Bell Telephone Laboratories, a new group of tungsten-bronze ferroelectrics were discovered and extensively investigated. These are the alkali alkaline-earth niobates, such as $Sr_2KNb_5O_{15}$[12-13], $Ba_2NaNb_5O_{15}$[12,14], $Ba_2KNb_5O_{15}$[12], $Sr_2NaNb_5O_{15}$[15], $K_3Li_2Nb_5O_{15}$[16-17], $KNbO_3$-$PbNb_2O_6$[15], $K(Sr-Ba)_2Nb_5O_{15}$[15], $K(Ba-Pb)_2Nb_5O_{15}$[15] and $K(Sr-Pb)_2Nb_5O_{15}$[15].

$K_3Li_2Nb_5O_{15}$ (KLN) is a typical compound ferroelectric material of completely filled tungsten-bronze structure and belongs to a tetragonal crystallographic system with a point group symmetry of 4mm[18]. Ferroelectricity in crystals grown from $K_3Li_2Nb_5O_{15}$ composition was reported by Van Uitert et al. in 1967[17]. It is well known that the KLN is one of the most interesting materials for various applications because of the excellent electro-optic, nonlinear optic and piezoelectric properties[16-21]. However, it is very difficult to obtain high-quality large-size single crystals because the KLN is not congruently melting composition. An approach for the solution of this problem is to grow epitaxial films of this crystal[22].

In this thesis, growth and properties of tungsten-bronze ferroelectric crystals and films are studied and discussed in detail from an applicational point of view. The first four chapters (Chapts. 2-5) describe tungsten-bronze bulk crystals and the second four chapters (Chapts. 6-9) present thin films. The thesis is organized into the follwing chapters: In Chapter 2, experimental results of crystal growth, and dielectric and ferroelectric properties of KLN are described. Chapter 3 contains the measured results of all the elastic, piezoelectric and dielectric constants as well as their temperature coefficients. In Chapter 4, electrical and optical properties of Na-modified KLN are studied and presented. Chapter 5 is concerned with studies of the ferroelectric and elastic properties of a $K_2BiNb_5O_{15}$ crystal. Further the photo-elastic properties are measured by the Dixon-Cohen method for application to an acousto optic device. In Chapter 6, epitaxial growth of KLN single-crystal films on KBN substrates by the EGM technique are investigated. In Chapters 7 and 8, the epitaxial growth of KLN single-crystal films on KBN and sapphire substrates by an rf sputtering technique, respectively, are described and applied to the purpose of fabricating optical waveguides. Chapter 9 is concerned with calculated SAW characteristics of tungsten-bronze layered structures of (KLN film)/(substrate) and (PKN)/(substrate) combinations. In addition, preliminary experiment on SAW properties of the layered structure of KLN film deposited on sapphire substrate is also described. Finally, conclusions and suggestions for further study are summarized in Chapter 10.

References

[1] J. Valasek: Phys. Rev. 17 (1921) 475 ; Phys. Rev. 19 (1922) 639 ; Phys. Rev. 24 (1924) 560.

[2] G. Busch and P. Scherrer: Naturwiss. 23 (1935) 737.

[3] E. Wainer and A. N. Salomon: Titanium Alloy Manufacturing Company, Elec. Rep. 8 (1942) cited in Rev. Mod. Phys. 22 (1950) 221.

[4] T. Ogawa: Presented at the Meeting of the Research Institute of High Dielectric Constant Materials (1944) cited in Busseiron Kenkyu No.6 (1947) 1.

[5] B. Wul: Nature 156 (1945) 484.

[6] A. von Hippel, R. G. Breckenridge, A. P. De Bretteville Jr., J. M. Brownlow, F. G. Chesley, G. Oster, L. Tisza and W. B. Westphal: N. D. R. C. Rept. No. 300 (1944), cited in Rev. Mod. Phys. 22 (1950) 221.

[7] B. Wul: Nature 157 (1946) 808.

[8] T. Mitsui, S. Nomura, M. Adachi, J. Harada, T. Ikeda, E. Nakamura, E. Sawaguchi, T. Shigenari, Y. Shiozaki, I. Tatsuzaki, K. Toyoda, T. Yamada, K. Gesi, Y. Makita, M. Marutake, T. Shiosaki and K. Wakino: *Landolt-Börnstein, Numerical Data and Functional Relationships in Science and Technology, New Series, Group III: Crystal and Solid State Physics, Vol. 16, Ferroelectrics and Related Substances*, Berlin, Heidelberg, New York, Springer 1981.

[9] A. Magnéli: Arkiv Kemi: 1 (1949) 213.

[10] G. Goodman: J. Am. Ceram. Soc. 36 (1953) 368.

[11] M. H. Francombe and Lewis: Acta Cryst. 11 (1958) 696.

[12] G. E. Burns, E. A. Giess, and D. F. O'Kane: IBM Tech. Discl. Bull. 10 (1967) 618.

[13] E. A. Giess, G. Burns, D. F. O'Kane and A. W. Smith:

Appl. Phys. Letters 11 (1967) 233.

[14] J. E. Geusic, H. J. Levinstein, J. J. Rubin, S. Singh, and L. G. Van Uitert: Appl. Phys. Letters 11 (1967) 269.

[15] E. A. Giess, B. A. Scott, G. Burns, D. F. O'Kane and A. Segmüller: J. Am. Ceram. Soc. 52 (1969) 276.

[16] W. A. Bonner, W. H. Grodkiewicz and L. G. Van Uitert:J. Cryst. Growth 1 (1967) 318.

[17] L. G. Van Uitert, S. Singh, H. J. Levinstein, J. E. Geusic and W. A. Bonner: Appl. Phys. Letters 11 (1967) 161.

[18] L. G. Van Uitert, J. J. Rubin and W. A. Bonner: IEEE Trans. Quantum Electron. QE-4 (1968) 622.

[19] T. Nagai and T. Ikeda: Jpn. J. Appl. Phys. 12 (1973) 199.

[20] Y. Uematsu and S. Koide: Jpn. J. Appl. Phys. 9 (1970) 336.

[21] M. Adachi and A. Kawabata: Jpn. J. Appl. Phys. 17 (1978) 1969.

[22] M. Adachi, K. Kumagawa, T. Shiosaki and A. Kawabata: Jpn. J. Appl. Phys. Suppl.20-4 (1981) 17.

CHAPTER 2 GROWTH OF POTASSIUM LITHIUM NIOBATE (KLN) CRYSTALS

2.1 INTRODUCTION

Among various ferroelectric materials, a number of ferroelectric niobates having tetragonal or related orthorhombic tungsten-bronze structures with general chemical formula $(A_1)_2(A_2)_4C_4(B_1)_2(B_2)_8O_{30}$ have attracted much attention for electro-optic, nonlinear-optic, bulk wave and surface acoustic wave (SAW) applications.

A $K_3Li_2Nb_5O_{15}$ (KLN) is tetragonal with a point group 4mm and is a typical compound of completely filled tungsten-bronze ferroelectrics [1]. It is well known that these filled tungsten-bronze compounds have a high stability to intense laser radiation [1,2]. So far, crystal growth of KLN have been successfully attempted by various people for several different purposes: those are Bonner et al. [3], Van Uitert et al. [1,2] and Nagai et al. [4] for electro-optic and nonlinear-optic applications, Fukuda [5], Scott et al. [6] and Ikeda et al. [7] for detailed phase equilibrium studies, Abrahams et al. [8] for investigation of crystal structure, and finally Uematsu et al. [9] and Adachi et al. [10] for acoustic applications.

In this chapter, experimental results of crystal growth, dielectric and ferroelectric properties of KLN are described.

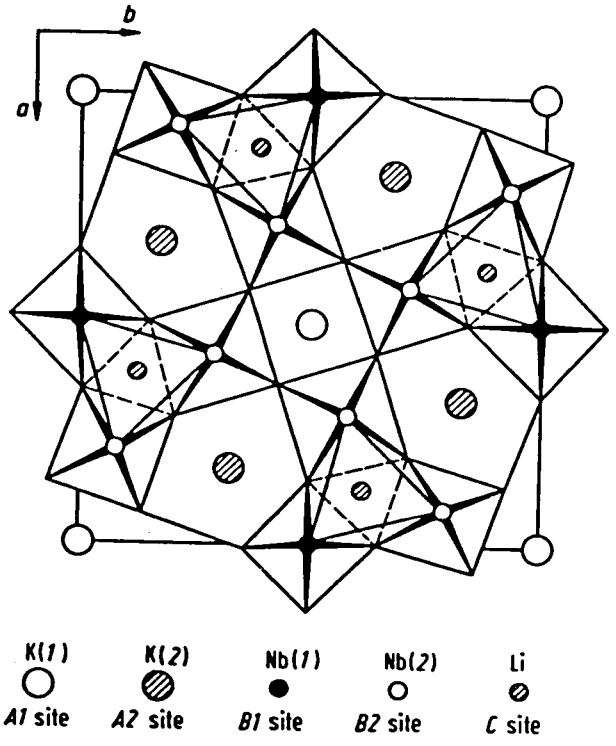

Fig. 2.1 Representation of KLN structure along the polar axis. The nearest oxygen neighbor environment around the C site is indicated by the apices of the dashed equatorial triangle and by those of the solid lines representing the triangular faces of a trigonal prism.

2.2 CRYSTAL GROWTH

2.2.1 Crystal Structure of $K_3Li_2Nb_5O_{15}$

The tungsten-bronze structure was first found by Magnéli in K_xWO_3 [11]. It is characterized by a framework of BO_6 octahedra (B=Nb in KLN) sharing the corners with each other, and is represented by general chemical formula $(A_1)_2(A_2)_4C_4(B_1)_2(B_2)_8O_{30}$ corresponding to the contents of a unit cell with an approximate dimension of $12.5 \times 12.5 \times 4.0$ Å. A representation of the overall structure is given in Fig. 2.1, showing the interrelationships of A_1, A_2, B_1, B_2 and C sites. In this figure, the square A_1 site is 12 coordinated, the pentagonal A_2 site is 15 coordinated, both B sites are 6 coordinated, and the triangular C site is 9 coordinated.

$K_3Li_2Nb_5O_{15}$ has tetragonal tungsten-bronze structure with a 4mm point group. All the A_1 and A_2 sites are filled with K, and all the C sites are filled with Li. This was the first material reported as having a completely filled tetragonal tungsten-bronze structure [2,8].

2.2.2 Phase Equilibrium in K_2O-Li_2O-Nb_2O_5 System

Detailed phase equilibrium study of the K_2O-Li_2O-Nb_2O_5 ternary system was carried out by Scott et al. [6], and by Ikeda et al. [7], independently. Scott et al. found the tungsten-bronze type phase in the Nb-rich region where the Nb_2O_5 concentration is higher than 0.51, and concluded that the tungsten-bronze phase does not occur with completely filled alkali cation sites at the composition $K_3Li_2Nb_5O_{15}$.

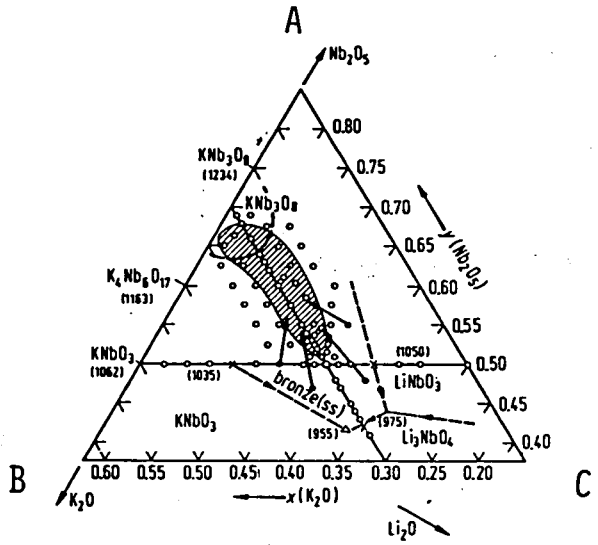

Fig. 2.2 The system K_2O-Li_2O-Nb_2O_5. Hatched area shows the field of tungsten-bronze solid solution. Short lines indicate the tie lines. Open circles: composition of samples; full circles: melt composition to examine tie lines; triangle: eutectic point; crosses: liquids boundary of the tungsten-bronze field. The arrows point to different composition of the melt and the solid crystal. (after Ref. [6].)

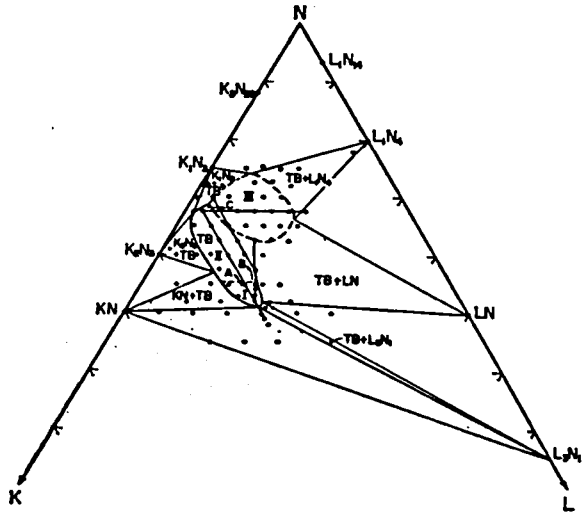

Fig. 2.3 Diagram of K_2O-Li_2O-Nb_2O_5 ternary system. (after Ref. [7].)

The diagram of the K_2O-Li_2O-Nb_2O_5 ternary system determined by Scott et al. is shown in Fig. 2.2, where the hatched area shows the field of tungsten-bronze type solid solution and several tie lines in the field are indicated by lines connecting the small solid circles. On the other hand, Ikeda et al. found a wider tungsten-bronze type area spreading toward the Nb-richer side than the range studied by Scott et al. , and also showed that the single phase region can be divided into three parts, I, II and III as shown in Fig. 2.3. The phases I and II are similar to the result shown by Scott et al., except a little deviation. Crystals in the phase I are ferroelectric and the Curie temperature shifts from 540 to 326 ^{o}C as the Nb_2O_5 concentration changes from 0.51 to 0.55. Crystals in the phase II, with the Nb_2O_5concentration changing from 0.55 to 0.63, have pseudo-tetragonal structure and are not ferroelectric. The phase III is located in the area where the concentration of K_2O is 0.17 ~ 0.28 and that of $Nb_2O_5$is 0.63 ~ 0.73.

In this study, potassium lithium niobate crystals in the phase I have been grown by rf-heating Czochralski technique from a melt with the composition, 35 mole % K_2CO_3, 17.3 mole % Li_2CO_3 and 47.7 mole % Nb_2O_5.

2.2.3 Sample Preparation

Single crystals of $K_3Li_2Nb_5O_{15}$ were grown by rf-heating Czochralski technique from a melt by using KOKUSAI DENKI type DP-500FM crystal pulling equipment. The starting materials were K_2CO_3, Li_2CO_3 of reagent grade, and Nb_2O_5 of 99.9 % purity. These oxides were mixed in nonstoichiometric proportion with potassium and lithium enriched composition, 35 mole % K_2CO_3,

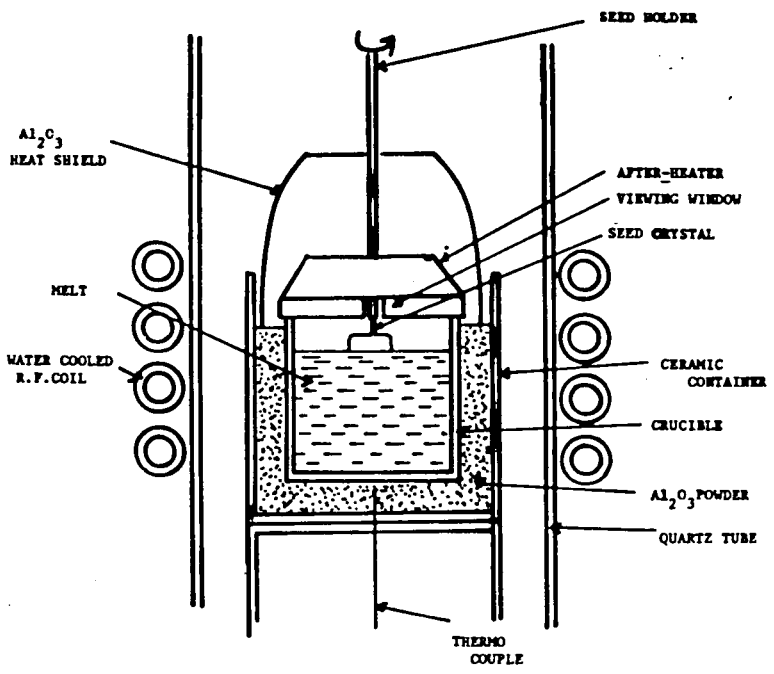

Fig. 2.4 A drawing of the crystal pulling equipment.

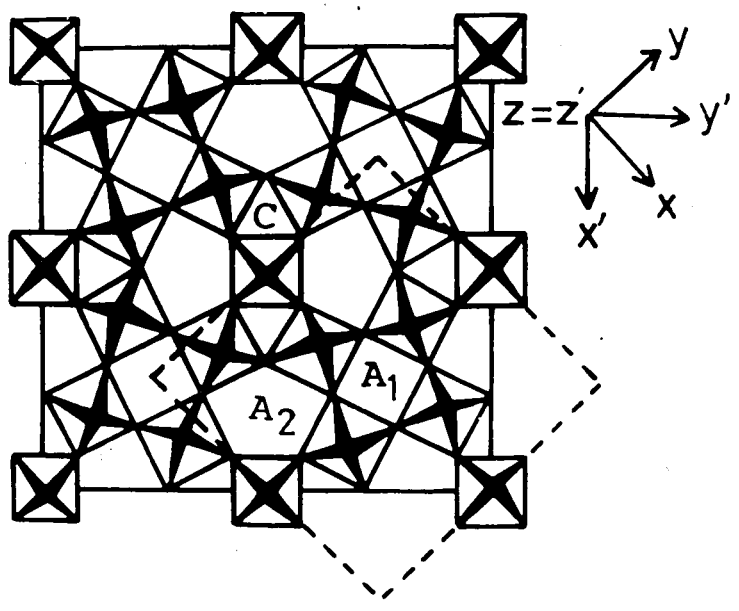

Fig. 2.5 Tungsten-bronze structure and reference axes. The (001) projection of KBN lattice is shown in relation to the KLN cell shown by dashed square.

17.3 mole % Li_2O and 47.7 mole % Nb_2O_5. The mixture was placed in a 150 ml platinum crucible and melted by rf-heating. A drawing of the crystal pulling equipment employed in this work is shown in Fig. 2.4. Both KLN and $K_2BiNb_5O_{15}$ (KBN: see Chapter 5 for this material) crystals were used as seeds because the crystal structures of KLN and KBN are both of the tungsten-bronze type as shown in Fig. 2.5 and melting temperature of KBN is higher by about 250 ^{o}C than that of KLN. The KBN crystal is orthorhombic on the contrary to tetragonal in KLN. The coordinate systems (x,y,z) for KLN and (x',y',z') for KBN are compared in Fig. 2.5 in relation to the crystallographic axes a_1, a_2 and c.

Optimum growth conditions were as follows; pulling rate: 1 mm/h and rotation rate: 40 rpm. The pulling axis was chosen in parallel to the x' or y' axis in order to minimize cracking taking place during the crystal growth.

2.3 EXPERIMENTAL PROCEDURES FOR EVALUATION OF KLN CRYSTALS

Analytical determination for the potassium, lithium and niobium in the crystals was done by chemical analysis. X-ray diffraction measurements were performed by means of a diffractometer (TOSHIBA ADX-102) using CuKα radiation. Lattice constants were calculated using reflection peaks in the $2\theta = 20$ to 60^{o} range. The dielectric constants ε_{11}^{T} and ε_{33}^{T} were measured at 100 KHz by using YHP type 4332A LCR meter.

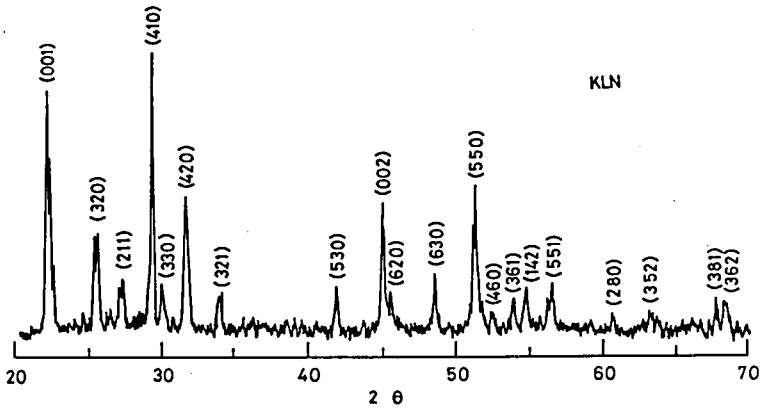

Fig. 2.6 X-ray diffraction pattern of KLN powder.

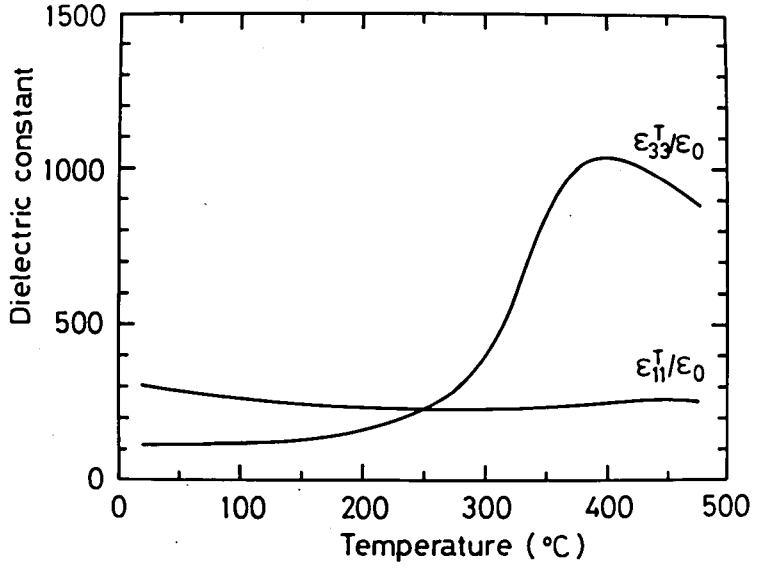

Fig. 2.7 Temperature dependence of dielectric constants of KLN.

2.4 RESULTS AND DISCUSSION

Single crystals of KLN could be grown with excess K_2CO_3 and Li_2CO_3 by rf-heating Czochralski method. It has been experienced that while the rate of crystallization along the c axis is much less than those along any other attempted directions, great difficulty is often encountered in obtaining large crystals in this pulling direction, due to the unavoidable occurrence of cracking. Therefore the pulling axis is chosen in parallel to [100] or [110] axis in order to minimize the cracking during the crystal growth. The crystals obtained are elongated in the lateral direction along the $[\bar{1}10]$ axis and are generally prismatic with clearly defined faces, (001) and (110). Pale-yellow single crystals up to about 8-10 mm in diameter and 30 mm in length were obtained.

Chemical analysis revealed that the grown crystal contained 78 wt% of Nb_2O_5, 3.2 wt% of Li_2O and 18.8 wt% of K_2O, which corresponded to a molar ratio of 33.4 K_2O 17.8 Li_2O and 48.8 Nb_2O_5. Taking account of the Curie temperature (405 ^{o}C) and the lattice constants of this crystal, the composition was determined as $K_{2.89}Li_{1.55}Nb_{5.11}O_{15}$.

Figure 2.6 shows the profile of X-ray powder diffraction patterns. The lattice constants a and c of KLN crystal obtained by X-ray diffraction measurement were 12.58 and 4.01 $\mathring{A}$, respectively. These values are in good agreement with Bonner's data [3].

The temperature dependences of dielectric constants at 100 KHz are shown in Fig. 2.7. The dielectric constants $\varepsilon_{11}^{T}/\varepsilon_0$ and $\varepsilon_{33}^{T}/\varepsilon_0$ at room temperature were 306 and 115, respectively. The constant ε_{33}^{T} shows a marked anomaly at the transition point of 405 ^{o}C. On the other hand, the dielectric constant ε_{11}^{T} does

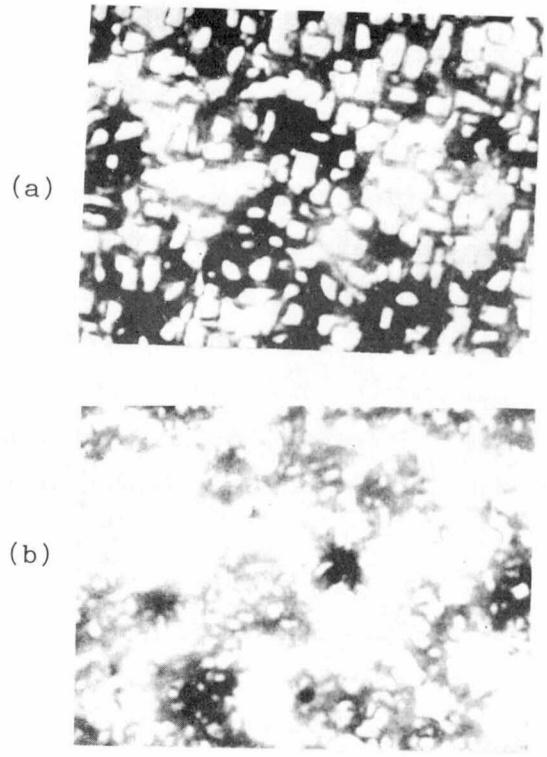

Fig. 2.8 Reflected microscopic photographs of (a) negative sense plane (-c surface), and (b) positive sense plane (+c surface) of the KLN crystal.

Table 2-I Fundamental properties of KLN and KBN.

	KLN ($K_{2.89}Li_{1.55}Nb_{5.11}O_{15}$)	KBN ($K_{1.93}Bi_{0.91}Nb_{5.07}O_{15}$)
Symmetry	Tetragonal	Orthorhombic (Pseudo-tetragonal)
Lattice constant	a=12.58Å c=4.01 Å	a=17.85 Å c=7.84 Å
Curie temperature	405°C	360°C
Dielectric constant	$\varepsilon^T_{11}/\varepsilon_0$=306 $\varepsilon^T_{33}/\varepsilon_0$=115	$\varepsilon^T_{11}/\varepsilon_0$=430 $\varepsilon^T_{33}/\varepsilon_0$=500
Spontaneous polarization	0.25 C/m²	—

not show any anomaly but decreases gradually with increasing temperature.

The crystals were poled by the field-cooling method under a DC field of about 300 V/cm along the c-axis. A spontaneous polarization in the tetragonal tungsten-bronze type KLN is parallel to either +c or -c axis direction. Poling completeness was confirmed by chemical etching. A mixed solution, $1HF:1HNO_3$ was used as an etchant, in which KLN crystals were boiled for a few minutes. The etched patterns were observed as shown in Fig. 2.8 by using a reflection optical microscope. As shown in Fig. 2.8, the negative side of (001) plane was etched faster than the positive side and on which square etched patterns were observed. On the other hand, the positive side was only slightly etched.

Fundamental properties of the present KLN crystals at room temperature in Table 2-I, are to be compared to those of KBN.

2.5 SUMMARY

Crystals of KLN were grown by the Czochralski method from a melt using a KLN or KBN crystal as the seed. Since the vapor pressure of K_2O and Li_2O is high at the melting point of KLN, the starting composition with excess K_2O and Li_2O was mainly used, which was necessary to obtain crystals of good quality. Pale-yellow single crystals up to about 8-10 mm in diameter and 30 mm in length were obtained. The composition of grown-crystals was analyzed as $K_{2.89}Li_{1.55}Nb_{5.11}O_{15}$.

X-ray, dielectric and chemical etching measurements were carried out in order to investigate crystallographic and

ferroelectric properties of KLN. From the measured results of the above properties, the lattice constants a and c were determined as 12.58 and 4.01 Å, respectively, and the dielectric constants $\varepsilon_{11}^T/\varepsilon_0$ and $\varepsilon_{33}^T/\varepsilon_0$ at room temperature were 306 and 115, respectively. The constant ε_{33}^T shows a marked anomaly at the transition point of 405°C. On the other hand, the ε_{11}^T does not show any anomaly, but decreases gradually with increasing temperature.

The KLN crystal is a suitable material for applications to the electro-optic, nonlinear-optic, bulk wave and SAW devices. However it has been very difficult to obtain large-size single crystals of KLN because the KLN is not congruently melting composition. The solution of this remaining problem will be needed in the future for device applications.

References

[1] L. G. Van Uitert, J. J. Rubin and W. A. Bonner: IEEE Trans. Quantum Electron. QE-4 (1968) 622.

[2] L. G. Van Uitert, S. Singh, H. J. Levinstein, J. E. Geusic and W. A. Bonner: Appl. Phys. Letters 11 (1967) 161.

[3] W. A. Bonner, W. H. Grodkiewicz and L. G. Van Uitert: J. Cryst. Growth 1 (1967) 318.

[4] T. Nagai and T. Ikeda: Jpn. J. Appl. Phys. 12 (1973) 199.

[5] T. Fukuda: Jpn. J. Appl. Phys. 8 (1969) 122.

[6] B. A. Scott, E. A. Giess, B. L. Olson, G. Burns, A. W. Smith and D. F. O'Kane: Mater. Res. Bull. 5 (1970) 47.

[7] T. Ikeda and K. Kiyohashi: Jpn. J. Appl. Phys. 9 (1970) 1541.

[8] S. C. Abrahams, P. B. Jamieson and J. L. Bernstein: J. Chem. Phys. 54 (1971) 2355.

[9] Y. Uematsu and S. Koide: Jpn. J. Appl. Phys. 9 (1970) 336.

[10] M. Adachi and A. Kawabata: Jpn. J. Appl. Phys. 17 (1978) 1969.

[11] A. Magnéli: Ark. Kemi. 1 (1949) 213.

CHAPTER 3 ELASTIC AND PIEZOELECTRIC PROPERTIES OF POTASSIUM LITHIUM NIOBATE CRYSTALS

3.1 INTRODUCTION

Potassium lithium niobate (KLN) is a ferroelectric material with a Curie temperature of 405 ^{o}C [1]. It has a tetragonal tungsten-bronze structure and belongs to the point group 4mm at room temperature [2].

For a complete understanding of detailed piezoelectric behavior, especially for bulk or surface acoustic wave (SAW) resonator and filter designs, a knowledge of temperature behavior of the elastic, piezoelectric and dielectric constants is a necessary adjunct to their room-temperature evalution. Uematsu and Koide [3] have reported some of the piezoelectric and elastic properties of KLN. They have shown that KLN has a large electro-mechanical coupling factor k_t. However, the mechanical or acoustical properties of this crystal have not been reported in detail yet.

In this chapter, the measured results of all the elastic, piezoelectric and dielectric constants as well as their temperature coefficients are described. Furthermore, SAW characteristics of KLN are also described.

3.2 PROCEDURES FOR DETERMINING ELASTIC AND PIEZOELECTRIC CONSTANTS

The crystal KLN is a tetragonal material at room temperature and belongs to the point group 4mm [2]. Crystals in class

Table 3-I Elasto-piezo-dielectric matrix for crystals belonging to the point group 4mm.

S_{11}	S_{12}	S_{13}	0	0	0	0	0	d_{31}
S_{12}	S_{11}	S_{13}	0	0	0	0	0	d_{31}
S_{13}	S_{13}	S_{33}	0	0	0	0	0	d_{33}
0	0	0	S_{44}	0	0	0	d_{15}	0
0	0	0	0	S_{44}	0	d_{15}	0	0
0	0	0	0	0	S_{66}	0	0	0
0	0	0	0	d_{15}	0	ε_{11}	0	0
0	0	0	d_{15}	0	0	0	ε_{11}	0
d_{31}	d_{31}	d_{33}	0	0	0	0	0	ε_{33}

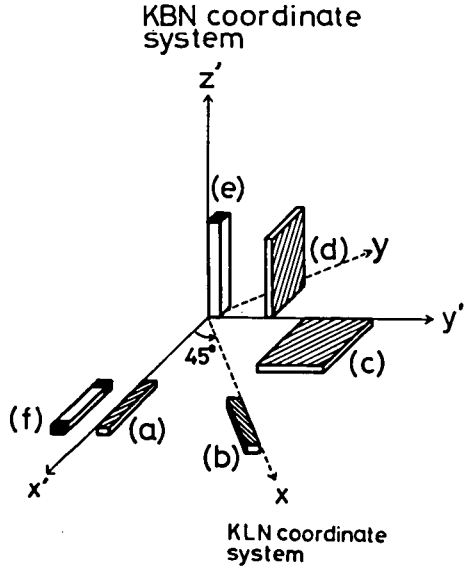

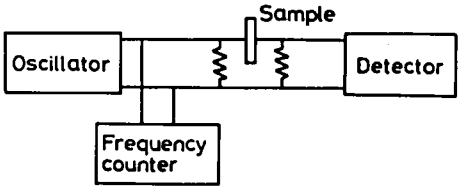

Fig. 3.2 The system for measuring the resonant and antiresonant frequencies.

Fig. 3.1 Shapes and orientations of specimens. The shaded portions indicate the electrode with gold thin films. (a) [100] bar, (b) [110] bar, (c) square z'-plate, (d) y'-plate, (e) [001] bar and (f) z'-plate in the x' y' z' coordinates.

4mm have six elastic, three piezoelectric, and two dielectric independent elements in its elasto-piezoelectric-dielectric matrix as shown in Table 3-I.

The crystals were poled by the field-cooling method under a DC field of about 300 V/cm along the c-axis. The specimens were cut from the crystals so as to take the shapes and orientations shown in Fig. 3.1, and were polished with #3000 alumina lapping powder.

In the measurements, x', y', z' coordinates were used for convenience as shown in Fig. 3.1, where x' and y' axes are rotated by 45° around the z axis from x and y axes. In the following, constants with prime and without prime are used to specify the reference axes; for example, s' is the elastic compliance refered to the x' y' z' coordinate system.

The system for measuring the resonant and antiresonant frequencies (f_R and f_A) is shown in Fig. 3.2. To minimize the stray capacitance parallel to the sample, the input and output circuits were shielded.

The procedures for determining elastic and piezoelectric constants are the same as those described by Berlincourt and Jaffe [4] in the case of tetragonal $BaTiO_3$. All values of elastic constants (s'), piezoelectric constants (d') and coupling factors (k') were determined, as mentioned below, by measuring f_R or f_A of various specimens shown in Fig. 3.1.

The elastic compliance $s_{11}^{E'}$ was obtained from f_R of the bar elongated in the x'direction with thickness along the z' axis (specimen (a)), using the relation

$$s_{11}^{E'} = 1/(4\rho f_R^2 \cdot l^2), \qquad (3\text{-}1)$$

where ρ is the density, 4.26×10^3 Kg/m^3, and l is the length.

The elastic compliance $s_{12}^{E'}$ was obtained from the $s_{11}^{E'}$ mentioned above and f_R of the square z'-plate (specimen (c)). The frequency constant ($f_R l$) for the extensional "breathing" mode of the square plate is given by Ekstein [5] as

$$f_R^2 l^2 = \frac{1}{4\rho(s_{11}^{E'} + s_{12}^{E'})}\left[1 + \left(1 - \frac{8}{\pi^2}\right)\left(\frac{s_{12}^{E'}}{s_{11}^{E'} - s_{12}^{E'}}\right)\right]. \quad (3\text{-}2)$$

To obtain the shear compliance $s_{66}^{E'}$, the elastic compliance s_{11}^{E} was determined from f_R of the bar oriented with length along the [110] direction (specimen (b)). The equation for this case is

$$s_{11}^{E} = \frac{1}{2}s_{11}^{E'} + \frac{1}{2}s_{12}^{E'} + \frac{1}{4}s_{66}^{E'}, \quad (3\text{-}3)$$

$$\text{where } s_{11}^{E} = 1/(4\rho f_R^2 l^2). \quad (3\text{-}4)$$

On the other hand, the shear compliance $s_{44}^{D'}$ was determined from the antiresonant frequency f_A of the y'-plate with thickness along the y' axis (specimen (d)), using the relation

$$s_{44}^{D'} = 1/(4\rho f_A^2 d^2), \quad (3\text{-}5)$$

where d is the thickness of the plate.

For the specimens (c) and (e) vibrating in piezoelectrically stiffened mode, the electric field is parallel to the direction of the elastic wave motion. The elastic stiffness $c_{33}^{D'}$ and the elastic compliance $s_{33}^{D'}$ are determined from the antiresonant frequencies of the z'-plate and the [001] bar shown in Figs. 3.1(c) and (e), respectively. However it is not easy to measure the f_A accurately because of the spurious response due to mode couplings in the case of the specimen (c) and also

because of the very small value of clamped capacitance in the case of specimen (e). Therefore, their antiresonant frequencies and coupling factors k_t' and k_3', to obtain the constants $c_{33}^{D'}$ and $s_{33}^{D'}$, were determined from the measurement of fundamental and higher harmonic resonant frequencies by the overtone method of Onoe, Tiersten and Meitzler [6]. Onoe et al. found that each resonant frequency of the fundamental and higher harmonic modes is given as the solution of the following equation:

$$\tan x = x/k^2, \tag{3-6}$$

$$x = \omega d/2v, \tag{3-7}$$

where x is the normalized frequency, k is the coupling factor, ω is the angular frequency, d is the thickness and v is the phase velocity of the elastic wave. As is evident from the above equation (3-6), the ratio of the higher harmonic resonant frequency to the fundamental one is only dependent on the coupling factor k. Table 3-II is the relation between the coupling factor k and the ratio of the higher harmonic resonant frequency to the fundamental one deduced from the equation (3-6) given by Onoe [7]. To obtain the value of the elastic stiffness coefficient $c_{33}^{D'}$, the coupling constant k_t' of the specimen (c) was first determined from the ratio of the measured higher harmonic frequencies to the fundamental one by using the Table 3-II. The antiresonant frequency f_A and the elastic stiffness coefficient $c_{33}^{D'}$ were then obtained from k_t' and the fundamental resonant frequency, using the relation

Table 3-II The relation between the coupling factor k and the ratio of the higher harmonic resonant frequencies to the fundamental one. (after Ref. [7].)

K	F_2/F_1	F_3/F_1	F_4/F_1	K	F_2/F_1	F_3/F_1	F_4/F_1
0.00	3.0000	5.0000	7.0000	0.50	3.3438	5.6142	7.8756
0.01	3.0001	5.0001	7.0002	0.51	3.3617	5.6459	7.9208
0.02	3.0004	5.0007	7.0011	0.52	3.3803	5.6790	7.9679
0.03	3.0009	5.0017	7.0025	0.53	3.3998	5.7136	8.0171
0.04	3.0017	5.0031	7.0044	0.54	3.4201	5.7496	8.0683
0.05	3.0027	5.0048	7.0069	0.55	3.4414	5.7872	8.1218
0.06	3.0039	5.0070	7.0100	0.56	3.4636	5.8265	8.1777
0.07	3.0053	5.0095	7.0136	0.57	3.4868	5.8675	8.2360
0.08	3.0069	5.0125	7.0178	0.58	3.5110	5.9104	8.2970
0.09	3.0088	5.0158	7.0226	0.59	3.5364	5.9553	8.3608
0.10	3.0109	5.0196	7.0280	0.60	3.5630	6.0023	8.4276
0.11	3.0132	5.0237	7.0339	0.61	3.5909	6.0516	8.4976
0.12	3.0157	5.0283	7.0404	0.62	3.6202	6.1032	8.5709
0.13	3.0185	5.0333	7.0476	0.63	3.6509	6.1573	8.6479
0.14	3.0215	5.0387	7.0553	0.64	3.6832	6.2142	8.7287
0.15	3.0247	5.0446	7.0637	0.65	3.7172	6.2740	8.8136
0.16	3.0282	5.0508	7.0726	0.66	3.7529	6.3369	8.9029
0.17	3.0320	5.0575	7.0822	0.67	3.7906	6.4032	8.9970
0.18	3.0360	5.0647	7.0925	0.68	3.8304	6.4731	9.0963
0.19	3.0402	5.0723	7.1033	0.69	3.8725	6.5470	9.2011
0.20	3.0447	5.0804	7.1149	0.70	5.9169	6.6251	9.3118
0.21	3.0495	5.0890	7.1271	0.71	3.9641	6.7077	9.4292
0.22	3.0545	5.0980	7.1400	0.72	4.0141	6.7955	9.5536
0.23	3.0598	5.1076	7.1536	0.73	4.0674	6.8887	9.6858
0.24	3.0654	5.1176	7.1680	0.74	41.240	6.9879	9.8265
0.25	3.0713	5.1282	7.1830	0.75	4.1846	7.0938	9.9766
0.26	3.0775	5.1393	7.1989	0.76	4.2493	7.2069	10.1370
0.27	3.0840	5.1509	7.2154	0.77	4.3187	7.3282	10.3089
0.28	3.0908	5.1631	7.2328	0.78	4.3934	7.4585	10.4935
0.29	3.0979	5.1758	7.2510	0.79	4.4739	7.5990	10.6925
0.30	3.1053	5.1891	7.2700	0.80	4.5609	7.7507	10.9075
0.31	3.1131	5.2031	7.2899	0.81	4.6554	7.9154	11.1407
0.32	3.1212	5.2176	7.3107	0.82	4.7584	8.0947	11.3946
0.33	3.1297	5.2328	7.3323	0.83	4.8711	8.2908	11.6722
0.34	3.1386	5.2487	7.3549	0.84	4.9951	8.5062	11.9772
0.35	3.1478	5.2652	7.3785	0.85	5.1321	8.7443	12.3141
0.36	3.1575	5.2824	7.4031	0.86	5.2846	9.0090	12.6887
0.37	3.1675	5.3004	7.4287	0.87	5.4554	9 3054	13.1080
0.38	3.1780	5.3191	7.4554	0.88	5.6484	9.6400	13.5813
0.39	3.1889	5.3386	7.4831	0.89	5.8685	10.0214	14.1207
0.40	3.2003	5.3589	7.5121	0.90	6.1225	10.4611	14.7425
0.41	3.2122	5.3800	7.5422	0.91	6.4194	10.9750	15.4690
0.42	3.2245	5.4020	7.5735	0.92	6.7727	11.5857	16.3323
0.43	3.2374	5.4249	7.6062	0.93	7.2017	12.3270	17.3799
0.44	3.2508	5.4488	7.6402	0.94	7.7371	13.2515	18.6862
0.45	3.2647	5.4736	7.6755	0.95	8.4300	14.4471	20.3755
0.46	3.2792	5.4995	7.7124	0.96	9.3742	16.0753	22.6753
0.47	3.2944	5.5264	7.7507	0.97	10.7658	18.4732	26.0620
0.48	3.3102	5.5545	7.7907	0.98	13.1136	22.5162	31.7709
0.49	3.3266	5.5837	7.8323	0.99	18.4432	31.6878	44.7196
0.50	3.3438	5.6142	7.8756				

$$k_t'^2 = \frac{\pi f_R}{2f_A} \cot\left(\frac{\pi f_R}{2f_A}\right), \tag{3-8}$$

$$c_{33}^{D'} = 4\rho f_A^2 d^2 . \tag{3-9}$$

The coupling factor k'_{33} and the elastic compliance $s_{33}^{D'}$ of the specimen (e) were also determined in a similar way to the procedure described above in the case of the specimen (c), using the relationship

$$k_{33}'^2 = \frac{\pi f_R}{2f_A} \cot\left(\frac{\pi f_R}{2f_A}\right), \tag{3-10}$$

$$s_{33}^{D'} = 1/4\rho f_A^2 l^2. \tag{3-11}$$

The coupling factor k'_{31} was obtained from the resonant and antiresonant frequencies of the [100] bar (specimen (a)) by using the relation

$$\frac{k_{31}'^2}{1 - k_{31}'^2} = \frac{\pi f_A}{2f_R} \tan\left(\frac{\pi \Delta f}{2f_R}\right), \tag{3-12}$$

where $\Delta f = f_A - f_R$.

The shear coupling factor k'_{15} was obtained from the resonant and antiresonant frequencies of the y'-plate (specimen (d)) by using the relationship

$$k_{15}'^2 = \frac{\pi f_R}{2f_A} \cot\left(\frac{\pi f_R}{2f_A}\right). \tag{3-13}$$

The constant-field compliances $s_{33}^{E'}$ and $s_{44}^{E'}$, and stiffness $c_{33}^{E'}$ were determined from $s_{33}^{D'}$, $s_{44}^{D'}$ and $c_{33}^{D'}$, respectively, as

$$s_{33}^{E'} = s_{33}^{D'} /(1 - k_{33}'^2), \tag{3-14}$$

$$s_{44}^{E'} = s_{44}^{D'} /(1 - k_{15}'^2), \tag{3-15}$$

$$c_{33}^{E'} = (1 - k_t'^2)c_{33}^{D'}. \tag{3-16}$$

The constant-charge density compliances $s_{11}^{D'}$ and $s_{12}^{D'}$ were obtained from $s_{11}^{E'}$ and $s_{12}^{E'}$ by the relations:

$$s_{11}^{D'} = (1 - k_{31}'^2)\, s_{11}^{E'}, \tag{3-17}$$

$$s_{12}^{D'} = s_{12}^{E'} - k_{31}'^2\, s_{11}^{E'}. \tag{3-18}$$

The value of $c_{44}^{E'}$ is given by parallel field excitation measurement [8] on z'-plate of the specimen (f) with the applied field along the x' axis, using the relation

$$c_{44}^{E'} = 4\rho f_R^2\, d^2, \tag{3-19}$$

which serves as a check for reliability in the measurements made by the shear mode excitation. The piezoelectric constants (d') were determined from the respective coupling constants, compliances and permittivities as

$$g_{31}' = k_{31}' \,(s_{11}^{E'} / \varepsilon_{33}^{T'}), \tag{3-20}$$

$$g_{33}' = k_{33}' \,(s_{33}^{E'} / \varepsilon_{33}^{T'}), \tag{3-21}$$

$$g_{15}' = k_{15}' \,(s_{44}^{E'} / \varepsilon_{11}^{T'}), \tag{3-22}$$

$$d_{31}' = \varepsilon_{33}^{T'}\, g_{31}' \tag{3-23}$$

$$d_{33}' = \varepsilon_{33}^{T'}\, g_{33}' \tag{3-24}$$

$$d'_{15} = \varepsilon'^{T'}_{11} g'_{15} \ . \qquad (3\text{-}25)$$

All values in the s' matrix except s'_{13} were thus determined. The value of s'_{13} was calculated from the s' matrix and already determined c'_{33} as follows:

$$s'_{13}{}^{2} = \frac{(s'_{11} + s'_{12})(c'_{33}s'_{33} - 1)}{2c'_{33}} \ . \qquad (3\text{-}26)$$

The dielectric constants $\varepsilon'^{T'}_{33}$ and $\varepsilon'^{T'}_{11}$ were measured at 100 KHz by using YHP type 4332A LCR meter or 1 KHz by using MEGURO DENPA SOKKI universal Bridge.

The elastic, piezoelectric and dielectric constants without primes in the xyz coordinates are calculated from those referred to the x' y' z' coordinate system through the following relations.

$$s_{11} = s_{22} = \frac{s'_{11}}{2} + \frac{s'_{12}}{2} + \frac{s'_{66}}{4} \ ,$$

$$s_{12} = s_{21} = \frac{s'_{11}}{2} + \frac{s'_{12}}{2} - \frac{s'_{66}}{4} \ ,$$

$$s_{33} = s'_{33} \ ,$$

$$s_{44} = s_{55} = s'_{44} \ ,$$

$$s_{66} = 2(s'_{11} - s'_{12}) \ , \qquad (3\text{-}27)$$

$$d_{31} = d'_{31} \ , \ d_{33} = d'_{33} \ , \ d_{15} = d'_{15} \ , \qquad (3\text{-}28)$$

$$\varepsilon_{11} = \varepsilon'_{11} \quad \text{and} \quad \varepsilon_{33} = \varepsilon'_{33} \ . \qquad (3\text{-}29)$$

3.3 RESULTS

All the piezoelectric, elastic and dielectric (See: Chapt. 2) constants of KLN determined above are listed in Table 3-III. The coupling factors k_{15}, k_{31}, k_{33} and k_t are

$$k_{15} = 0.34, \quad k_{31} = 0.18,$$

$$k_{33} = 0.52 \text{ and } k_t = 0.53$$

at room temperature.

It is worthwhile to note that KLN crystal has considerably large electromechanical coupling for shear mode. For example, the coupling factor k_{15} is larger than the value of 0.21 for x cut and 0.24 for y cut in BNN [9], while k_{33} and k_t are somewhat smaller than those for BNN.

The temperature dependences of the elastic compliances, the piezoelectric constants and the coupling factors are shown in Figs. 3.3, .4 and .5 from room temperature to about 120 $^{\circ}$C. Temperature dependences of the elastic compliances are fairly small. The elastic compliances s_{11}^E, s_{12}^E and s_{66}^E increase with increasing temperature, but s_{13}^E, s_{33}^E and s_{44}^E decrease monotonically. Piezoelectric constants d_{31} and d_{33}, and the coupling factors k_{31} and k_{33} is little temperature dependent, but d_{15} and k_{15} decrease gradually with increasing temperature. Temperature coefficients of these constants are given in Table 3-IV, where it is noticed the values Ts_{33}^E, Ts_{44}^E and Ts_{66}^E are fairly small.

Table 3-III Physical constants of KLN.

$\varepsilon_{11}^T/\varepsilon_0$	306	$\varepsilon_{11}^S/\varepsilon_0$	271
$\varepsilon_{33}^T/\varepsilon_0$	115	$\varepsilon_{33}^S/\varepsilon_0$	83
s_{11}^E	5.59×10^{-12} m²/N	s_{11}^D	5.41×10^{-12} m²/N
s_{12}^E	−1.24	s_{12}^D	−1.42
s_{13}^E	−2.37	s_{13}^D	−1.61
s_{33}^E	11.8	s_{33}^D	8.58
s_{44}^E	14.7	s_{44}^D	13.0
s_{66}^E	14.3	s_{66}^D	14.3
c_{11}^E	2.20×10^{11} N/m²	c_{11}^D	2.21×10^{11} N/m²
c_{12}^E	0.74	c_{12}^D	0.74
c_{13}^E	0.59	c_{13}^D	0.55
c_{33}^E	1.09	c_{33}^D	1.50
c_{44}^E	0.68	c_{44}^D	0.77
c_{66}^E	0.70	c_{66}^D	0.70
d_{15}	6.8×10^{-11} C/N	e_{15}	4.6 C/m²
d_{31}	−1.4	e_{31}	−0.6
d_{33}	5.7	e_{33}	5.5
ρ	4.26×10^3 kg/m³		

$k_{15}=0.34$, $k_{31}=0.18$,
$k_{33}=0.52$ and $k_t=0.53$
at room temperature.

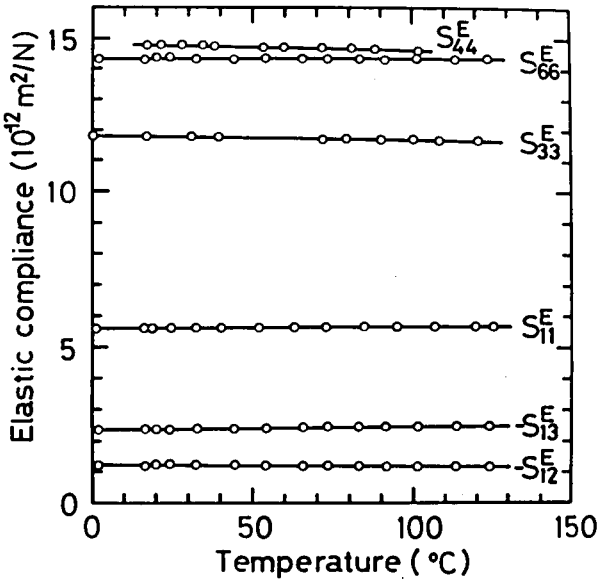

Fig. 3.3 Temperature dependence of elastic compliances of KLN.

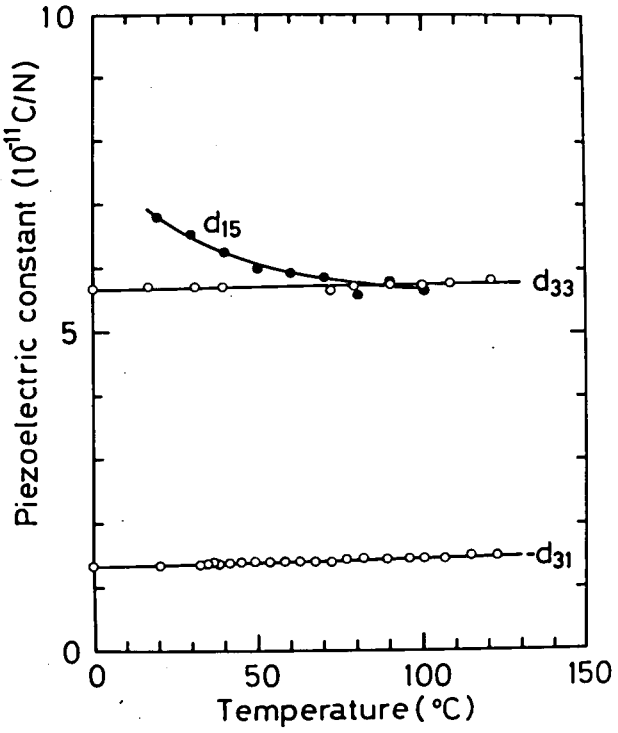

Fig. 3.4 Temperature dependence of piezoelectric constants of KLN.

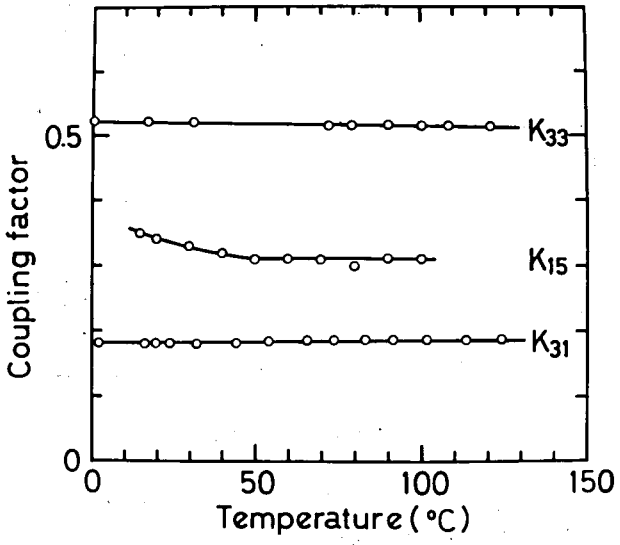

Fig. 3.5 Temperature dependence of mechanical coupling factors of KLN.

Table 3-IV Temperature coefficients of electro-acoustical constants in KLN at room temperature.

Ts_{11}^E	1.6×10^{-4}/°C	Td_{15}	nonlinear
Ts_{12}^E	−3.4	Td_{31}	8.5×10^{-4}/°C
Ts_{13}^E	5.6	Td_{33}	2.3
Ts_{33}^E	−0.98		
Ts_{44}^E	−1.2	Tk_{15}	nonlinear
Ts_{66}^E	0.075	Tk_{31}	3.0×10^{-4}/°C
$T\epsilon_{11}^T$	-20×10^{-4}/°C	Tk_{33}	−1.5
$T\epsilon_{33}^T$	9.4	Tk_t	−4.4

3.4 DISCUSSION

In the usual proper ferroelectrics, the temperature dependences of piezoelectric constants and mechanical coupling factors are often explained by the electrostrictive argument. Namely, it is assumed that the piezoelectric effect in the ferroelectric phase is due to the electrostrictive effect in the paraelectric phase biased by the spontaneous polarization. Then we have

$$d_{31} = 2Q_{12}P_S\varepsilon_0 (\varepsilon_{33}^T/\varepsilon_0 - 1), \tag{3-30}$$

$$d_{33} = 2Q_{11}P_S\varepsilon_0 (\varepsilon_{33}^T/\varepsilon_0 - 1), \tag{3-31}$$

$$\text{and} \quad d_{15} = 2Q_{44}P_S\varepsilon_0 (\varepsilon_{11}^T/\varepsilon_0 - 1), \tag{3-32}$$

where Q_{11} , Q_{12} and Q_{44} are the electrostrictive constants in the paraelectric phase. Using the value of 0.25 C/m^2 [10] for the spontaneous polarization P_S, the electrostrictive constants were determined as Q_{11} = 0.11 m^4/C^2 , Q_{12} = -0.027 m^4/C^2 and Q_{44} = 0.048 m^4/C^2 at room temperature. These values can be presumed to be nearly constant in the measured temperature range. They are comparable to those measured for other oxygen octahedra ferroelectrics [1,11,12] . Experimentally, the piezoelectric constants (d_{31} and d_{33}) and the coupling factors (k_{31} and k_{33}) are almost constant against temperature from room temperature to about 120 ^oC, while d_{15} and k_{15} decrease gradually with increasing temperature. These temperature characteristics are caused by the temperature dependence of dielectric constants.

In recent years, intensive efforts have been made by many

people to search for high piezoelectric coupling and temperature compensated SAW materials [13-16]. Among various materials thus found to date, tungsten-bronze ferroelectrics have attracted much attention as promising candidates for the temperature-stable and high piezoelectric coupling SAW applications.

Recently, the SAW characteristics of the present $K_{2.89}Li_{1.55}Nb_{5.11}O_{15}$ have also been calculated theoretically by Yamashita et al. [17], using the material constants determined by this author as thus described in this chapter. They showed that this material can be temperature-compensated at x-axis cylinder 45° cut. Figure 3.6 shows the SAW properties of KLN calculated by them. The values of the power flow angle (PFA), temperature coefficient of time delay (TCD), SAW coupling factor k_s^2 ($=2\Delta v/v$), and SAW velocity v obtained by them are 0.0 deg., 0.0 ppm/°C, 0.92 % and 3114 m/s at the x-axis cylinder 45° cut, respectively.

The SAW characteristics of various SAW materials given by O'Connell [15], are shown compared with that of KLN in Table 3-V. Further, Fig. 3.7 shows the TCD versus SAW coupling factor relation for various promising SAW materials. As can be seen from this figure, the KLN crystal is one of the most useful materials for SAW applications.

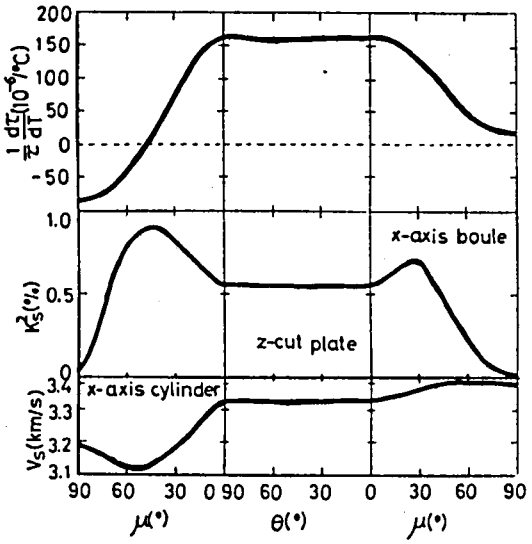

Fig. 3.6 The variation of SAW velocity, TCD, and 2Δv/v for x- and z-axis boule, x- and z-cut plate, x-axis cylinder KLN. (after Ref. [17].)

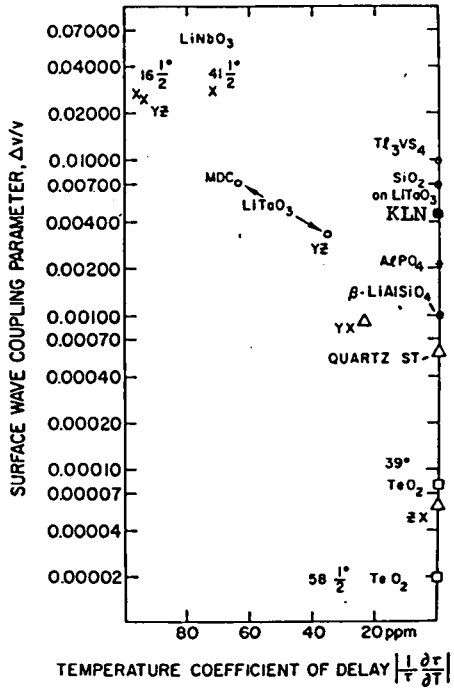

Fig. 3.7 Temperature coefficient of time delay versus piezoelectric coupling for various SAW materials. (after Ref. [15].)

Table 3-V Temperature compensated cuts of various materials.

Material	Orientation	Euler angles λ	μ	θ	TCD (ppm/°C)	Power flow angle φ (deg.)	Slope of power flow angle (∂φ/∂θ)	Δv/v (x10^{-2})	SAW velocity (m/sec)
$K_3Li_2Nb_5O_{15}$	X-axis cyl. 45°	0	45	90	0.0	....	.....	0.46	3114
$Pb_2KNb_5O_{15}$	X cut 10.6°	90	90	10.6	0.0	-2.5	.....	0.84	2493
	Z-axis cyl. 24.4°	24.4	90	0	0.0	0.0	0.150	0.033	2516
	Z-axis cyl. 74.4°	74.4	90	0	0.0	0.0	-0.268	0.73	2505
	Y-axis boule 66.6°	90	66.6	0	0.0	0.0	-0.241	0.94	2525
SiO_2	ST cut	0	132.75	0	0.0	0.0	0.378	0.058	3158
β-LiAlSiO	X cut 69°	90	90	69	0.0	18	.....	0.100	3662
	Doubly rotated	0	57	62	0.0	0.0	0.32	0.035	3258
Tl_3VS_4	(110) cut 70°	-45	90	70	0.0	-17	.....	1.0	900
	(110) cyl. 24°	45	24	90	0.0	0.0	.....	0.617	1010
Tl_3TaSe_4	(110) cyl. 54°	45	54	90	0.0	0.0	.....	0.508	879
$SiO_2/LiTaO_3$	Y cut, Z prop.	0	90	90	0.0	0.0	.....	0.7	3455
TeO_2	X cut 39°	90	90	39	0.0	0.0	.....	0.008	1424
	X-axis boule 58.2°	0	58.2	0	0.0	0.0	.....	0.002	1387

3.5 SUMMARY

All the elastic, piezoelectric and dielectric constants were determined in this chapter. The electromechanical coupling factors k_{15} , k_{31} , k_{33} and k_t are 0.34, 0.18, 0.52 and 0.53, respectively. The temperature coefficients of elastic compliances Ts_{33}^E , Ts_{44}^E and Ts_{66}^E are considerably small, suggesting that the KLN crystal is potentially suitable for applications to electromechanical bulk transducers in the thickness shear or longitudinal modes.

For SAW applications, it is shown that the KLN crystal also possesses a zero-temperature coefficient of time delay and zero-electromechanical power flow angle at x-axis cylinder 45° cut. The values of k_s^2 and v were calculated by Yamashita et al. to be 0.92 % and 3114 m/s at this cut, respectively. Accordingly, it is concluded that the KLN crystal is one of the most promising materials for SAW applications.

References

[1] M. Adachi and A. Kawabata: Jpn. J. Appl. Phys. 17 (1978) 1969.

[2] S. C. Abrahams, P. B. Jamieson and J. L. Bernstein: J. Chem. Phys. 54 (1971) 2355.

[3] Y. Uematsu and S. Koide: Jpn. J. Appl. Phys. 9 (1970) 336.

[4] D. Berlincourt and H. Jaffe: Phys. Rev. 111 (1958) 143.

[5] H. Ekstein: phys. Rev. 66 (1944) 108.

[6] M. Onoe, H. F. Tiersten and A. H. Meitzler: J. Acoust. Soc. Amer. 35 (1963) 36.

[7] M. Onoe, H. F. Tiersten and A. H. Meitzler: Trans. IECE.

Japan 46 (1963) 330 [in Japanese].

[8] T. Yamada: J. Appl. Phys. 46 (1975) 2894.

[9] A. W. Warner, G. A. Coquin and J. L. Fink: J. Appl. Phys. 40 (1969) 4353.

[10] L. G. Van Uitert, S. Singh, H. J. Levinstein, J. E. Geusic and W. A. Bonner: Appl. Phys. Letters 11 (1967) 161.

[11] M. Adachi and A. Kawabata: Jpn. J. Appl. Phys. 11 (1972) 1855.

[12] T. Yamada: J. Appl. Phys. 43 (1972) 328.

[13] A. J. Slobodnik, Jr., E. D. Conway and R. T. Delmonico: USAF Cambridge Research Laboratory Report No. AFCRL-TR-73-0597, (1973) .

[14] T. L. Szabo and A. J. Slobodnik, Jr.: IEEE Trans. Sonic and Ultrason. SU-20 (1973) 240.

[15] R. M. O'Connell and P. H. Carr: Optical Engineering 16 (1977) 440.

[16] R. W. Whatmore: J. Cryst. Growth 48 (1980) 530.

[17] K. Yamashita and H. Takeuchi: The 40th Annual Meeting of Japan Soc. Appl. Phys. No. 2a-Q-5, (1979) [in Japanese].

CHAPTER 4 ELECTRICAL AND OPTICAL PROPERTIES OF Na-MODIFIED POTASSIUM LITHIUM NIOBATE

4.1 INTRODUCTION

Interest in the quantum electronics field has led to many studies of the optical properties of a ferroelectric family with the tungsten-bronze structure. For materials to be useful in the quantum optical electronics field and for the related purposes with a laser:

1) good quality material must be growable in reasonable sizes;
2) it must not be susceptible to optically induced inhomogeneities(laser damage) which is a very serious problem in $LiNbO_3$;
3) it should have reasonable coefficients so that excessive voltages or intensities of laser are not required.

This family with "filled tungsten-bronze structure" such as KLN and BNN , to a reasonable extent, have all three of the properties required for useful crystals. Much information has been accumulated on the tungsten-bronze type ferroelectric materials. Total number of the ferroelectrics belonging to this family discovered till 1978 are about 104, including pure and complex compounds.

It is well-known that the KLN crystal has a completely filled tungsten-bronze structure and that possesses useful properties for electro-mechanical, electro-optic and nonlinear optic applications, because it is remarkably stable to intense laser radiation [1-7].

In this chapter, the crystal growth, electrical and optical properties of Na-modified KLN crystals are described.

Table 4-I Starting compositions of KNLN.

Sample	Starting compositions (mole %)			
	K_2O	Na_2O	Li_2O	Nb_2O_5
KLN	35.0		17.3	47.7
KNLN-10	31.5	3.5	17.3	47.7
KNLN-20	28.0	7.0	17.3	47.7
KNLN-25	26.2	8.8	17.3	47.7
KNLN-30	24.5	10.5	17.3	47.7

4.2 EXPERIMENTS AND RESULTS

4.2.1 Crystal Growth

The starting compositions are specified here by the value of x in a formula $K_{3(1-x)}Na_{3x}Li_2Nb_5O_{15}$ (hereafter abbreviated as KNLN except $x = 0$), which is obtained from the replacement of a part of K by Na in $K_3Li_2Nb_5O_{15}$ (KLN). The raw materials were K_2CO_3, Li_2CO_3, Na_2CO_3 of reagent grade, and Nb_2O_5 of 99.9 % purity. The crystals were grown by the same Czochralski method as described in Chapter 2. The attempted values for x are 0, 0.1, 0.2, 0.25 and 0.3 as shown in Table 4-I. The mixture was loaded in a platinum crucible and melted by rf-heating. Optimum growth conditions are as follows: pulling rate; 1 mm/h and rotation rate; 40 rpm. The pulling axis was chosen perpendicular to the c axis in order to minimize cracking taking place during the growth. It is found that the melting point shifts towards higher temperature with Na concentrations, that is, with the x value. In spite of a number of repeated attempts, it was not very successful to grow reasonably large and crackless crystals. The crystal often contains cracks presumably due to the thermal stress unavoidably generated when crossing the Curie temperature. This result should be compared to that obtained for KLN. This kind of difficulty, as described in Chapter 2, was not experienced in the attempt to grow KLN crystals, for which $x = 0$ and pale-yellow single crystals up to about 8-10 mm in diameter and 30 mm in length were successfully obtained.

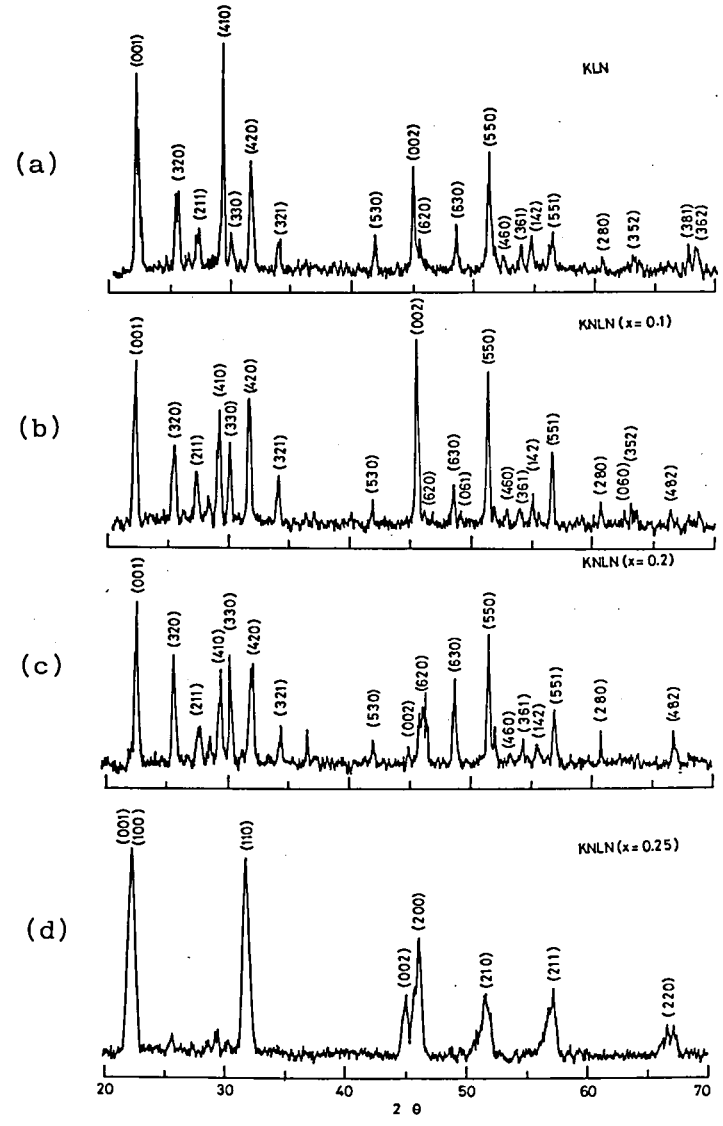

Fig. 4.1 X-ray diffraction patterns of KNLN. (a): x = 0 (KLN), (b): 0.1, (c): 0.2 and (d): 0.25.

4.2.2 Crystal Structure of KNLN

In order to determine the crystal structure and the phase boundary, X-ray diffraction measurements were carried out with a diffractometer using Ni filtered CuKα radiation. The obtained X-ray diffraction spectra were compared with those of another known tungsten-bronze and perovskite oxides such as KLN, $K_2BiNb_5O_{15}$ and $K(Ta_xNb_{1-x})O_3$.

The X-ray diffraction analyses revealed that the single phase region could be devided into two parts, namely, the tungsten-bronze and perovskite structure phases. Figure 4.1 shows the profiles of X-ray powder diffraction patterns of KNLN. As can be seen from the figures, the diffraction patterns in Figs. 4.1(a)-(c) are of tungsten-bronze, while those in Fig. 4.1 (d) are of perovskite. Accordingly, the limits of stability for the tungsten-bronze structure appear to be $x = 0.2$ to 0.25. Lattice constants (a and c), axial ratio (R) in the perovskite subunit and Curie temperature of KNLN are shown in Table 4-II together with the measured compositions of KLN and KNLN-10. The axial ratio R relates the hight (c) to the length of its edge ($a/\sqrt{10}$) in tungsten-bronze structure and represents the tetragonal distortion within the subunits. In Table 4-II, the axial ratio and Curie temperature of KNLN in the tungsten-bronze phase decrease with increasing x up to 0.2, whereas those in the perovskite phase increase discontinuously with increasing x beyond 0.25.

4.2.3 Dielectric Properties

Dielectric constants ε_{11}^T and ε_{33}^T were measured at 100 KHz

Table 4-II Lattice constants, axial ratio and Curie temperature of KNLN.

	$K_{3(1-x)}Na_{3x}Li_2Nb_5O_{15}$		Lattice constants		Axial ratio	Curie
	Starting composition	Composition in crystals	a(Å)	c(Å)	R	temperature T_c (°C)
KLN	x= 0	$K_{2.89}Li_{1.55}Nb_{5.11}O_{15}$	12.58	4.01	1.01	405
KNLN-10	0.1	$K_{2.27}Na_{0.49}Li_{0.79}Nb_{5.29}O_{15}$	12.56	3.96	1.00	350
KNLN-20	0.2		12.54	3.93	0.99	125
KNLN-25	0.25		3.94	4.00	1.02	500
KNLN-30	0.30		3.91	4.01	1.03	520

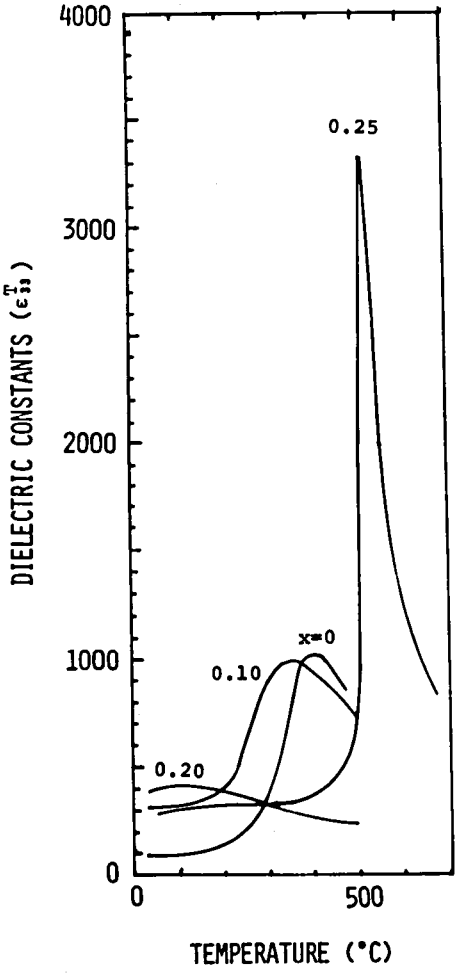

Fig. 4.2 Temperature dependence of dielectric constants $\varepsilon_{33}^T/\varepsilon_0$ of KNLN.

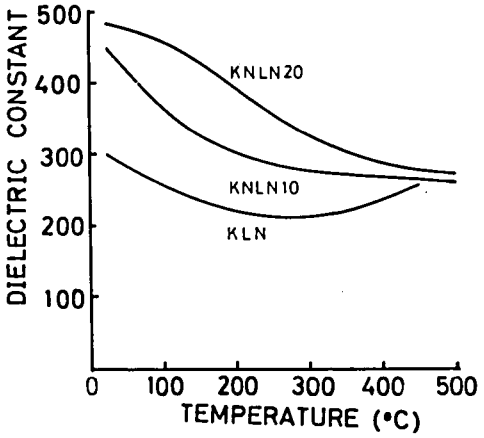

Fig. 4.3 Temperature dependence of dielectric constants $\varepsilon_{11}^T/\varepsilon_0$ of KNLN.

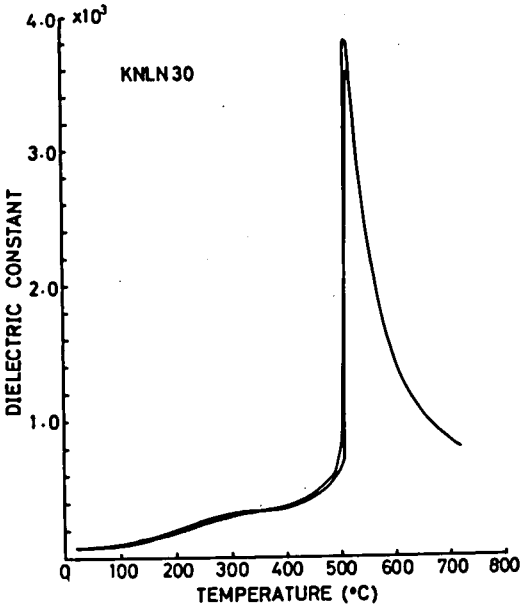

Fig. 4.4 Temperature dependence of dielectric constant of KNLN-30.

by using YHP type 4332A LCR meter. The output of the LCR meter was recorded on the Y axis of X-Y recorder, while the specimen temperature was recorded on the X-axis by means of CA thermocouple placed next to the specimen in the furnace. Paradium silver paste was used as an electrode for high temperature up to about 650 ^{o}C. The temperature dependence of dielectric constants of KNLN is shown in Figs. 4.2-4.4. In Fig. 4.2, two characteristic features can be seen. One is that the Curie temperature moves markedly to lower temperature and the peak of dielectric constant ε_{33}^{T} broadens with increasing x up to 0.2. The other feature is that the Curie temperature shifts discontinuously toward the higher temperature of about 500 ^{o}C at x = 0.25. The structural phase change from tungsten-bronze to perovskite structures is found to be around x between 0.20 and 0.25 in KNLN. These results are in agreement with those obtained from the X-ray measurements shown in the section 4.2.2. Figure 4.3 shows the dielectric constants ε_{11}^{T} of KNLN in the tungsten-bronze region. The constants ε_{11}^{T} do not show any anomaly, but decrease gradually with increasing temperature. On the other hand, the temperature dependence of dielectric constant for the KNLN-30 crystal located in the perovskite region is shown in Fig. 4.4. Its Curie temperature was about 520 ^{o}C. Further, the reciprocal dielectric constant $1/\varepsilon$ satisfied the Curie Weiss law and the Curie constant was determined as 1.8×10^{5} K. In addition, the phase transition from the tetragonal to orthorhombic structure was also observed at temperature of about 300 ^{o}C.

4.2.4 Electro-Mechanical Properties

Electrical poling treatment of KNLN crystals were attempted by the field-cooling method. It was found that the crystals with x value larger than 0.20 could not be effectively poled because the composition approaches the limits of stability of tungsten-bronze structure, and presumably the material is no longer ferroelectric in the vicinity of $x = 0.2$. In the present section, a part of electro-mechanical constants in KNLN-10 is determined, as compared with those of KLN described in Chapt. 3, by the overtone method [8].

A c-cut plate ($t = 0.61$ mm) of KNLN-10 was poled by the field-cooling technique under a dc field of about 200-300 V/cm along the c axis. From fundamental, 3rd harmonic and 5th harmonic resonanse frequencies, 4.312, 13.669 and 22.685 MHz, respectively, the electro-mechanical coupling factor k_t, elastic constants c_{33}^D and c_{33}^E, and dielectric constant $\varepsilon_{33}^S/\varepsilon_0$ were caluculated by using the Table 3-II shown in Chapt. 3 and the following formulae:

$$k_t^2 = \frac{\pi f_R}{2f_A} \cot\left(\frac{\pi f_R}{2f_A}\right), \tag{4-1}$$

$$c_{33}^D = \rho(2f_A d)^2 , \tag{4-2}$$

$$c_{33}^E = (1 - k_t^2)\, c_{33}^D , \tag{4-3}$$

$$\varepsilon_{33}^S/\varepsilon_0 = (1 - k_t^2)\, \varepsilon_{33}^T/\varepsilon_0 . \tag{4-4}$$

These constants of KNLN-10 are shown compared with those of KLN in Table 4-III. In KNLN-10, the value of k_t is smaller than that of KLN. It is presumed that piezoelectricity in KNLN

Table 4-III Dielectric, elastic constants and coupling factors of KNLN-10 and KLN.

Constants	KNLN-10	K L N
$\varepsilon_{11}^{T}/\varepsilon_0$	460	306
$\varepsilon_{33}^{T}/\varepsilon_0$	320	115
$\varepsilon_{11}^{S}/\varepsilon_0$		271
$\varepsilon_{33}^{S}/\varepsilon_0$	279	83
k_t	0.36	0.53
C_{33}^{E} (N/m^2)	1.23×10^{11}	1.09×10^{11}
C_{33}^{D} (N/m^2)		1.50×10^{11}
ρ (Kg/m^3)	4.53×10^{3}	4.26×10^{3}
T_c (°C)	350	405

crystals becomes weaker as Na concentration increases.

4.2.5 Linear Electro-Optic Properties

Linear electro-optic effect is commonly described in terms of a third-rank r-tensor defined by the expression

$$\Delta(1/n^2)_{ij} = \sum_k r_{ij,k} E_k \ . \qquad (4\text{-}5)$$

In eq. (4-5), the unit of r are m/V, E_k is the k_{th} Cartesian component of the externally applied electric field, and the pair of indices (ij) is separated by a comma from the third index k to emphasize that these indices can be interchanged.

Ferroelectric KLN and KNLN-10 crystals belong to the point group 4mm. Therefore there are only three different, non-zero electro-optic elements:

$$r_{13} = r_{23} \ ,$$

$$r_{33} \ , \qquad (4\text{-}6)$$

$$r_{42} = r_{51} \ .$$

A light incident along the a axis, and linearly polarized at 45^o to the c axis suffers an optical retardation

$$\phi = 2\pi l (n_o - n_e)/\lambda \ , \qquad (4\text{-}7)$$

where l is the optical path-length, n_o and n_e are ordinary and extra-ordinary refractive indices, respectively, and λ is

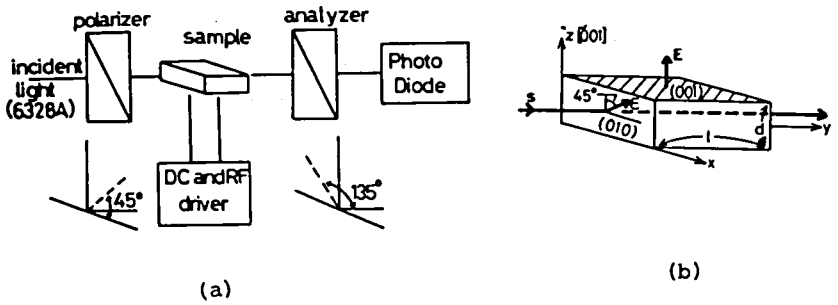

Fig. 4.5 A schematic diagram of the electro-optical measurement (a) and the crystal configuration (b).

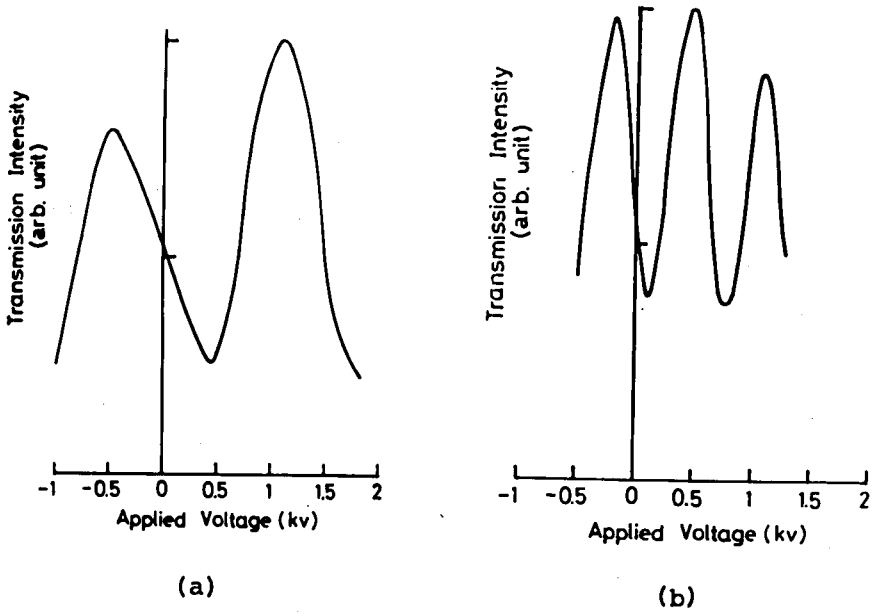

Fig. 4.6 Transmitted light as a function of applied voltage for KLN (a) and KNLN-10 (b).

Table 4-IV Crystal dimensions and values of the half-wave voltage.

	Length ℓ (mm)	Thickness d (mm)	Half-wave voltage V_π (V)	v_π (V)
K L N	3.40	2.95	900	1040
KNLN-10	3.94	1.82	350	750

the wavelength of the incident light in vacuum. Since z-directed electric field (E_3) changes both n_o and n_e it gives rise to a field-induced retardation

$$\Delta\phi = \pi n_e^3 \ell r_c E_c/\lambda \ , \qquad (4\text{-}8)$$

where r_c has been defined as

$$r_c = r_{33} - (n_o/n_e)\, r_{13} \ . \qquad (4\text{-}9)$$

A schematic diagram of the electro-optic measurements is shown in Fig. 4.5. The polarizer and analyzer were crossed at 45° to the crystal c axis. A photo-diode was used to detect the maxima and minima in the transmitted light corresponding to even and odd multiples of π retardations in the crystal. Figures 4.6(a) and (b) show transmitted light intensities as a function of a applied voltage for KLN and KNLN-10, respectively. The half-wave voltages V_π were determined as 900 and 350 V, for KLN and KNLN-10, respectively, from Figs. 4.6(a) and (b). The reduced half-wave voltage v_π is, in general, used for electro-optical materials comparison and it is defined as the voltage required to achieve one half-wave of phase retardation in a crystal having an electrode spacing equal to the optical path length, that is, defined as follows:

$$v_\pi = V_\pi \ell/d \ , \qquad (4\text{-}10)$$

where d is electrode spacing.

The obtained half-wave voltage V_π and v_π are given in Table 4-IV, together with sample dimensions. The value of v_π of KLN was 1040 V, which is close to that of the KLN crystal reported by

Van Uitert et al. [3]. On the other hand, the v_π for KNLN-10 is much smaller than that for KLN. The electro-optic constant r_c was calculated from the v_π by the following equation:

$$r_c = \frac{\lambda}{n_e^3} \frac{1}{v_\pi} \quad . \tag{4-11}$$

The calculated value of r_c for KLN is 6.0×10^{-10} m/V using the value of $n_e = 2.163$ measured by Van Uitert et al. [3]. While, the r_c for KNLN-10 was not determined in the present study because of no obtained value of n_e. It is found in this section that the v_π decreases with doping of Na ions in the KLN crystal as is evident from Table 4-IV.

4.2.6 Nonlinear Optic Properties

In this section, the nonlinear optical properties of KLN and KNLN-10 are described in order to examine the influence of Na doped in KLN. It is customary in nonlinear-optics to define a third rank d tensor by the relations,

$$P_i(2\omega) = \sum_{j,k} \epsilon_0 d_{ijk} E_j(\omega) E_k(\omega) \quad , \tag{4-12}$$

in the rationalized MKSA unit system. Here $P_i(2\omega)$ is a component of the second harmonic polarization of frequency 2ω generated by the electrical field of light frequency ω, $E(\omega)$. The commonly used second harmonic generation (SHG) coefficient $d_{i\lambda}$ is defined by $d_{i\lambda} = d_{ijk}$ for all combinations of j and k. Crystals in class 4mm, such as the KLN and KNLN-10, have three independent SHG coefficients, d_{15}, d_{31} and d_{33} .

In general, type I and type II phase matching processes

are possible for the nonlinear-optic materials. The phase matching conditions for the negative uniaxial crystal are given by

$$\text{Type I} \qquad n_o^{\omega} = n_e^{2\omega}(\theta) \ , \qquad (o + o \rightarrow e) \ , \tag{4-13}$$

$$\text{Type II} \qquad \frac{1}{2}[n_e^{\omega}(\theta) + n_o^{\omega}] = n_e^{2\omega}(\theta) \ , \qquad (o + e \rightarrow e), \tag{4-14}$$

where the subscripts e and o denote extraordinary and ordinary waves, respectively. For type I, a plot of the normal index surfaces for the ordinary and extraordinary rays at ω and 2ω is shown in Fig. 4.7. If $n_e^{2\omega}$ is smaller than n_o^{ω}, the respective index surfaces intersect and the condition $n_e^{2\omega}(\theta) = n_o^{\omega}$ is satisfied at $\theta = \theta_m$ and $\theta = \pi - \theta_m$. In other words, index matching is obtained if the fundamental beam is an ordinary ray while the second harmonic beam is an extraordinary beam, both beams propagate in a direction making an angle θ_m with the optic axis as shown in Fig. 4.7. The index-matching condition $n_e^{2\omega}(\theta_m) = n_o^{\omega}$ can be rewritten as

$$\left[\frac{1}{n_e^{2\omega}(\theta_m)}\right]^2 = \frac{1}{(n_o^{\omega})^2} \ . \tag{4-15}$$

On the other hand, $n_e^{\omega}(\theta_m)$ is expressed by

$$n_e^{\omega}(\theta_m) = n_o^{\omega} n_e^{\omega} / \{(n_o^{\omega})^2 \sin^2\theta_m + (n_e^{\omega})^2 \cos^2\theta_m\}^{1/2} \ . \tag{4-16}$$

From eqs. (4-15) and (4-16), the index-matching angle is given by

$$\sin^2\theta_m = \frac{(n_o^{\omega})^{-2} - (n_o^{2\omega})^{-2}}{(n_e^{2\omega})^{-2} - (n_o^{2\omega})^{-2}} \ . \tag{4-17}$$

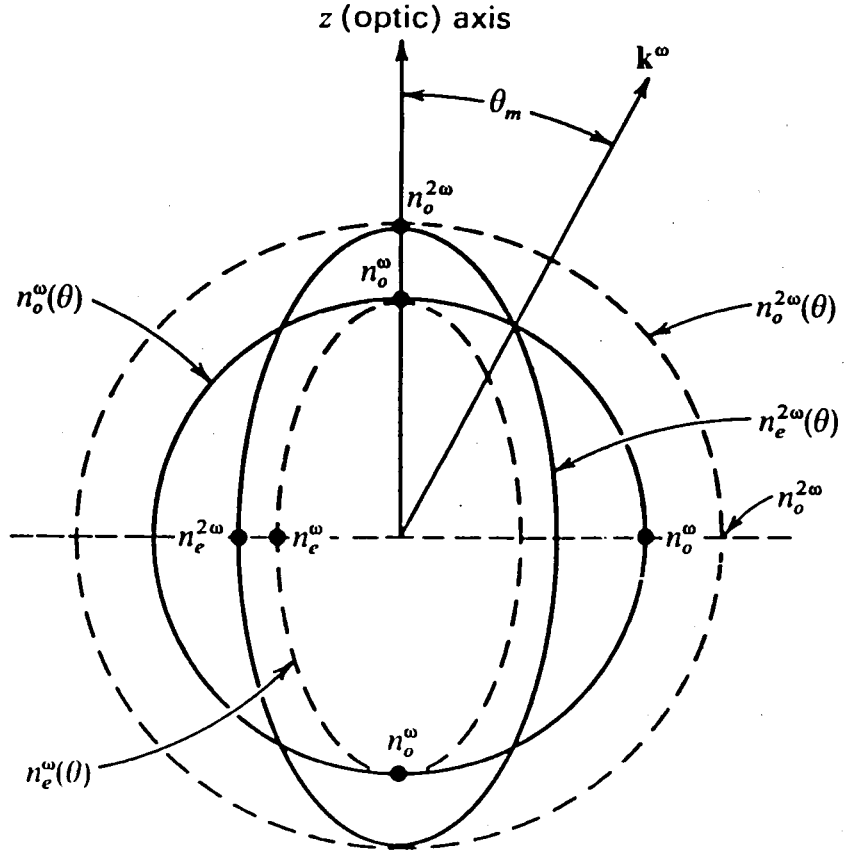

Fig. 4.7 The normal (index) surfaces for the ordinary and extraordinary rays in a negative uniaxial crystal.

The refractive indices of KLN are: $n_e^{2\omega} = 2.197$, $n_o^{2\omega} = 2.326$ at 0.532 μm; and $n_e^{\omega} = 2.112$, $n_o^{\omega} = 2.208$ at 1.064 μm, respectively [3]. On the other hand, those of the commercially available $LiNbO_3$ (UNION CARBIDE INCORPORATED) measured in this section for comparison are: $n_e^{2\omega} = 2.2350$, $n_o^{2\omega} = 2.3241$, $n_e^{\omega} = 2.15504$ and $n_o^{\omega} = 2.2309$ [9]. By using these refractive indices and eq. (4-17), the phase matching angles θ_m for KLN and $LiNbO_3$ were calculated as 72.3^o and 79.3^o, respectively. However, eq. (4-14) for type II was not satisfied by the above-mentioned refractive indices for KLN and $LiNbO_3$. Therefore, the process for type II is not considered in this study.

Nonlinear-optic measurements were carried out by observing the intensity of SHG at the phase matching angles from a continuously pumped 1.0642 μm YAG/Nd laser. A block diagram of the experimental arrangement is shown in Fig. 4.8. The laser beam was chopped at 460 Hz and it was lightly focused into the crystal by a lens of 5 cm focal length. The sample was mounted on a rotatable stage, whose rotation axis was perpendicular to the c-axis. After passing through IRQ-80 (infrared cut-off filter) filters and a lens of 10 cm focal length, the SH 0.532 μm radiation was detected by an RCA-7102 photo-multiplier. According to the theory [10] for the phase-matched SHG for the case of optimum focussing, the SH power $P^{2\omega}$ generated by a single-mode Gaussian beam of power P^{ω} in this experimental arrangement, is given by

$$P^{2\omega} = \frac{128\pi^2\omega^3 d_{eff}^2 \, l_{eff}}{c^4 n_o^{\omega^2} \, b} P^{\omega^2}, \qquad (4\text{-}18)$$

where P^{ω} is the fundamental power, ω is the frequency of the fundamental optical wave, d_{eff} is the effective nonlinear coefficient and is given by $d_{eff} = d_{31} \sin\theta_m$ in this experi-

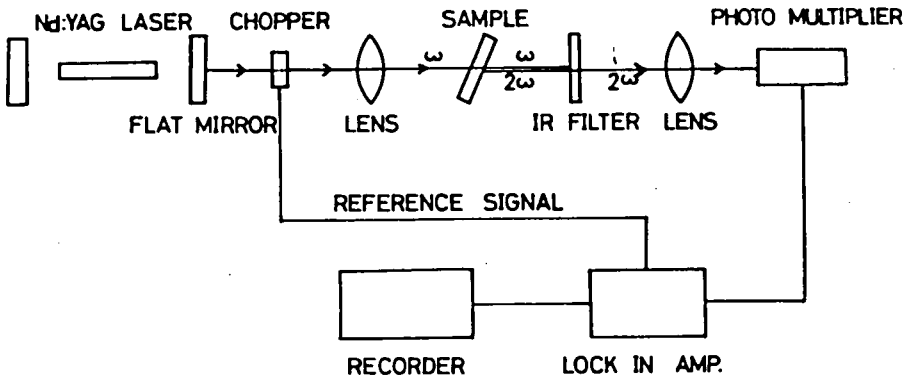

Fig. 4.8 A schematic diagram of experimental apparatus.

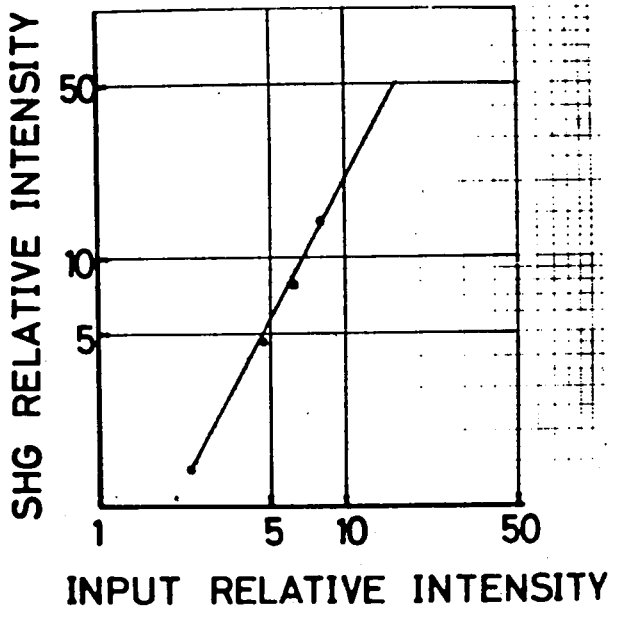

Fig. 4.9 Dependence of the SH power on the fundamental input power in the reference $LiNbO_3$ crystal.

mental arrangement. l_{eff} is the effective interaction length in the crystal, c is the light velocity in vacuum, n_o^{ω} is the ordinary refractive index at angular frequency ω, and b is the confocal parameter. An example of the dependence of the SH output intensity on the fundamental input intensity is shown in Fig. 4.9. The square dependence is in agreement with the theoretical prediction of eq. (4-18). Figures 4.10(a), (b) and (c) show the SH output intensities as a function of the internal incident angle in the crystals of $LiNbO_3$, KLN and KNLN-10, respectively. From these figures, the measured values of the phase matched angle θ_m were determined as 82.3^o, 75.9^o and 81.1^o for $LiNbO_3$, KLN and KNLN-10, respectively. These results are given in Table 4-V, compared with the values of the previously calculated phase matched angle θ_m. This discrepancy between the calculated and the measured values of θ_m may be due to a small difference in the crystal composition. The nonlinear optic coefficient d_{31} of the $LiNbO_3$ used as a reference material is $11.9 \times d_{36}^{KDP}$, which was reported by Boyd et al. [11]. Therefore, from each peak of the SH intensities shown in Fig. 4.10, the d_{31} of KLN and KNLN-10 can be determined by comparing the relative intensities with each other, referring to that of $LiNbO_3$. The thus-determined values of d_{31} are also given in Table 4-V. As can be seen from the table, the d_{31} of KLN is less than that of $LiNbO_3$. On the other hand, Van Uitert et al. [3] reported that the d_{31} of KLN is the same level with that of $LiNbO_3$. This discrepancy may be caused by optical inhomogeneity and defect stemming from the crystal growth or by off-stoichiometry effect of optical inhomogeneity mainly due to compositional variation on characteristics for SHG. As compared with the d_{31} of KLN and KNLN-10, the d_{31} of KNLN-10 is somewhat larger than that of KLN and is determined as

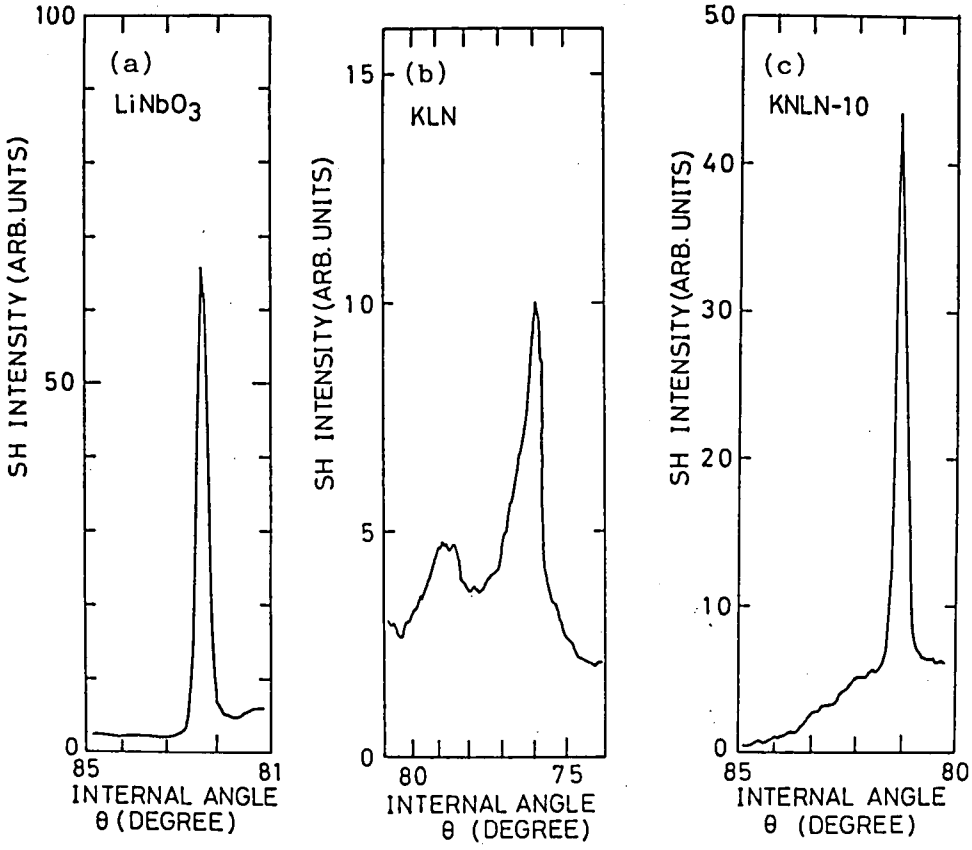

Fig. 4.10 SH intensities as a function of the internal inciedent angle in crystals of $LiNbO_3$ (a), KLN (b) and KNLN-10 (c).

Table 4-V Values of the phase matched angle θ_m and d_{31}.

Sample	Calculated θ_m	Measured θ_m	d_{31}
$LiNbO_3$	79.3°	82.3°	11.9 x d_{36}^{KDP}
K L N	72.2°	75.9°	7.7
KNLN-10		81.1°	11.7

$$d_{31}^{(KNLN-10)} = 1.6\ d_{31}^{KLN} .$$

From this results, it is concluded that the addition of small amount of Na to KLN results in a more preferable non-linear optic behavior than that pure KLN.

of

4.3 DISCUSSION

In this section, the influence of Na ions doped in the KLN crystal is considered. The completely filled tungsten-bronze KLN is represented by the formula $(A_1)_2(A_2)_4C_4(B_1)_2(B_2)_8O_{30}$ as described in Chapt. 2. A structural phase change due to the replacement of K ions by Na can be explained by considering the cation-anion distances and the coordination numbers in each site. The ionic radii of each atom and correction factors for different coordination numbers are given in Tables 4-VI and VII. The simplified environments of each site are illustrated with the interatomic O - O distances in Figs. 4.11(a) to (d), where the square A_1, pentagonal A_2, octahedral (B_1,B_2) and triangular C sites are 12, 15, 6 and 9 coordinated, respectively. Maximum allowable ion radius (r_{A_1}, r_{A_2}, r_B and r_C) of each anion surrounded by O^{2-} ions are also given in these figures, by assuming that the Nb - O distance in B site is 2.04 Å as reported by Shannon and Prewitt [12]. As can be seen from the figures, there is a possibility that the Na ions doped in KLN could occupy either A_1 or A_2 site, judging from its ionic radii. Now, consider the following process. The K ions in the A_1 site are first substituted by Na ions. The A_1 site is fully occupied by Na ions at x = 0.33. For x larger than 0.33, the K ions in the A_2 site are substituted by Na ions.

Table 4-VI Ionic radii in Å.

Li^+	0.74
Na^+	1.02
K^+	1.38
Nb^{5+}	0.64
O^{2-}	1.40

Table 4-VII Correction factors for different coordination numbers.

Coordination number	Ratio of interatomic distance to sum of standard radii
6	1
9	1.06
12	1.10
15	1.13

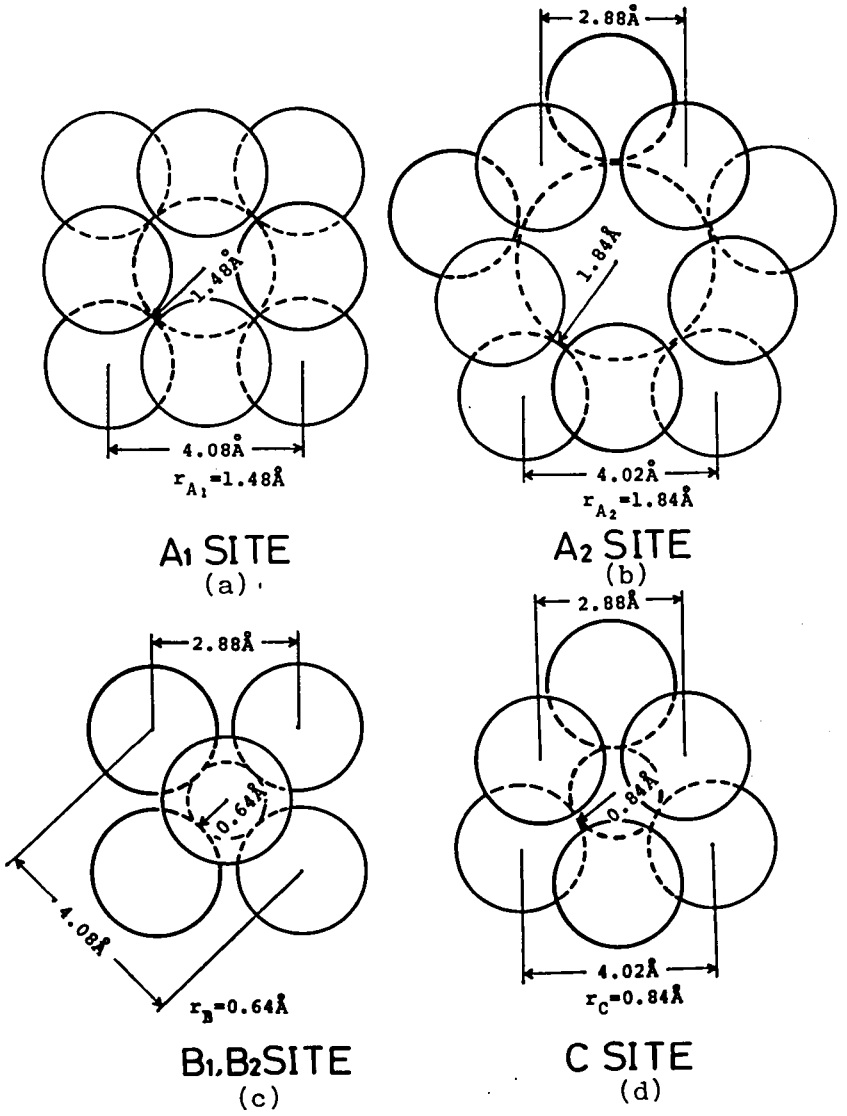

Fig. 4.11 Environments of A_1 (a), A_2 (b), B_1 and B_2 (c), and C (d) sites in the tungsten-bronze structure.

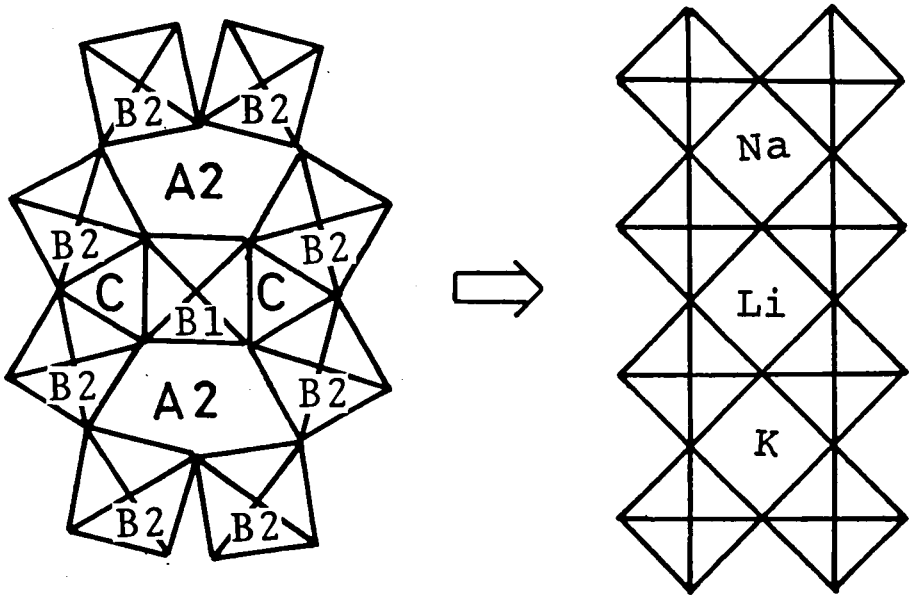

Fig. 4.12 An illustration of the structural phase transition.

However, as explained by Goldschmidt's packing principle [13], the A_2 site becomes progressively less stable as the K ion is replaced by the Na ion. Because the ionic radii of Na is too small to sustain the coordination number of 15 for the pentagonal A_2 site. Therefore, as shown in Fig. 4.12, a structural change takes place to adjust the coordination number from 15 to 12. With this structural change, the C site loses one Li ion and the B_1 site loses one Nb ion and three O ions. It is seen that the resulting new structure has a perovskite form. Thus it is theoretically expected that the crystal changes its structure form a tungsten-bronze form to a perovskite form at $x = 0.33$. However, the experimental results given in section 4.2.2 suggests the possibility that the structural change takes place at some x value between 0.2 and 0.25. The discrepancy between the experimentally obtained x value and that theoretically expected is due to the compositional deviation in the grown crystal.

4.4 SUMMARY

Crystals of KNLN were grown by the Czochralski method. The attempted values for x were 0, 0.1, 0.2, 0.25 and 0.3. However, it was not very successful to grown reasonably large and crackless crystals, when x value increased. X-ray and dielectric measurements were carried out in order to determine the crystal structure and the phase boundary of KNLN. From the measured results, the structural phase change from tungsten-bronze to perovskite structures was found to be around x between 0.20 and 0.25 in KNLN.

Further, it was found that the crystals with x value

larger than 0.20 could not be effectively poled because the composition approaches the limits of stability of the tungsten-bronze structure, and presumably the material was no longer ferroelectric in the vicinity of $x = 0.20$. Therefore, the electromechanical, linear electro-optic and nonlinear-optic properties of KLN and KNLN-10 were investigated to clarify the influence of Na doped in KLN. In KNLN-10, the value of k_t was smaller than that of KLN. It is found that piezoelectricity in KNLN crystals becomes weaker as Na concentration increases. On the other hand, the v_π for KNLN-10 was much smaller than that for KLN. Further, the d_{31} of KNLN-10 was somewhat larger than that of KLN and was determined as

$$d_{31}^{(KNLN-10)} = 1.6\ d_{31}^{(KLN)} \quad .$$

From these results, it is concluded that the addition of small amount of Na to KLN results in more preferable linear optical and nonlinear-optic behaviors than pure KLN.

References

[1] Y. Uematsu and S. Koide: Jpn. J. Appl. Phys. 9 (1970) 336.

[2] M. Adachi and A. Kawabata: Jpn. J. Appl. Phys. 17 (1978) 1969.

[3] L. G. Van Uitert, S. Singh, H. J. Levinstein, J. E. Geusic and W. A. Bonner: Appl. Phys. Letters 11 (1967) 161.

[4] T. Nagai and T. Ikeda: Jpn. J. Appl. Phys. 12 (1973) 199.

[5] J. E. Geusic, H. J. Levinstein, J. J. Rubin, S. Singh and L. G. Van Uitert: Appl. Phys. Letters 12 (1968) 224.

[6] L. G. Van Uitert, J. J. Rubin and W. A. Bonner: IEEE Trans.

Quantum Electron. QE-4 (1968) 622.

[7] B. A. Scott, E. A. Giess, B. L. Olson, G. Burns, A. W. Smith and D. F. O'Kane: Mater. Res. Bull. 5 (1970) 47.

[8] M. Onoe, H. F. Tiersten and A. H. Meitzler: J. Acoust. Soc. Am. 35 (1963) 36.

[9] D. S. Smith, H. D. Riccius and R. P. Edwin: Opt. Commun. 17 (1976) 332.

[10] G. D. Boyd and D. A. Kleinman: J. Appl. Phys. 39 (1968) 3597.

[11] G. D. Boyd, R. C. Miller, K. Nassau,W. L. Bond and A. Savage: Appl. Phys. Letters 5 (1964) 234.

[12] R. D. Shannon and C. T. Prewitt: Acta Cryst. B25 (1969) 925.

[13] V. M. Goldschmidt: Geochemistry, Oxford (1954).

CHAPTER 5 CRYSTAL GROWTH AND FUNDAMENTAL PROPERTIES OF POTASSIUM BISMUTH NIOBATE (KBN)

5.1 INTRODUCTION

A large number of ferroelectric materials with tungsten-bronze structure have been grown and have attracted much attention for electro-optic, nonlinear optic and piezoelectric applications. Among various tungsten-bronze type ferroelectric materials, "filled" tungsten-bronze ferroelectrics, where all the A_1 and A_2 site are occupied by cations as shown in Fig.2.1 (see Chapt. 2), have a high stability to intense laser radiation [1, 2] and furthermore have excellent electro-optic and nonlinear optical properties as exampled by $Ba_2NaNb_5O_{15}$ [3].

Pottasium bismuth niobate (hereafter abbreviated as KBN) is one of the filled tungsten-bronze crystals. KBN has an orthorhombic structure, and its melting point is 1310 ^{o}C. So far some number of studies have been made on the crystal structure, the crystal growth, and the dielectric and optical properties of KBN [4-6]. The crystal structure was studied by Ismailzade [4] and Sugai et al. [6] using ceramics and crystals, respectively. The phase diagram of the ternary system K_2O-Bi_2O_3-Nb_2O_5 was investigated in detail by Sugai et al. [6]. The Curie temperature is reported as about 350 ^{o}C, and the refractive indices are given as $n_z = 2.264$, $n_x = n_y = 2.227$ at 632.8 nm [7]. No additional detailed study of this material has been reported yet. For further investigation of KBN, this chapter is concerned with studies of the ferroelectric and elastic properties of this material. Further the photo-elastic properties are measured by

the Dixon-Cohen method [8] for application to acousto-optic devices.

5.2 EXPERIMENTS AND RESULTS

5.2.1 Crystal Growth

Single crystals of KBN were grown by rf-heating Czochralski method from the melt with stoichiometric composition (a): 25 mole % K_2CO_3, 12.5 mole % Bi_2O_3 and 62.5 mole % Nb_2O_5; and with potassium and bismuth enriched composition (b): 26.5 mole % K_2CO_3, 13.3 mole % Bi_2O_3 and 60.2 mole % Nb_2O_5. The mixture was charged in a platinum crucible (150 cc) and melted at the temperature of about 1310 ^{o}C. The optimum growth conditions are follows:

Seed orientation	[001] ,
Pulling rate	4 mm/h ,
Seed rotation	10 - 40 rpm ,
Crucible rotation	0 - 10 rpm ,
Atmosphere	O_2 (350 cc/m at 1 atm) ,
Cooling rate	60 - 80 ^{o}C/h .

Large pale-yellow transparent single crystals of KBN up to about 30 mm in diameter and 40 mm in length were easily obtained as shown in Fig. 5.1.

The chemical analysis revealed that the compositions in the grown crystals from the melt with the compositions (a) and (b) were $K_{1.63}Bi_{0.67}Nb_{5.27}O_{15}$ and $K_{1.93}Bi_{0.91}Nb_{5.07}O_{15}$, respectively, as given in Table 5-I. A survey of the phase diagram of

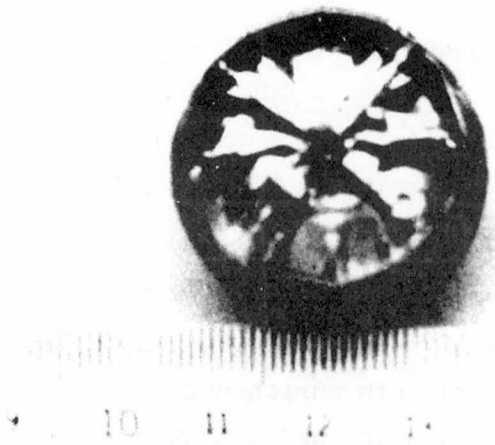

Fig. 5.1 A photograph of an as-grown KBN crystal.

Table 5-I Composition of the melt-pulled crystals.

Sample	K_2O	Bi_2O_3 (wt%)	Nb_2O_5	compositions
KBN-a	8.3	16.9	75.8	$K_{1.63}Bi_{0.67}Nb_{5.27}O_{15}$
KBN-b	9.4	22	69.8	$K_{1.93}Bi_{0.91}Nb_{5.07}O_{15}$

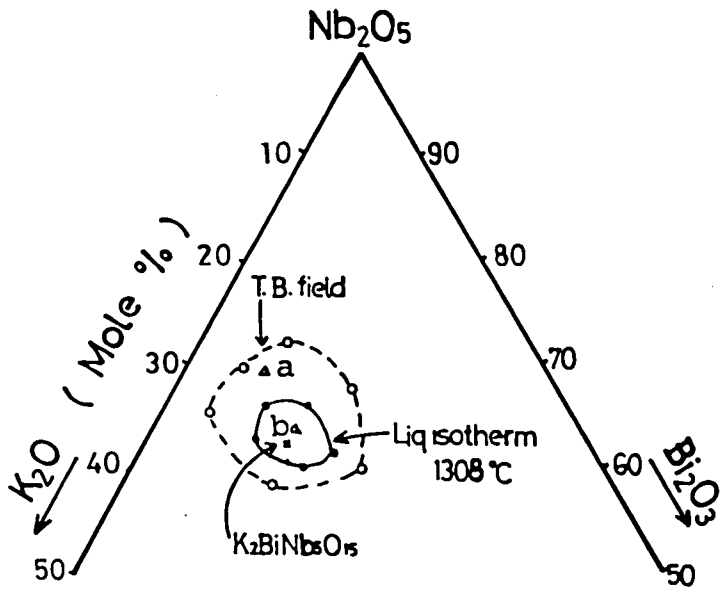

Fig. 5.2 The K_2O-Bi_2O_3-Nb_2O_5 system with ternary compounds.

the ternary system K_2O-Bi_2O_3-Nb_2O_5 is shown in Fig. 5.2, which is the result obtained by Sugai et al. [7]. They have revealed that $K_2BiNb_5O_{15}$ is not the congruently melting composition, and that the composition with highest stability of the tungsten-bronze phase lies somewhere on the Nb_2O_5-rich side of the $KNbO_3$-$Bi_{1/3}NbO_3$ section of the K_2O-Bi_2O_3-Nb_2O_5 ternary system as shown in Fig. 5.2. The compositions corresponding to the present crystals (a) and (b) are also marked in Fig. 5.2. As can be seen from the figure, the composition of the melt pulled crystal with the stoichiometric composition (a) was close to the phase boundary of the tungsten-bronze region. It should be noted that K_2O and Bi_2O_3 evaporated during the crystal growth, and that the melt pulled crystals contain excess Nb because the vapor pressure of both K_2O and Bi_2O_3 is high at the melting point of KBN (1310 ^{o}C). The crystal (a), as judged by the result of X-ray measurement, had the tungsten-bronze structure. However the dielectric constants of it did not show any anomaly corresponding to its Curie temperature (ferroelectric phase transition), but only increase gradually with increasing temperature. Therefore, the crystal (a) seems to be non-ferroelectric. On the other hand, the dielectric constants of the crystal (b) exhibited anomalies at the Curie temperature of about 380 ^{o}C, corresponding to the ferroelectric phase transition. Accordingly, the starting composition (b) with excess K_2O and Bi_2O_3 was mainly used for the crystal growth of KBN. This technique is important to obtain large KBN crystals of good quality.

5.2.2 Crystal Structure at Room Temperature

Ismailzade [4] and Krainik et al. [5] reported that KBN belongs to the orthorhombic system with lattice constants a = 17.75, b = 17.90 and c = 7.84 Å. On the other hand, Sugai et al. [6] has shown that it belongs to the tetragonal system with lattice constants a = b = 17.85 and c = 7.84 Å.

In this section, X-ray diffraction measurements were carried out in order to determine the class of the crystal system in KBN. An example of X-ray powder diffraction measurements is shown in Fig. 5.3, indicating the same tungsten-bronze structure as shown in KLN (see Chapt. 2). In the figure, (hkl)-(khl) doublets produced by the orthorhombic symmetry were not obviously observed in the present KBN powder. Therefore studies on the crystal system in KBN were further carried out, using the crystal sample instead of the powder by X-ray measurements. Figure 5.4 shows an example of X-ray diffraction patterns for the (10, 0, 0) and (0, 10, 0) diffractions from the the a- and b- surface plates to compare with each other. The peaks corresponding to the diffractions from the (10, 0, 0) and (0, 10, 0) KBN plates were clearly separated. The diffraction angles 2θ for the (10, 0, 0) and (0, 10, 0) $CuK\alpha_1$ diffractions were determined as 51.050° and 51.013°, respectively, referring to Si standard. The lattice constants a, b and c of the KBN crystal obtained were 17.878, 17.888 and 7.853 Å, respectively. An example of the X-ray back Laue patterns for the surface-normal axis of the (001) KBN possesses four-fold symmetry as shown in Fig. 5.5.

From the experimental results obtained by the X-ray measurements, it is concluded that KBN is an orthorhombic material, but its spontaneous deformation b/a is nearly equal to 1.

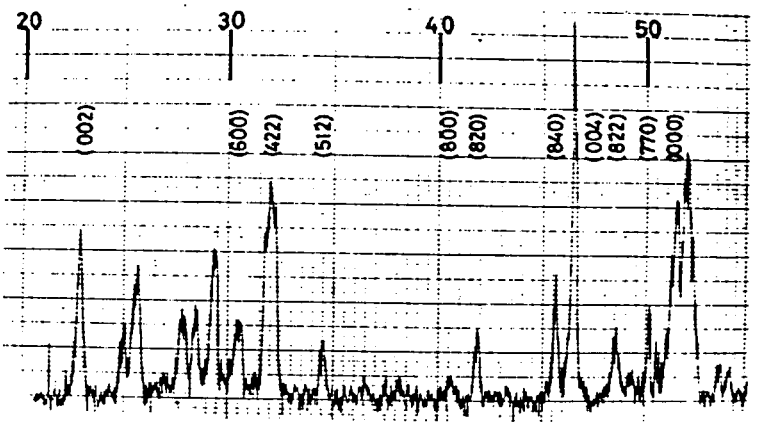

Fig. 5.3 An X-ray diffraction pattern of KBN powder.

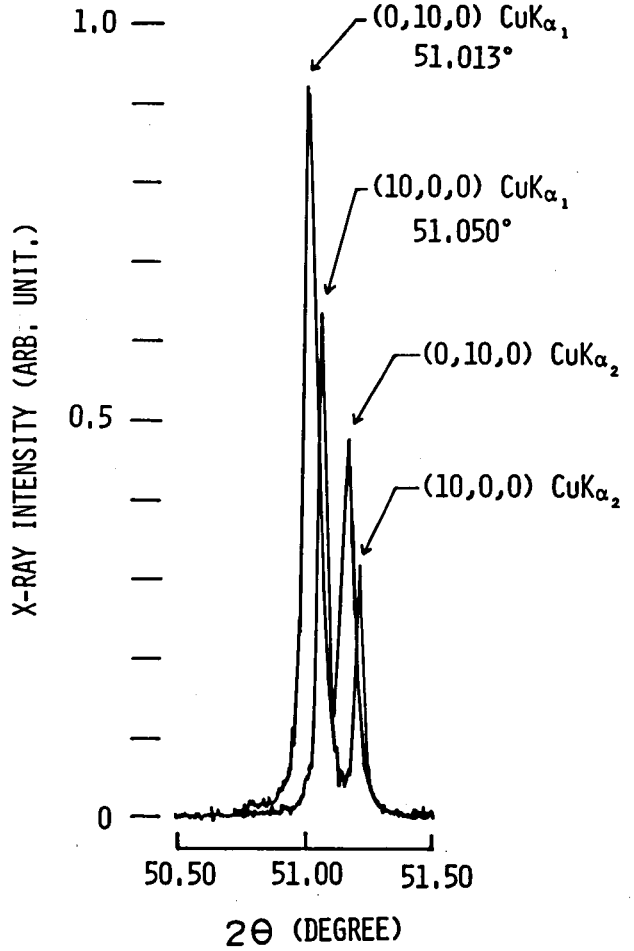

Fig. 5.4 X-ray diffraction patterns for the (10,0,0) and (0,10,0) diffractions of the a- and b-surfaces of KBN crystal.

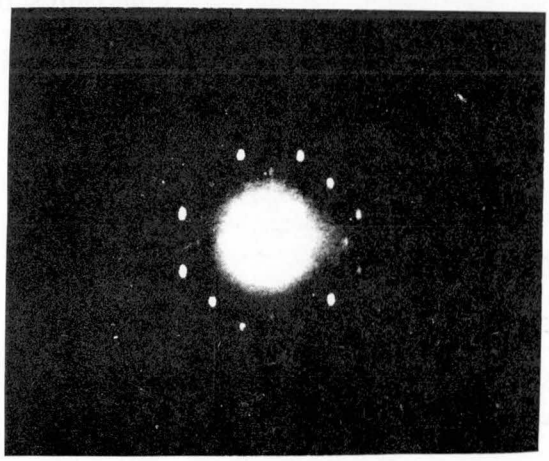

Fig. 5.5 An X-ray Laue pattern for the (001) KBN surface.

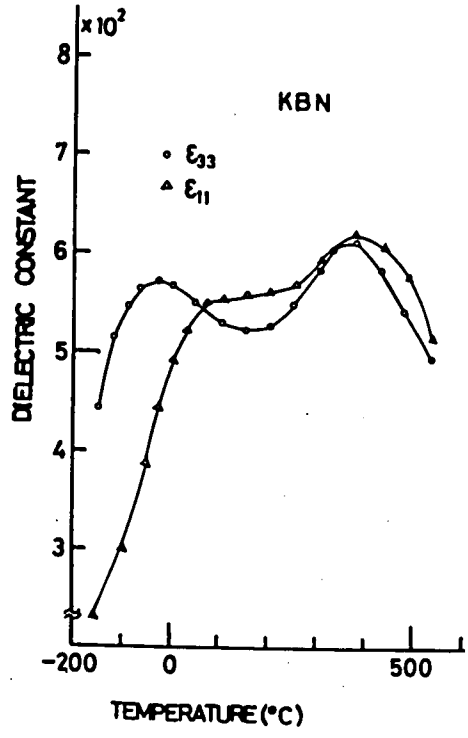

Fig. 5.6 Temperature dependence of dielectric constants of KBN.

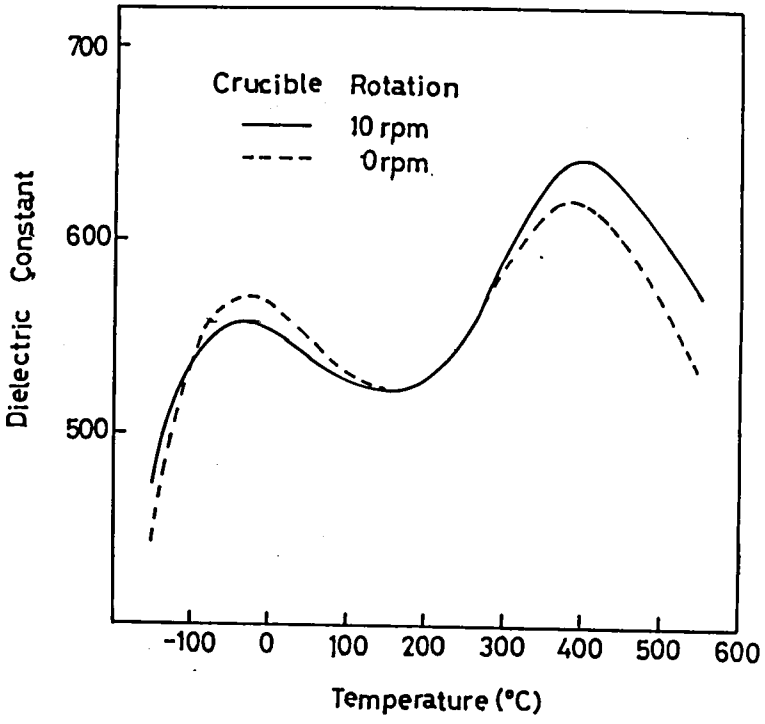

Fig. 5.7 Temperature dependence of dielectric constants with the crucible rotation.

5.2.3 Dielectric Properties

The dielectric constants ε_{11} (or ε_{22}) and ε_{33} were measured at 100 KHz by the YHP type 4332A LCR meter. The output of the LCR meter was recorded on the Y axis of an X-Y recorder, while the specimen temperature was recorded on the X-axis by means of a CA thermocouple placed next to the specimen in a furnace or cryostat. Evaporated gold and paradium silver paste were used as electrodes for low temperature measurements below 0 ^{o}C and for high temperature up to 550 ^{o}C, respectively.

The temperature dependences of dielectric constants of KBN grown without crucible rotation are shown in Fig. 5.6. The dielectric constants $\varepsilon_{11}^{T}/\varepsilon_{0}$ ($\simeq\varepsilon_{22}^{T}/\varepsilon_{0}$) and $\varepsilon_{33}^{T}/\varepsilon_{0}$ at room temperature were 530 and 560, respectively. Both the dielectric constants exhibit anomalies at the Curie temperature of about 380 ^{o}C. The Curie temperature is found to be strongly dependent on the crysral composition and therefore the peaks of the dielectric constants are broad because of the inhomogeneities in the composition. The temperature dependences of the dielectric constants $\varepsilon_{33}^{T}/\varepsilon_{0}$ of the KBN grown from the melt with crucible rotations 0 and 10 rpm, are shown in Fig. 5.7. It is found that inhomogeneities in the crystals are improved by the crucible rotation.

5.2.4 Poling and Chemical Etching Treatments

A ferroelectric crystal is defined as a crystal which belongs to the pyroelectric family and whose direction of the spontaneous polarization can be reversed by an electric field. In General, ferroeletricity in a given material can be most

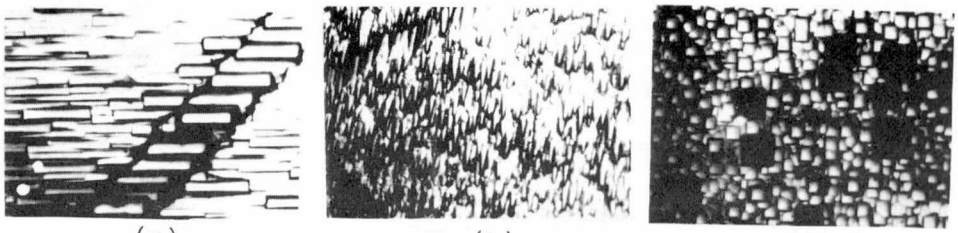

(a) (b) (c)

Fig. 5.8 Etched patterns of (100) (a), (110) (b) and (001) (c) plates.

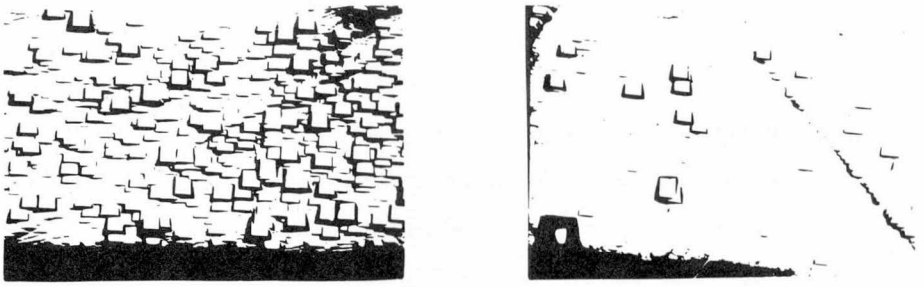

(a) (b)

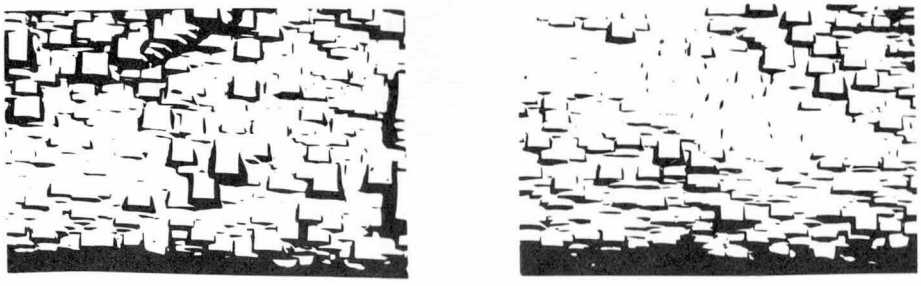

(c) (d)

Fig. 5.9 Etched figures on an (001) plate.
(a) and (c): negative sense plane;
(b) and (d): positive sense plane.

simply verified by the existence of D-E hysteresis loop. However, such a hysteresis loop was not observed in the present KBN crystals. Therefore, a chemical etching technique was next employed, as an alternative method as described in Chapt. 2 , to examine the possible ferroelectric properties. The etchant was a mixed solution of one part hydrofluoric acid (containing 47 % HF) and one part nitric acid at its boiling point. The etched figures of (100), (110) and (001) plates cut from an as-grown crystal of KBN are shown in Figs. 5.8(a), (b) and (c), respectively. The Ni-Cr electrodes were evaporated on the surfaces of the plates described above. By means of the field-cooling method through the Curie temperature under a dc electric field applied along the [100], [110] and [001] axes, poling treatment was attempted to obtain a single-domain of KBN crystal. The plate was then etched to examine the poling effect. Contrary to the expectation, however, no difference was observed between the appearance of the positive side surface and that of the negative surface of the etched plate. This result suggests that the field-cooling method alone is not good enough to develop a large single-domain. Accordingly, in order to improve the poling effect, application of a compressive stress was then incorporated during the field-cooling treatment. The stress was applied to the sample in perpendicular to the electric field.

Chemical etching analysis showed that KBN could be poled only in the case of the (001) plate. The etched figures of the negative and positive side surfaces of the (001) plate are shown in Figs. 5.9 (a) and (b), respectively. The difference in the etched appearance is clearly seen, suggesting that this sample was effectively poled. On the other hand, such difference was not seen either in the (100) or in the (110) plate.

After being poled, the (001) plate was inserted into the

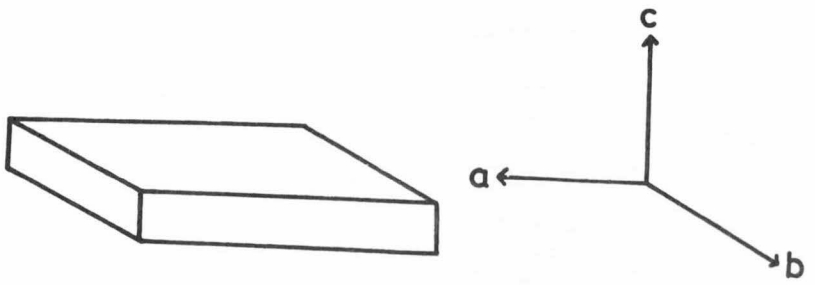

(a)

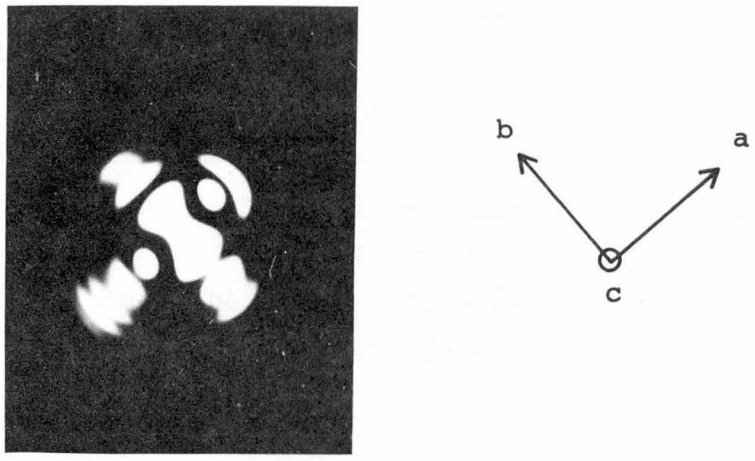

(b)

Fig. 5.10 The shape and orientation (a) of the specimen, and the interference figure (b).

furnace kept at a temperature above the Curie point, and then cooled without applying either the electric field or the compressive stress. In this case, the difference in the appearance of the two surfaces of the plate was not observed as shown in Figs. 5.9 (c) and (d).

From these results, it is concluded that the polar axis of KBN is parallel to the [001] axis.

5.2.5 Conoscopic Observation

The experimental results described in the previous section showed that in KBN estimated as belonging to the orthorhombic system, application of uniaxial compressive stress is essential to developing a single ferroelectric domain. This fact suggests that KBN is possibly a ferroelastic material. "Ferroelasticity" is defined on the analogy of "ferroelectricity", mechanical strain and stress in the former corresponding to electric polarization and field in the latter respectively [9]. Exsistence of ferroelasticity, in a material belonging to the orthorhombic system, can be verified in a direct manner by viewing conoscopically the switching of the optic axis under application of uniaxial stress (conoscopic observation) [10]. In the conoscopic method, interference figures created by light diverging through the crystal are examined in a polarizing microscope.

Consider the case observed in the KBN crystal as shown in Fig. 5.10. For the light propagated in the c axis direction, the interference figure showed the existence of two optic axes lying in the a-c plane. Although the angle between the two optic axes is very small, the above observation suggests

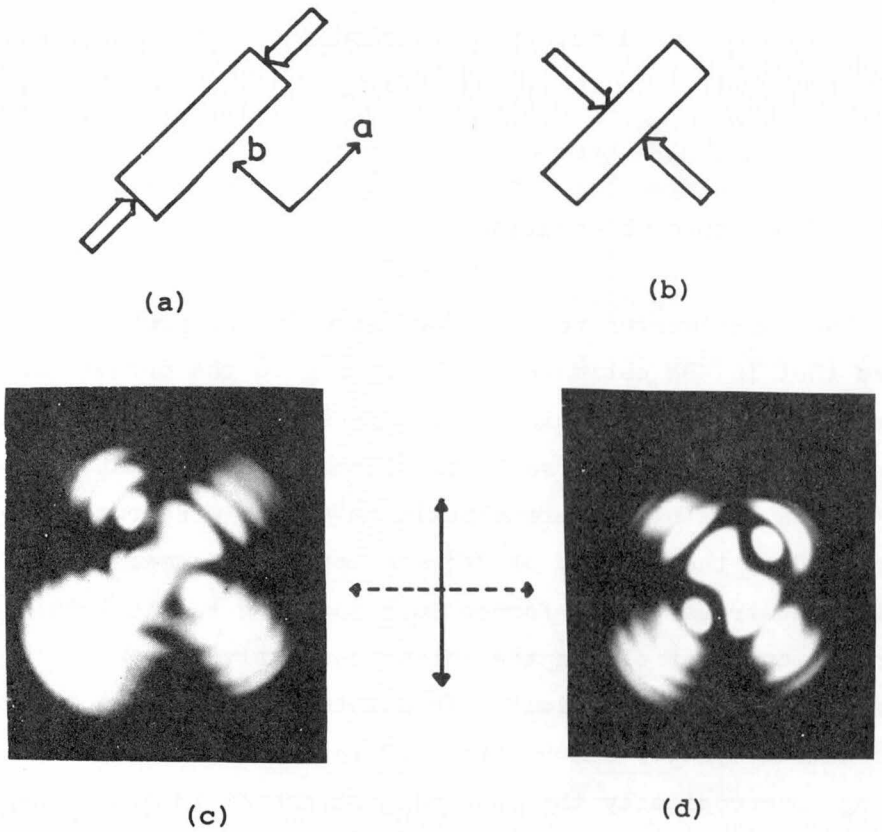

Fig. 5.11 Compressive stress directions (a) and (b), and interference figures (c) and (d).

that the KBN crystal is positive and biaxial in optical sense.

When a compressive stress along the a axis was applied through the Curie point, as shown in Fig. 5.11 (a), the interference figure was observed with the optic axes lying in the b-c plane as shown in Fig. 5.11 (c). On the other hand, when the compressive stress was applied along the b axis by the same way as described above, the optic axes changed their directions from in the b - c plane to the a - c plane as shown in Fig. 5.11 (d).

Thus the optic-axial plane can be rotated through 90° by changing the direction of uniaxial compressive stress. Accordingly, it is confirmed that the KBN crystal has a ferroelastic character.

5.2.6 Thermal Expansion

Figure 5.12 shows thermal expansion along the [100], [010] and [001] axes as a function of temperature, measured by a dilatometer with a straingage. The lengths of each sample were about 12 mm. The thermal expansion $\Delta l/l$ for the [001] axis increases abruptly with increaing temperature and slightly changes its slope in the vicinity of the phase transition temperature at about 350° C. On the other hand, the thermal expansion along the [100] and [010] axes increases gradually with increasing temperature, and their curves are in almost agreement with each other. An enlarged diagram of thermal expansion along the [001], [100], [010], [110] and [011] axes is shown in Fig. 5.13. Each curve shows a slight anomaly caused by the phase transition at the temperature of about 350° C. The thermal expansion coefficients for various orientations are

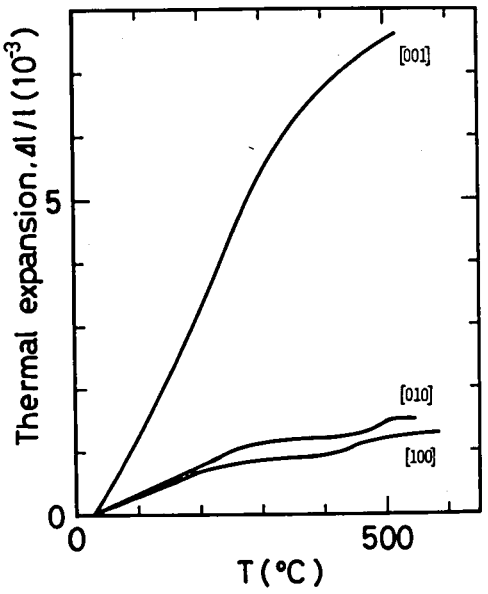

Fig. 5.12 Thermal expansion along the [100], [010] and [001] axes.

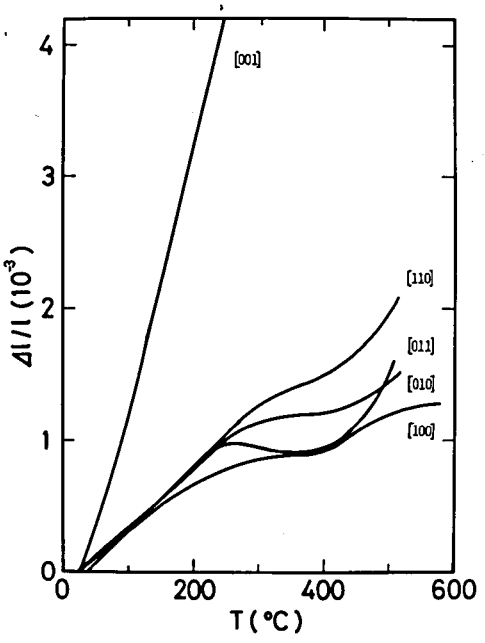

Fig. 5.13 Thermal expansion along the [001], [110], [010], [011] and [100]axes.

Table 5-II Thermal expansion coefficients of KBN. The unit is $10^{-6}(°C)^{-1}$.

Temperature (°C)	25-100	100-200	200-300	300-400	400-500
[100] axis	3.67	2.95	1.62	1.46	2.98
[010] axis	4.52	4.44	1.94	0.29	3.72
[001] axis	17.67	21.31	19.51	10.36	6.67
[110] axis	4.89	4.14	4.09	1.87	6.42
[011] axis	4.88	4.43	-0.71	1.13	9.32

listed in Table 5-II.

5.2.7 Elastic Properties

The KBN crystal is an orthorhombic material and probably belongs to the point group mm2 at room temperature. The elastic tensor matrix for crystals in class mm2 has 9 independent elements. These are shown in Table 5-III. The elastic constants are mathematically related to the velocity of propagation for longitudinal and trasverse waves along various crystallographic directions. So that, by measuring velocities for various orientations of KBN, all the elastic constants can be determined. The equations relating velocities of propagation and elastic constants, which are used for the present measurement, are given in Table 5-IV [11]. Ultrasonic velocity measurements were done by the pulse echo method using two specimens. One specimen had three pairs of parallel faces cut normal to the [100], [010] and [001] axes, and the other had three pairs of parallel faces cut normal to the [110], [1$\bar{1}$0] and [101] axes, respectively. These surface orientations were determined with respect to the cleavage planes (001) and (100), and each parallel face was ground and polished.

Two 163°- and 36°- rotated y-cut $LiNbO_3$ transducers with fundamental frequencies of 40 and 18 MHz were used as thickness shear and longitudinal mode transducers, respectively. The transducers were bonded to the surfaces of the specimens by phenyle salicylate to generate ultasonic acoustic waves in the crystal. A dc electric pulse with 0.05 μsec width was applied to the transducer. The excited ultrasonic pulse traveled back and forth between the ends of the specimen and created a slowly

Table 5-III Elastic elements.

$$\begin{bmatrix} C_{11} & C_{12} & C_{13} & 0 & 0 & 0 \\ C_{12} & C_{22} & C_{23} & 0 & 0 & 0 \\ C_{13} & C_{23} & C_{33} & 0 & 0 & 0 \\ 0 & 0 & 0 & C_{44} & 0 & 0 \\ 0 & 0 & 0 & 0 & C_{55} & 0 \\ 0 & 0 & 0 & 0 & 0 & C_{66} \end{bmatrix}$$

Table 5-IV Velocity-moduli relations for orthorhombic symmetry.

Mode [a]	Direction of particle motion	Formula for elastic moduli [b]
	Propagation along X-axis	
L	X	$c_{11} = \rho V'^2$
S	Y	$c_{66} = \rho V'^2$
S	Z	$c_{55} = \rho V'^2$
	Propagation along Y-axis	
L	Y	$c_{22} = \rho V'^2$
S	X	$c_{66} = \rho V'^2$
S	Z	$c_{44} = \rho V'^2$
	Propagation along Z-axis	
L	Z	$c_{33} = \rho V'^2$
S	X	$c_{55} = \rho V'^2$
S	Y	$c_{44} = \rho V'^2$
		Propagation along X' for rotations around Z-axis
QL	$\perp Z$	$c_{12} = [(c^2 c_{11} + s^2 c_{66} - \rho V^2)(c^2 c_{66} + s^2 c_{22} - \rho V'^2)/c^2 s^2]^{1/2} - c_{66}$
QS	$\perp Z$	(*Ibid.* above)
S	Z	$\rho V'^2 = c^2 c_{55} + s^2 c_{44}$
		Propagation along Y' for rotations around X-axis
QL	$\perp X$	$c_{23} = [(c^2 c_{22} + s^2 c_{44} - \rho V'^2)(c^2 c_{44} + s^2 c_{33} - \rho V'^2)/c^2 s^2]^{1/2} - c_{44}$
QS	$\perp X$	(*Ibid.* above)
S	X	$\rho V'^2 = c^2 c_{66} + s^2 c_{55}$
		Propagation along Z' for rotations around Y-axis
QL	$\perp Y$	$c_{13} = [(s^2 c_{11} + c^2 c_{55} - \rho V'^2)(s^2 c_{55} + c^2 c_{33} - \rho V'^2)/c^2 s^2]^{1/2} - c_{55}$
QS	$\perp Y$	(*Ibid.* above)
S	Y	$\rho V^2 = s^2 c_{66} + c^2 c_{44}$

[a] L = longitudinal, S = shear, QL = quasi-longitudinal, QS = quasi-shear.
[b] s = sine and c = cosine of respective rotation angle, ρ = density, V = velocity of propagation of respective mode.

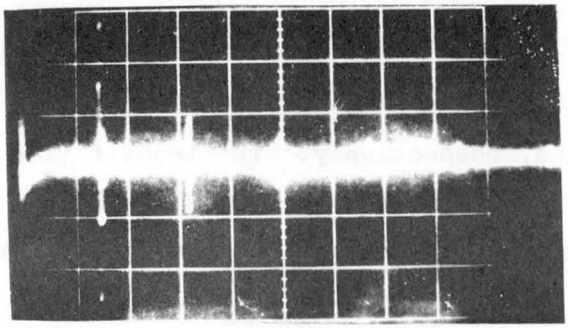

Fig. 5.14 Pulse echo train.
x: 2μs/div.

Table 5-V Ultrasonic velocities in KBN.

Direction	Mode	Velocity(m/s)
[100]	S[001]	3417
	S[010]	3477
	L	5542
[010]	S[001]	3425
	S[100]	3481
	L	5553
[001]	S[010]	3459
	S[100]	3455
	L	5345
[110]	S[001]	3207
	S[1$\bar{1}$0]	3477
	QL	5671
[101]	S[$\bar{1}$01]	3434
	S[010]	3418
	QL	5430

S: shear, L: longitudinal, Q: quasi.

Table 5-VI Elastic constants of KBN.

C_{11} = 1.61	x 10^{11} N/m^2
C_{12} = -0.371 ± 4.8%	
C_{13} = -0.387 ± 0.6%	
C_{22} = 1.62	
C_{33} = 1.50	
C_{44} = 0.621 ± 1.0%	
C_{55} = 0.619 ± 1.1%	
C_{66} = 0.634 ± 0.1%	

decaying echo train as shown in Fig. 5.14. The ultrasonic pass length was 9, 12, 6 and 6 mm in the [100], [010], [001] and [110] directions, respectively. The transit time for the ultrasonic wave propagated in the specimens was longer than 2 μsec, and accuracy of the measured velocity was much better than 3 %. The velocities measured for various propagation directions at room temperature are given in Table 5-V. As is evident from the table, each velocity for the one longitudinal and two shear waves propagating along the [100] direction in KBN is in agreement within the experimental erros with that for the waves propagating along the [010] direction. Furthermore, the velocities for the shear waves propagating along the [001] direction with the displacement parallel to the [100] and [010] axes, respectively, are almost the same. These results suggest that although the KBN belongs to the orthorhombic system, it has a tetragonal like (pseudo-tetragonal) character in elastic properties.

All the elastic constants calculated from the data presented in the Table 5-V are shown in Table 5-VI. From the present ultrasonic propagation measurements, it is found that the velocities of KBN are somewhat smaller than those of $LiNbO_3$ [12]. This result is also expected from the fact that KBN containes the heavy metal such as Bi.

5.2.8 Acousto-Optic Properties

The experimental results described in the previous section suggest that KBN is suitable material for the acousto-optic application because its ultrasonic velocities are smaller than those of oxide ferroelectric materials such as $LiNbO_3$ and $LiTaO_3$.

Table 5-VII Elasto-optic constants in the orthorhombic system.

$$\begin{bmatrix} p_{11} & p_{12} & p_{13} & 0 & 0 & 0 \\ p_{21} & p_{22} & p_{23} & 0 & 0 & 0 \\ p_{31} & p_{32} & p_{33} & 0 & 0 & 0 \\ 0 & 0 & 0 & p_{44} & 0 & 0 \\ 0 & 0 & 0 & 0 & p_{55} & 0 \\ 0 & 0 & 0 & 0 & 0 & p_{66} \end{bmatrix}$$

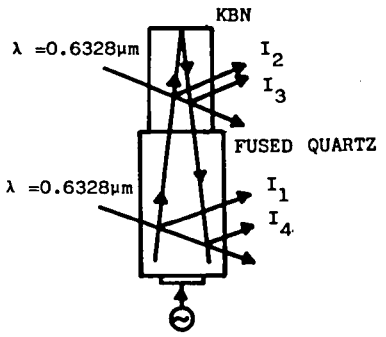

Fig. 5.15 Dixon-Cohen method.

In this section, partial photo-elastic constants and figures of merit of KBN are determined by the Dixon-Cohen method [8].

Since KBN is orthorhombic, it has 12 independet elasto-optic constants as shown in Table 5-VII. After surface orientations of an as-grown KBN crystal were determined with respect to the observation of the X-ray back Laue pattern, the sample was mechanically cut with a diamond cutter, and ground, and then polished to be optically flat. The parallelepiped size of the sample was x × y × z = 6.91 × 8.97 × 9.50 mm. Figure 5.15 shows the schematic illustration of the Dixon-Cohen method [8] employed in the present measurements. A fused quartz buffer rod was used as a standard reference material. A 36°-rotated y-cut $LiNbO_3$ transducer with fundamental frequency of 39 MHz was bonded to the buffer rod to generate the longitudinal wave. The acoustic contact between the KBN sample and the fused quartz was achieved by phenyle salicylate. A coherent light source was 632.8 nm He-Ne laser for both the fused quartz and the KBN. According to the Raman-Nath theory [13], when the ratio of the first-order diffracted light intensity to that of zeroth-order in the absence of the acoustic field, I_1/I_0, is much less than unity, the first-order diffracted light intensity I_1, can be approximated as

$$I_1 = I_0 (\pi^2/2\lambda_0^2) (L/H) MP_A , \qquad (5\text{-}1)$$

where λ_0 is the wavelength of the incident light in vacuum, L and H are the width and height of the acoustic beam, and M is the figure of merit of the material. Therefore, the first-order diffracted intensity I_1 is proportional to the acoustic power P_A, and hence, to the input electrical power applied to the transducer. For the geometry shown in Fig. 5.15 under such conditions, we have equation (5-2) as below, for the figures of

merit M and M^R

$$M/M^R = (I_2 \cdot I_3/I_1 \cdot I_4)^{1/2}, \qquad (5\text{-}2)$$

$$\text{and} \quad M = n^6 p^2/\rho v^3, \qquad (5\text{-}3)$$

where M^R is the figure of merit of the reference material and n is the refractive index, p is the photoelastic constant, ρ is the density, and v is the acoustic velocity. As shown in Fig. 5.15, I_2 and I_3 are the relative first-order diffracted light intensities for the KBN due to the acoustic pulse outgoing from the transducer and to the pulse reflected from the free end of the KBN, respectively. Similarly, I_1 and I_4 are the relative first-order diffracted intensities for the fused quartz due to the outgoing pulse and due to the reflected pulse, respectively. The value of $(I_2 \cdot I_3/I_1 \cdot I_4)^{1/2}$ dose not depend on the quality of the bond at the interface between the KBN and the fused quartz, nor on the acoustic loss in the materials provided only that the acoustic transmission through the bond is reciprocal. Consequently, the figure of merit M for the KBN is determined from the measurements of I_1, I_2, I_3 and I_4 with the standard value for M^R (= 1.56×10^{-18} sec^3/g). Representative examples of relations between relative intensity of the first-order diffracted light and input electrical power measured by the Dixon-Cohen method are shown in Fig. 5.16. The linear dependence of I_1, I_2, I_3 and I_4 on the input electrical power applied to the transducer assures the validity of the application of equation (5-2). The calculation employing a method of least squares gives $M/M^R = 1.04$ in the case shown in Fig. 5.16 (a). The photoelastic tensor elements relating to this diffraction geometry are p_{31} for the KBN and p_{12} for the fused quartz. In what

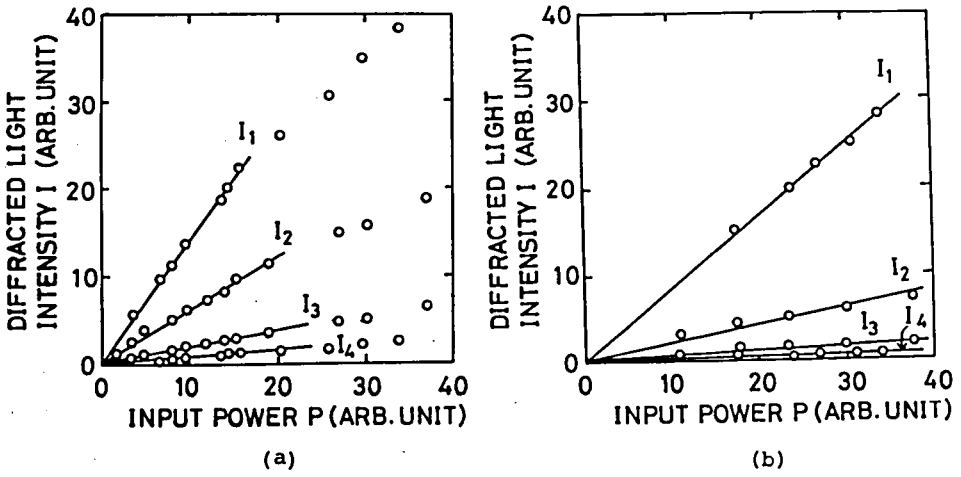

Fig. 5.16 Relations between relative intensity of the first-order diffracted light and electrical input power applied to the transducer.
Longitudinal acoustic waves propagate along the [100] axis and the incident 632.8 nm light is transmitted in the [010] direction with polarization parallel to the [001] axis (a), and along the [001] axis and the incident light is transmitted in the [010] direction with the polarization parallel to the [100] axis (b).

follows, the notation M_{ij} is adopted as the relevant figure of merit corresponding to the photo-elastic element p_{ij}. Accordingly, the figure of merit M_{31} is determined as 1.62×10^{-18} sec^3/g. Similarly, M_{13} was obtained as 1.06×10^{-18} sec^3/g from Fig. 5.16 (b).

Figures of merit M_{11}, M_{13}, M_{31} and M_{33} are given in Table 5-VIII. Four of the 12 independent photo-elastic tensor elements were calculated from the figure of merit M_{ij} determined above. The next figure of merit,

$$M' = n^7 p^2 / \rho v \quad , \tag{5-4}$$

was introduced by Gordon [14, 15] for the specific device applications, where the diffraction bandwidth and the diffraction efficiency are important performance parameters. The last figure of merit,

$$M'' = n^7 p^2 / \rho v^2 \quad , \tag{5-5}$$

was defined by Dixon [16] for the case where the acoustic beam height is as small as the optical beam diameter. These figure of merit M' and M'' are also listed in Table 5-VIII. Photoelastic constants are shown in Table 5-IX compared with those of $LiNbO_3$ and $LiTaO_3$.[17,18]. As is evident from Table 5-IX, the photo-elastic constants p_{11} and p_{33} of KBN are greater than those of $LiNbO_3$ and $LiTaO_3$.

Table 5-VIII Acousto-optic properties of KBN.

Acoustic wave		Optical wave at 632.8 nm.				Figure of merit		
Polarization and propagation direction	Velocity v(10^5cm/sec)	Incident direction	Polarization direction	Refractive index n[a)]	p	M	M'	M''
Long. in[100]	5.54	[010]	[100]	2.227	$\lvert p_{11}\rvert$	6.46	4.41	7.96
Long in[001]	5.35	[010]	[100]	2.227	$\lvert p_{13}\rvert$	1.06	9.79	18.3
Long. in[100]	5.54	[010]	[001]	2.264	$\lvert p_{31}\rvert$	1.62	1.14	2.06
Long. in[001]	5.35	[010]	[001]	2.264	$\lvert p_{33}\rvert$	6.41	4.14	7.74

M in 10^{-18} sec^3/g, M' in 10^{-6} cm^{2}sec/g, M'' in 10^{-12} cmsec^2/g.
a): Ref. [7].

Table 5-IX Photo-elastic constants of KBN, $LiNbO_3$ and $LiTaO_3$.

Sample	p_{11}	p_{12}	p_{13}	p_{14}	p_{21}	p_{22}	p_{23}	p_{31}	p_{32}	p_{33}	p_{44}	p_{55}	p_{66}
K B N	$\lvert 0.217\rvert$		$\lvert 0.084\rvert$					$\lvert 0.104\rvert$		$\lvert 0.195\rvert$			
$LiNbO_3$[a)]	-0.026	0.090	0.133	-0.075	$=p_{12}$	$=p_{11}$	$=p_{13}$	0.179	$=p_{31}$	0.071	0.146	$=p_{44}$	-0.058
$LiTaO_3$[b)]	-0.081	0.081	0.093	-0.026	$=p_{12}$	$=p_{11}$	$=p_{13}$	0.089	$=p_{31}$	-0.044	0.028	$=p_{44}$	-0.081

a): see Ref. [17], b): Ref. [18].

5.3 DISCUSSION

In this section the crystal system and ferroelectricity in KBN are discussed based on the results obtained in the previous section. Ismailzade [4] found that the crystal structure of KBN ceramics is very similar to that of ferroelectric (orthorhombic) phase of $PbTa_2O_6$, and the lattice constants of KBN are a = 17.75, b = 17.90 and c = 7.84 Å. This $PbTa_2O_6$ is a ferroelectric material with Curie temperature of 260 °C and has the orthorhombic tungsten-bronze structure, though its A-sites are only 5/6-filled [19]. From the expectation of the identity of the structures of KBN and $PbTa_2O_6$ determined by X-ray powder diffraction measurements, Ismailzade pointed out that KBN is possibly a ferroelectrics with the orthorhombic tungsten-bronze structure. On the other hand, Sugai et al. [6] have reported that KBN has tetragonal tungsten-bronze structure with a = b = 17.85 and c = 7.84 Å. In the present study, it is clear from the preceding section that KBN is ferroelectric and that it has the orthorhombic structure with a = 17.878, b = 17.888 and c = 7.853 Å. The value of the spontaneous deformation b/a is, however, nearly equal to 1 and is much smaller than that reported by Ismailzade [4].

Jamieson et al. [20,21] proposed, based on the detailed structure analysis, a ferroelectric mechanism in the tungsten-bronze materials such as $Ba_xSr_{1-x}Nb_2O_6$ and $Ba_2NaNb_5O_{15}$. According to their proposal, all metal atoms are displaced from their nearest mean planes of oxygen atoms in the ferroelectric state and move into oxygen layers at the Curie temperature. These displacement of the metal atoms from their nearest mean planes of oxygen atoms are directly related to the ferroelectric polarization. The ferroelectric mechanism may also be applicable

to KBN because KBN shows the isostructure with $Ba_2NaNb_5O_{15}$. In general, many orthorhombic tungsten-bronze niobates have the polar axis perpendicular to the [001] axis, when the axial ratio R (see Chapt. 4) is less than about 0.997 [22]. However, in the present KBN, the [001] polar axis is retained as shown in the preceding section 5.2.3, even R calculated from the values of the lattice constants is 0.982. This fact means that the displacement of metal atoms along the c axis is the origin of ferroelectricity in KBN.

5.4 SUMMARY

Since the vapor pressure of K_2O and Bi_2O_3 is high at the melting point of KBN (1310 ^{o}C), the starting composition with excess K_2O and Bi_2O_3 was mainly used, which was necessary to obtain large crystal of good optical quality. Large pale-yellow transparent single-crystals of KBN up to about 35 mm in diameter and 40 mm in length were easily obtained by the Czochralski method.

X-ray, dielectric, chemical etching, conoscopic and thermal expansion measurements were carried out in order to assess fundamental properties of KBN. From the experimental results, it is concluded that KBN is a ferroelectric materials with the polar axis parallel to the [001] axis and that it has the orthorhombic tungsten-bronze structure with a = 17.878, b = 17.888 and c = 7.853 $\mathring{A}$.

However, further study would be needed for better understanding of the ferroelectricity in this material, because no hysteresis loop was observed.

Furthermore, all the elastic constants and four of the

twelve independent photo-elastic constants of KBN were determined for applications to acousto-optic devices.

References

[1] A. Ashkin, G. D. Boyd, J. M. Dziedzie, R. G. Smith, A. A. Ballman, H. J. Levinstein, and K. Nassau: Appl. Phys. Letters 9 (1966) 72.

[2] L. G. Van Uitert, H. J. Levistein, J. J. Rubin, C. D. Capio, E. F. Deaborn and W. A. Bonner: Mater. Res. Bull. 3 (1968) 47.

[3] J. E. Geusic, H. J. Levinstein, J. J. Rubin, S. Singh and L. G. Van Uitert: Appl. Phys. Letters 11 (1967) 269.

[4] I. G. Ismailzade: Soviet Physics-Crystallography 8 (1963) 274.

[5] N. N. Krainik, V. A. Isupov, M. F. Bryzhina and A. I. Agranovskaya: Soviet Physics-Crystallogrphy 9 (1964) 281.

[6] T. Sugai and M. Wada: Jpn. J. Appl. Phys. 11 (1972) 1863.

[7] T. Sugai and M. Wada: Annual Report of Study Group on Applied Ferroelectrics in Japan, 21A (1972) 57 [in Japan.]

[8] R. W. Dixon and M. G. Cohen: Appl. Phys. Letters 8 (1966) 205.

[9] K. Aizu: J. Phys. Soc. Japan 27 (1969) 387.

[10] A. Kumada: Jpn. J. Appl. Phys. 39 (1970) 258.

[11] H. J. Mcskimin: *Physical Acoustics*, edited by W. P. Mason (Academic Press, New York and London, 1964) Vol. 1, Part A, p. 271.

[12] R. T. Smith and F. S. Welsh: J. Appl. Phys. 42 (1971) 2219.

[13] C. V. Raman and N. S. N. Nath: Proc. Indian Acad. Soc. 2A

(1935) 406; 2A (1935) 413; 3A (1936) 75; 3A (1936) 119; and 4A (1937) 222.

[14] E. I. Gordon: Proc. IEEE 54 (1966) 1391.

[15] E. I. Gordon: IEEE J. Quantum Electron. QE-2 (1966) 104.

[16] R. W. Dixon: J. Appl. Phys. 38 (1967) 5149.

[17] L. P. Avakyants, D. F. Kiselev and N. N. Schchitov: Soviet-Physics-Solid State [English Transl.] 18 (1976) 899.

[18] L. P. Avakyants, D. F. Kiselev and N. N. Schchitov: Soviet-Physics- Solid State [English Transl.] 18 (1976) 1242.

[19] E. C. Subbarao, G. Shirane, and F. Jona: Acta Cryst. 13 (1960) 226.

[20] P. B. Jamieson, S. C. Abrahams and J. L. Bernstein: J. Chem. Phys. 48 (1968) 5048.

[21] P. B. Jamieson, S. C. Abrahams and J. L. Bernstein: J. Chem. Phys. 50 (1969) 4352.

[22] E. A. Giess, B. A. Scott, G. Burns, D. F. O'Kane and A. Segmueller: J. Am. Ceram. Soc. 52 (1969) 276.

CHAPTER 6 EPITAXIAL GROWTH OF KLN SINGLE-CRYSTAL FILMS ON KBN SINGLE CRYSTALS BY THE EGM TECHNIQUE

6.1 INTRODUCTION

In recent studies on integrated optics, ferroelectric single-crystal thin films have attracted considerable interest in their applications to active optical IC devices, e.g., waveguide light modulators, light deflectors, second harmonic generators, and directional couplers; and several fabrication techniques have been investigated for growing single-crystal thin films of ferroelectric materials. For instance, $LiNbO_3$ single-crystal thin film has been fabricated by epitaxial growth by melting (EGM) [1], liquid phase epitaxial growth (LPE) [2], capillary liquid epitaxial growth (CLE) [3] and rf sputtering methods [4]. Potassium lithium niobate (KLN) crystal is one of the most interesting materials for various applications because of its excellent electro-optic, nonlinear optic and piezoelectric properties [5,6]. Accordingly, KLN single-crystal thin films would be excellent active media for integrated optics. The typical crystallographic properties and refractive indices of KLN at room temperature are shown compared with those of KBN (see Chapt. 5) in Table 6-I.

A single-crystal thin film of KLN also be grown on a KBN substrate by the same techniques as described above, because the crystal structures of KLN and KBN are the same tungsten-bronze type structure, and because the melting point of KBN is higher by about 250 ^{o}C than that of KLN, as shown in Table 6-I.

Table 6-I Crystallographic properties and refractive indices of KLN and KBN at room temperature.

	KLN	KBN[7] ($K_{1.5}Bi_{1.0}Nb_{5.1}O_{15}$)
Symmetry	Tetragonal[6]	Orthorhombic (pseudo-tetragonal)
Lattice constant	$a=12.58$ Å[6] $c=4.01$ Å[6]	$a\sim b=17.85$ Å $c=7.84$ Å
Melting temperature	1050°C[6]	1312°C
Refractive index	$n_o=2.294$[8] $n_e=2.156$[8] (632.8 nm)	$n_o=2.237$ $n_e=2.253$ (450.0 nm)

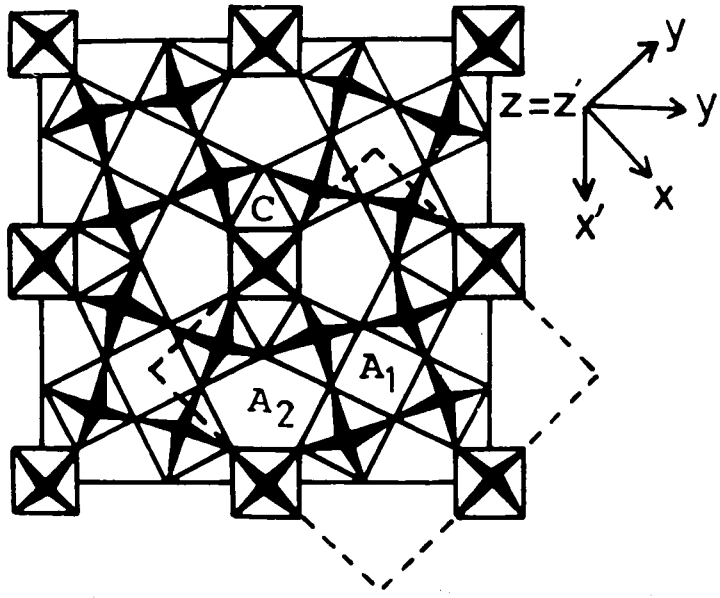

Fig. 6.1 Tungsten-bronze structure and reference axes. The (001) projection of KBN lattice is shown in relation to the KLN cell shown by dashed square.

The lattice mismatch between the KLN film and the KBN substrate is about 0.32 % and 2.3 % at room temperature for the a and c axes in the KLN coordinate system, as shown in Fig. 6.1, because the KBN crystal is orthorhombic , as opposed to the KLN crystal, which is tetragonal. Thus, a KBN crystal is a useful substrate for growing a single-crystal KLN film epitaxially. Furthermore, it is expected that a single-crystal thin film of KLN grown on a KBN substrate will act as an optical waveguide, and it can be also used as an optical waveguide modulator by coupled wave interaction between the guided and radiation modes [9].

In this chapter, we describe the epitxial growth of KLN single-crystal films on KBN substrates by the EGM technique.

6.2 EXPERIMENTAL PROCEDURE

Single-crystals of KBN were grown by an rf heating Czochralski method. As mentioned in Chapt. 5, optimum growth conditions were a 4 mm/h pulling rate and a 40 rpm rotation rate. The pulling axis was chosen to be parallel to the [001] axis. It was found very easy to obtain large crystals under the above conditions. (001) or (100) KBN substrates were cut from as-grown crystals, and their top surfaces were lapped and optically polished. On the other hand, reagent grade carbonates of lithium and potassium, and 99.9 % pure niobium pentaoxide were used as starting materials for the fabrication of KLN single-crystal film. A material with composition 35 mole % K_2CO_3, 17.3 mole % Li_2CO_3, and 47.7 mole % Nb_2O_5 was mixed well with acetone in a ball mill, dried, pressed into a disk, and calcined at 800 ^{o}C for three hours. The calcined material of KLN was then ground thoroughly. This powder of KLN was uniformly laid on the

polished surface of the KBN substrate with a sprayer. The substrate, with the powder on its top surface, was heated to about 1120 °C in a resistance furnace in order to melt the KLN crushed powder alone, and was then cooled slowly at a rate of 10 °C/h through the melting point (1050 °C) of KLN. In this way, the KLN film crystallized epitaxially onto the KBN substrate.

6.3 EXPERIMENTAL RESULTS AND DISCUSSION

Figures 6.2 (a) and (b) show microphotographs of a surface and a cleaved cross-section of the specimens, respectively. The top surface of the as-grown film was relatively rough, and the KLN film obtained was about 15 μm thick. Figure 6.3 shows X-ray diffraction patterns of KLN films grown epitaxially on the (001) and (100) KBN substrates. In the X-ray diffraction patterns, the peaks corresponding to diffractions from the KLN films and KBN substrates are clearly separated. Further, the value obtained for the standard deviation angle σ of the X-ray rocking curve, assuming a Gaussian distribution to good approximation, is small at 0.2°. The lattice constants a and c of the KLN film obtained by the X-ray diffraction measurement are 12.53 and 3.98 Å, respectively. These values agree well with those of the KLN single crystal, as shown in Table 6-I. The electron diffraction patterns for both KLN films calculated and epitaxially grown on KBN substrates are shown in Figs. 6.4 and 6.5, where the clear spots in Fig. 6.5 and also the Kikuchi pattern in Fig. 6.5 (a) indicate that the films are of a single-crystal of considerably good quality. These results show that a single-crystal film of (001) KLN is epitaxially grown on an

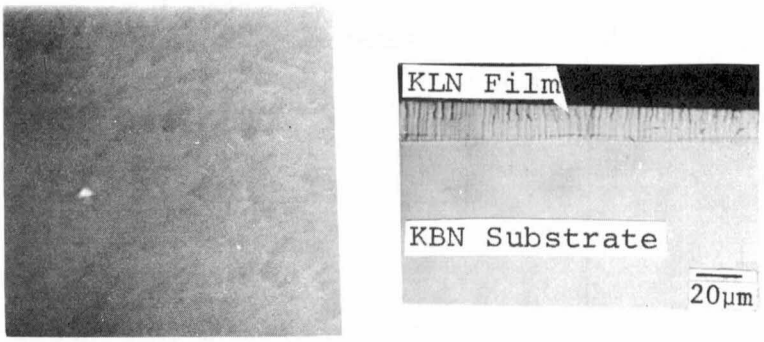

Fig. 6.2 The microphotographs of the surface (a) and cleaved cross section of an (001) KBN substrate with an epitaxially grown KLN film.

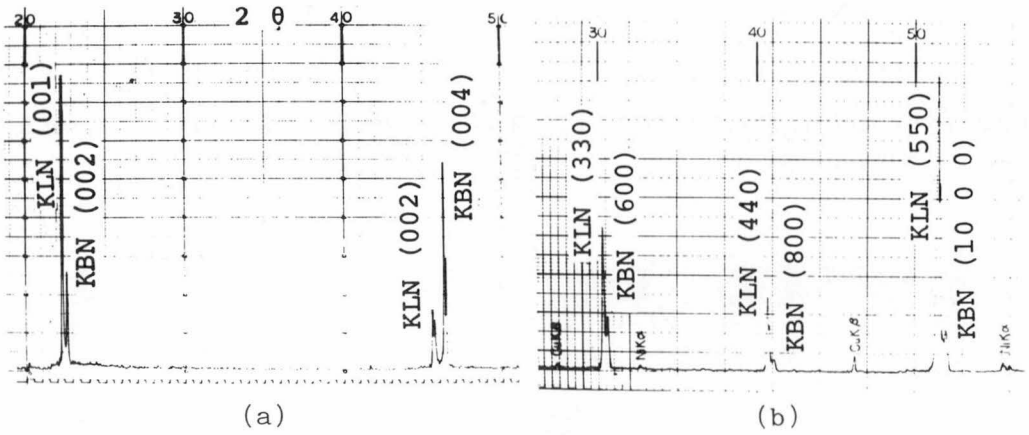

Fig. 6.3 X-ray diffraction patterns of KLN films grown epitaxially on an (001) KBN substrate (a), and a (100) KBN substrate (b).

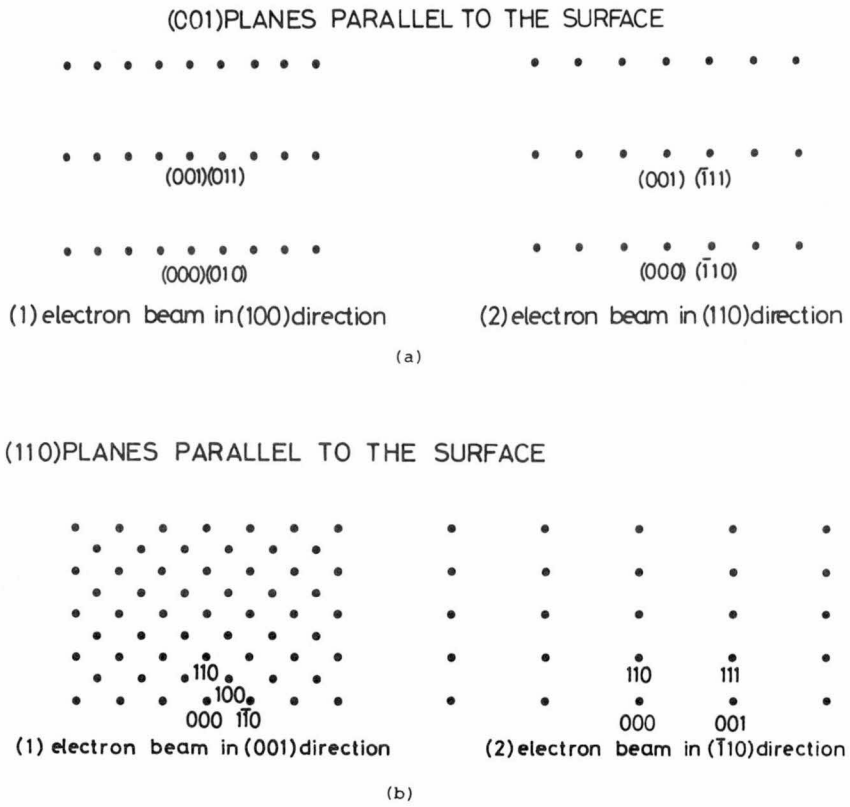

Fig. 6.4 RED patterns calculated by using the values of lattice constants of KLN.

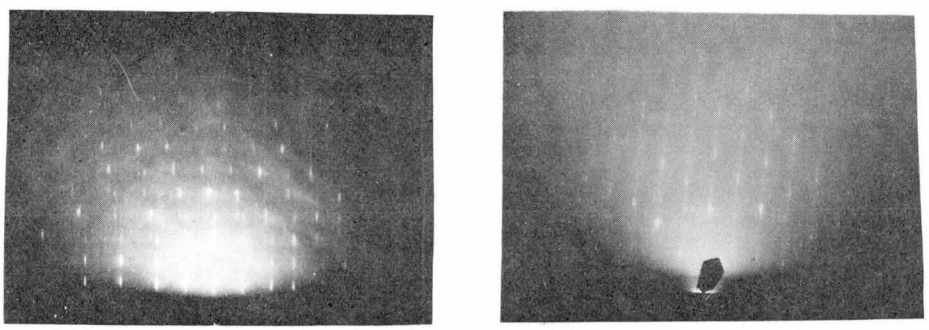

(a) (b)

Fig. 6.5 Reflection electron diffraction patterns of KLN thin films grown epitaxially on an (001) KBN substrate (a), and on a (100) KBN substrate (b).

(001) KBN substrate, and also that of (110) KLN is epitaxially grown on a (100) KBN substrate by the EGM method.

6.4 SUMMARY

KLN single-crystal films have been successfully grown with good epitaxy on KBN substrates by the "epitaxial growth by melting" (EGM) technique. The analyses on these KLN films by X-ray, reflection electron diffraction (RED) and scanning electron microscopy (SEM) methods indicated that a single-crystal film of (001) KLN is epitaxially grown on an (001) KBN substrate, and also that of (110) KLN is grown on a (100) KBN substrate. The KLN films obtained are single-crystals of high quality and also are transparent. However, the top surface of the as-grown film is relatively rough. Therefore, optical polishing would be needed for fabricating low loss optical waveguides.

References

[1] S. Miyazawa: Appl. Phys. Letters 23 (1973) 198.

[2] S. Kondo, S. Miyazawa, S. Fushimi and K. Sugii: Appl. Phys. Letters 26 (1975) 489.

[3] T. Fukuda and H. Hirano: Appl. Phys. Letters 28 (1976) 675.

[4] S. Takada, M. Ohnishi, H. Hayakawa and N. Mikoshiba: Appl. Phys. Letters 24 (1974) 490.

[5] L. G. Van Uitert, S. Singh, H. J. Levinstein, J. E. Geusic and W. A. Bonner: Appl. Phys. Letters 11 (1967) 161.

[6] M. Adachi and A. Kawabata: Jpn. J. Appl. Phys. 17 (1978) 1969.

[7] T. Sugai and M. Wada: Jpn. J. Appl. Phys. 11 (1972) 1863.

[8] A. W. Smith, G. Burns and B. A. Scott: J. Appl. Phys. 42 (1971) 684.

[9] N. Fudanuki, M. Nakajima and J. Ikenoue: The 10th Technical Meeting on Special Project Research"Optical Guided-Wave Electronics", of the Ministry of Educations, Science and Culture, Japan (1978) [in Japanese].

CHAPTER 7 EPITAXIAL GROWTH OF KLN SINGLE-CRYSTAL FILMS ON KBN SINGLE CRYSTALS BY RF SPUTTERING

7.1 INTRODUCTION

Since the proposal of general concept of integrated optics by Miller [1] in 1969, and the success in feeding a laser beam into ZnO and ZnS films by Tien [2] in the same year, many theoretical and experimental results on dielectric thin film waveguides have been reported and, particularly, $LiNbO_3$ ferroelectric single-crystal thin films [3-8] have attracted special interest in applications to the active and low loss optical waveguides. It is well-known that the KLN crystal is one of the most promising materials for electro-optic and nonlinear-optic applications because of its high stability to intense laser radiations (optical damage), and its large linear and nonlinear optical coefficients [9,10]. A half-wave voltage relating to the electro-optic coefficient r_c is determined to be about 1040 V (see Chapt. 4), which is about 1/3 times that of $LiNbO_3$[11] and the value of nonlinear coefficient d_{31} of KLN is equal to that of $LiNbO_3$[10]. The values of principal refractive indices n_o and n_e of the KLN crystal are 2.277 and 2.264 at 632.8 nm, respectively [12]. Those of KBN are 2.227 and 2.264 at 600.0 nm, respectively.[13]. Thus, it is expected that a single-crystal film of KLN grown on a KBN substrate will act as a dielectric optical waveguide, and it will be used as an optical waveguide modulator.

In this chapter, we describe the epitaxial growth of KLN single-crystal films on KBN substrates by an rf sputtering

Table 7-I Crystallographic and optical properties.

Material	K L N	K B N [d]	α-Al_2O_3	$LiNbO_3$ [e]	$LiTaO_3$ [e]
Lattice const. (Å)	a =12.58 [a] c =4.01 [a]	a =17.85 c =7.84	a_H=4.758 c_H=12.991	a_H=5.1483 c_H=13.863	a_H=5.1543 c_H=13.784
Melting temperature	1050°C [a]	1312°C	2050°C	1250°C	1670°C
Dielectric const.	ε_{11}^T=306 [a] ε_{33}^T=115 [a]	ε_{11}^T=430 ε_{33}^T=500	ε_{11}=9.34 ε_{33}=11.6	ε_{11}^S=43 ε_{33}^S=28	ε_{11}^S=41 ε_{33}^S=43
Refractive index	n_o=2.277 [b] n_e=2.163 [b]	n_o=2.227 n_e=2.264	n_o=1.766 n_e=1.758	n_o=2.289 n_e=2.201	n_o=2.176 n_e=2.180
Electro-optic coefficient r_{ij} ($\times 10^{-12}$ m/V)	r_{33}^T=79 [b] r_{13}^T= 9 [b] r_{15}^T=80 [c]			r_{13}^S=8.6 r_{22}^S=3.4 r_{33}^S=30.8 r_{52}^S=28	r_{13}^S=7.9 r_{22}^S=1 r_{33}^S=30.3 r_{52}^S=20
Nonlinear optic coefficient $\|d_{ij}\|$ ($\times 10^{-12}$m/V)	d_{31}=10.0 [b] d_{33}=18.1 [b]			d_{22}=4.0 d_{31}=7.5 d_{33}=52	d_{22}=2.6 d_{31}=1.6 d_{33}=25

a: see Ref. [14], b: Ref. [10], c: calculated from the phenomenological theory in Ref. [15] by using the value of P_S given in Ref. [16], d: Ref. [13], and e: Ref. [17].

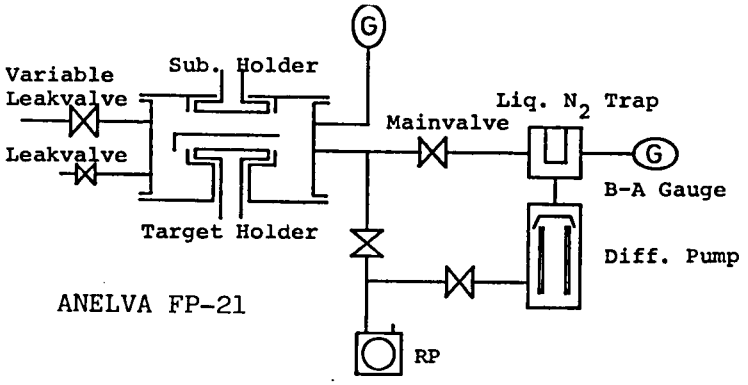

Fig. 7.1 Schematic diagram of the rf sputtering equipment.

technique for the purpose of fabricating optical waveguides.

7.2 EXPERIMENTAL PROCEDURE

7.2.1 Sample Preparation

The typical crystallographic and optical properties of KLN and KBN crystals compared with those of some other ferroelectric materials are shown in Table 7-I. As can be seen from this table, KLN crystals are optically negative and KBN positive. The electro-optic coefficient of KLN are significantly larger than those of $LiNbO_3$ and $LiTaO_3$, indicating the potential usefulness of this material in an optical waveguide modulator with waveguiding structure consisting of a KLN film on a KBN substrate or in the reverse.

In the present study, an rf diode sputtering equipment (ANELVA FP-21) was used to fabricate the KLN films as shown in Fig.7.1. This sputtering equipment is composed of a pumping system, an rf power supply and a substrate-heating system. The substrate holder was positioned above and parallel to the target, with a spacing variable from 3 to 8 cm. The pumping system has a 300 ℓ/s oil diffusion pump and gives a pressure of about 1×10^{-6} Torr within one hour. The substrate is held with metal clamps on the substrate holder and is heated by the heating system. Its temperature is controllable from 200 to 700 ^{o}C. The substrate temperature is measured with a thermocouple placed near the substrate. Three targets (a), (b) and (c) with different compositions used in our experiment were prepared by sintering pressed powder with potassium and lithium enriched composition of target (a): 33 mole % K_2CO_3, 22 mole %

Table 7-II Sputtering condition.

Input power	70-250 W
Substrate temperature	300-650 °C
Sputtering gas	Ar + O_2 (1:1)
Gas pressure	(0.8-1)x10^{-1} Torr
Target size	85 mmϕ x6mmt
Target-substrate distance	3-4cm
Deposition rate	800 Å/h.
Target composition	K_2CO_3: 33 mole%
	Li_2CO_3:22 mole%
	Nb_2O_5: 45 mole%

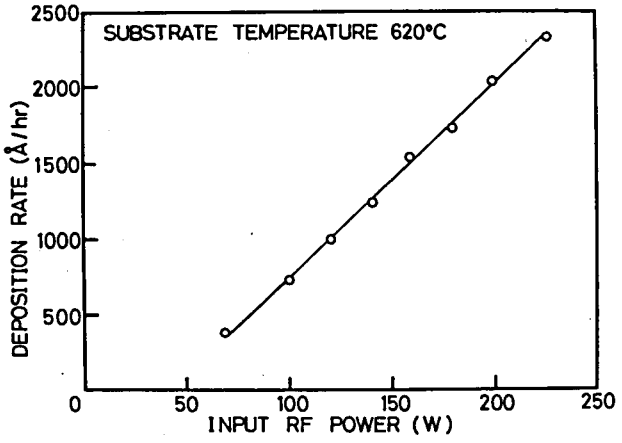

Fig. 7.2 Deposition rate versus rf input power.

Li_2CO_3 and 45 mole % Nb_2O_5; with potassium enriched composition of target (b): 35 mole % K_2CO_3, 17.3 mole % Li_2CO_3 and 47.7 mole % Nb_2O_5; and with stoichiometric composition of target (c): 30 mole % K_2CO_3, 20 mole % Li_2CO_3 and 50 mole % Nb_2O_5.

Single crystals of KBN were also used as the substrates by the same reasons as described in Chapt. 6. A substrate of (001) or (100) KBN was cut from as-grown crystals and their top surfaces were lapped and optically polished. Typical growth conditions of the KLN film by sputtering are shown in Table 7-II. The deposition rate under these conditions is about 2000 Å/h at an rf power of 200 W. The relation between the sputtering deposition rate and rf input power, when fused quartz was used as the substrate, is shown in Fig. 7.2, where the film-thickness was determined by measuring the coupling angles of a TiO_2 prism. The deposition rate did not depend on the substrate temperature from 300 to 700 °C.

7.2.2 Measuring Technique

The qualities of KLN films grown this way were evaluated from X-ray diffraction patterns and rocking curves obtained by a diffractometer using the Ni-filtered CuK_α radiation. Furthermore, RED patterns and SEM observations were also used in the evaluation. The dielectric constant was measured at 100 KHz with a YHP type 4332A LCR meter. The refractive index n_o and the film thickness of KLN films were determined by measuring coupling angles at which the light beam was fed into the KLN film through the prism coupler.

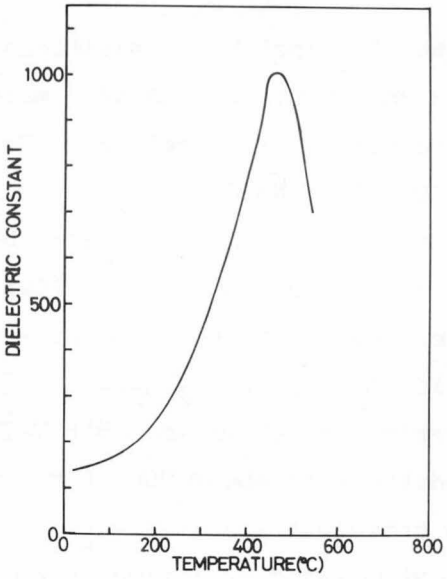

Fig. 7.3 Temperature dependence of dielectric constant of KLN film.

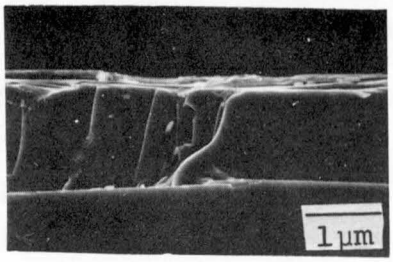

Fig. 7.5 An SEM photograph of the cleaved cross section.

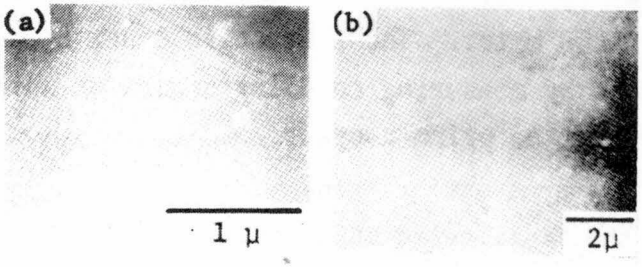

Fig. 7.4 SEM photographs of the surfaces of KLN films deposited on an (001) KBN substrate (a), and on a (100) KBN substrate (b).

7.3 EXPERIMENTAL RESULTS

7.3.1 Dielectric Properties of KLN Films

The KLN films obtained were transparent and their surfaces were smooth. The Curie temperatures, when Pt plates were used as substrates, were 460, 630 and 600 ^{o}C for targets (a), (b) and (c), respectively. As described in section 7.2, the composition of KLN films deposited using targets (b) and (c) were probably out side the tungsten-bronze region. Therefore target (a) was mainly used. The temperature dependence of the dielectric constant of an (001) axis oriented KLN film on a Pt substrate is shown in Fig. 7.3. The constant showed a marked anomaly at the transition point of 460 ^{o}C and its value at room temperature was 140.

7.3.2 Evaluation of KLN Films by SEM

Figure 7.4 shows the SEM photographs of the surfaces of the KLN films deposited on the (001) and (100) KBN substrates. Both film surfaces were clear and smooth as shown in Fig. 7.4. The SEM photograph of the cleaved cross-section of the (001) KBN substrate with an epitaxially grown KLN film is also shown in Fig. 7.5. The film-thickness was determined to be about 1.5 μm.

7.3.3 Evaluation of KLN Films by X-ray Diffraction and RED

Figure 7.6 shows X-ray diffraction patterns and rocking curves for KLN films on the (001) and (100) KBN substrates at

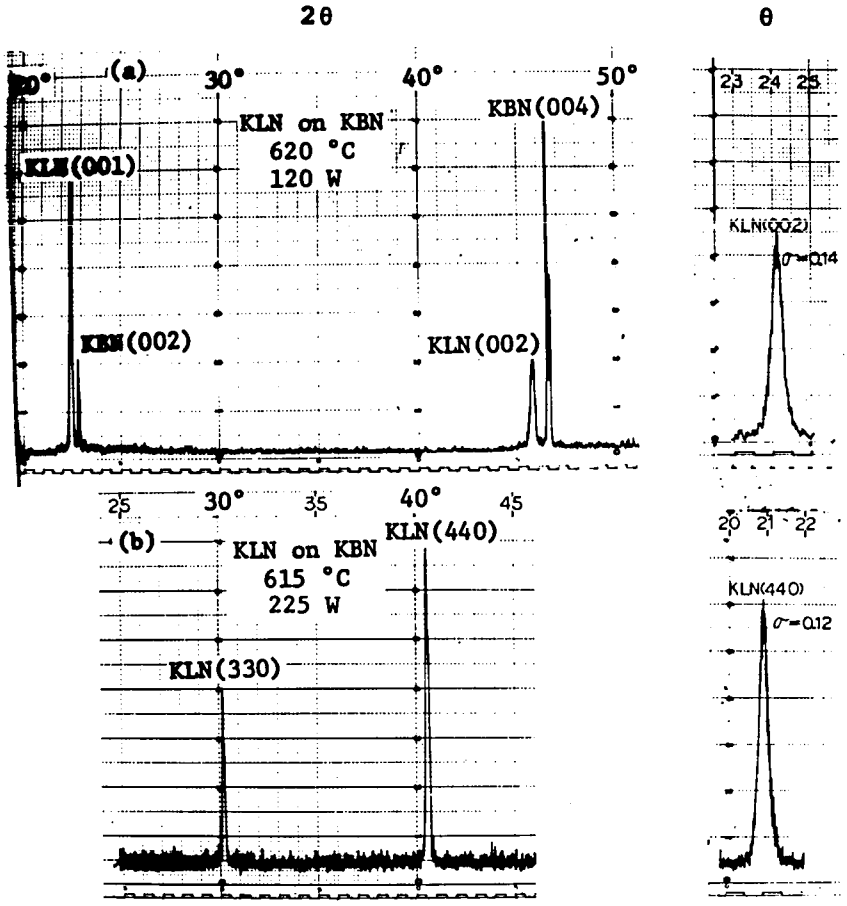

Fig. 7.6 X-ray diffraction patterns and their rocking curves of KLN thin films grown epitaxially on an (001) KBN substrate (a), and on a (100) KBN substrate (b).

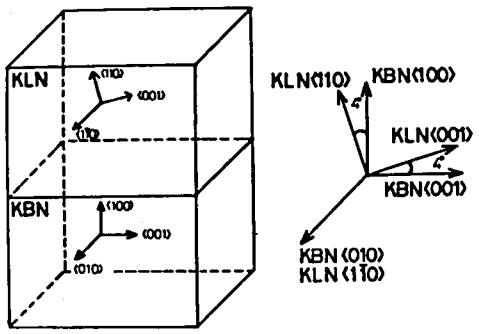

Fig. 7.7 Orientations between a (110) KLN film and a (100) KBN substrate.

a substrate temperature of about 620 °C. In the Fig. 7.6 (a), it is found that the peaks correponding to the diffractions from the KLN film and the KBN substrate are clearly separated. Furthermore, the value of the standard deviation angle σ of the rocking curve, which is derived from the assumption of Gaussian distribution of the curve, is a very small angle of 0.14°. On the other hand, in Fig. 7.6 (b), the peaks are not separated and the peaks from the KLN films are only observed. The value of σ for the (440) diffractions from the KLN film is also as small as 0.12° . The X-ray rocking measurement in Fig. 7.6 (b) suggests that the surface-normal axes of the (110) KLN film and the (100) KBN substrate differ from each other by 4° as shown in Fig. 7.7. The lattice constants a and c of the KLN film obtained by the X-ray diffraction measurements are 12.7 and 3.96 Å, respectively. These values are in fairly good agreement with those of the bulk KLN, shown in Table 7-I.

The diagrams of KLN film quality evaluated from the standard deviation angle σ of the X-ray rocking curves are shown in Fig. 7.8. The value σ for a high quality region of (001) and (110) KLN single-crystal films is defined as less than 0.2°. Evaluation of film quality in terms of this value σ is simple and also consistent with the RED measurement. As can be seen from Figs. 7.8 (a) and (b), optimum growth conditions for the high quality single-crystal thin films of KLN on the (001) and (100) KBN substrates are substrate temperatures of 570 to 630 °C and of 580 to 630 °C and rf input power below 150 W and below 250 W, respectively.

The RED patterns for KLN films epitaxially grown on KBN substrates are shown in Figs. 7.9 and 7.10. Appearance of the clear spots and Kikuchi patterns indicate that the films are of single crystal of considerably good quality.

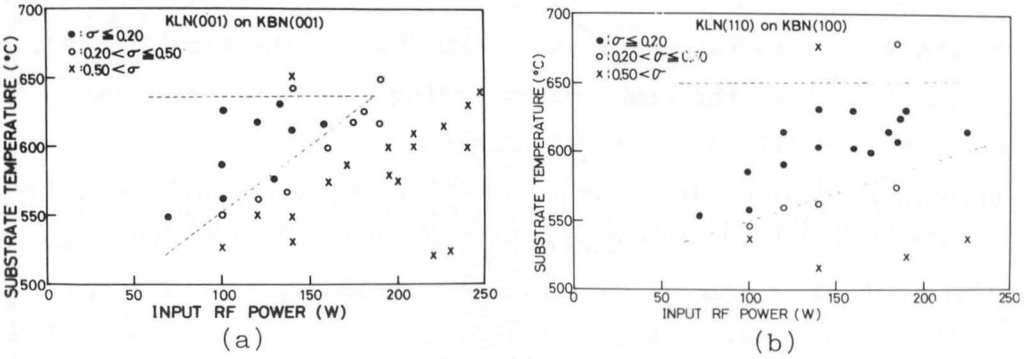

Fig. 7.8 Diagrams of the KLN film quality deposited on (001) KBN substrates (a), and on (100) KBN substrates (b), which have been evaluated from the standard deviation angle σ of the X-ray rocking curves.

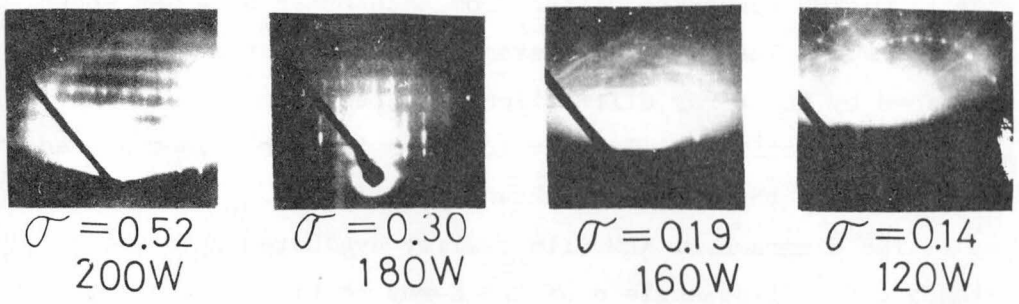

Fig. 7 9 Reflection electron diffraction patterns of KLN films sputtered on (001) KBN substrates.

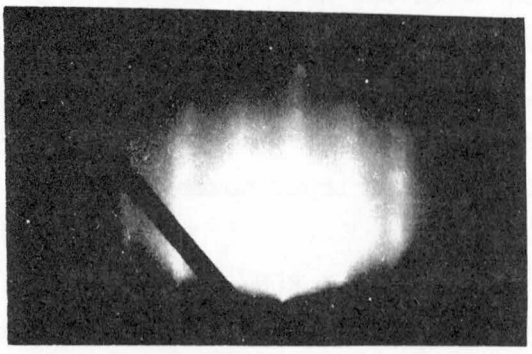

Fig. 7.10 RED patterns of KLN film sputtered on a (100) KBN substrate.

7.3.4 Optical Properties of KLN Films

Figure 7.11 shows the relation between the effective refractive index and film thickness for several optical waveguide modes calculated by using the values of indices in a bulk KLN as shown in Table 7-I. In the present study, the light beam was successfully fed through the prism coupler into the 2.1 μm thick KLN film deposited on the (001) KBN substrate by the sputtering. By measuring synchronous angles to the prism face, optical wavegude mode indices β/k, were determined as 2.26, 2.25, and 2.23 for TE_0, TE_1 and TE_2,respectively, as shown with circles in Fig. 7.11. The refractive index n_o in this KLN film was calculated as 2.27 from the mode indices as described above. This value is somewhat smaller than that of bulk KLN crystal as shown in Table 7-I. Measurements of propagation optical loss in this film were not attempted. However, it is expected that propagation losses of KLN film on KBN substrate can be made less than that of the KLN film on sapphire [18] by using a smoother KBN substrate.

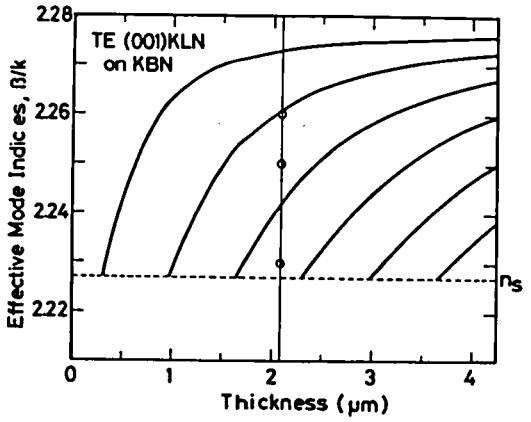

Fig. 7.11 The relation between the effective refractive indices and film thickness.

7.4 SUMMARY

Analyses with X-ray diffractometer, SEM and RED of the KLN films deposited on KBN substrates by the rf sputtering technique showed that the KLN films obtained were single crystals of considerably good quality. Further, a single-crystal film of KLN was epitaxially grown on a KBN substrate by the rf sputtering method. The light beam was successfully fed into the KLN film deposited on the (001)KBN substrate. More detailed measurements on the light propagation properties in these epitaxial thin films will be needed in the future for the optical IC devices.

References

[1] S. E. Miller: Bell Syst. tech. J. 48 (1969) 2059.

[2] P. K. Tien, R. Ulrich and R. J. Martin: Appl. Phys. Letters 14 (1969) 291.

[3] S. Miyazawa: Appl. Phys. Letters 23 (1973) 198.

[4] A. A. Ballman, H. Brown, P. K. Tien and R. J. Martin: J. Crysy. Growth 20 (1973) 251.

[5] S. Miyazawa, S. Fushimi and S. Kondo: Appl. Phys. Letters 26 (1975) 8.

[6] A. Baudrant, H. Vial and J. Daval: J. Cryst. Growth 43 (1978) 197.

[7] T. Fukuda and H. Hirano: Appl. Phys. Letters 28 (1976) 575.

[8] S. Takada, M. Ohnishi, H, Hayakawa and N. Mikoshiba: Appl. Phys. Letters 24 (1974) 490.

[9] L. G. Van Uitert, J. J. Rubin and W. A. Bonner: IEEE Trans. Quantum Electron. QE-4 (1968) 622.

[10] L. G. Van Uitert, S. Singh, H. J. Levinstein, J. E. Geusic and W. A. Bonner: Appl. Phys. Letters 11 (1967) 161.

[11] E. G. Spencer, P. V. Lenzo and A. A. Ballman: Proc. IEEE 55 (1967) 2074.

[12] A. W. Smith, G. Burns and B. A. Scott: J. Appl. Phys. 42 (1971) 684.

[13] T. Sugai and M. Wada: Jpn. J. Appl. Phys. 11 (1972) 1863.

[14] M. Adachi and A. Kawabata: Jpn. J. Appl. Phys. 17 (1978) 1969.

[15] M. DiDominico, Jr., and S. H. Wemple: J. Appl. Phys. 40 (1969) 720.

[16] S. H. Wemple, M. DiDominico, Jr. and I. Camlibel: Appl. Phys. Letters 12 (1968) 209.

[17] T. Mitsui et al.: *Landolt-Börnstein,,Numerical Data and Functional Relationships in Science and Technology, New Series Group III, Crystal and Solid State Physics, Vol. 16, Ferroelectrics and Related substances*, Berlin, Heidelberg, New York, Springer 1981.

[18] M. Adachi, M. Hori, T. Shiosaki and A. Kawabata: Jpn. J. Appl. Phys. 18 (1979) 1637.

CHAPTER 8 GROWTH OF POTASSIUM LITHIUM NIOBATE FILMS ON SAPPHIRE BY RF SPUTTERING

8.1 INTRODUCTION

Recently, considerable attention has been centered on the development of active and low-loss thin film optical waveguides. Several attempts have been made to grow single-crystal films which realize such waveguide, using ferroelectric materials such as $LiNbO_3$ [1-4], PLZT [5], $Sr_2Nb_2O_7$ [6] and KLN [7,8]. The top surfaces of as-grown $LiNbO_3$ films fabricated by liquid phase epitaxial growth, chemical vapor deposition, melting metod and so on, are relatively rough, so that they must be optically polished in order to feed the light beam into those films. On the other hand, the polishing process is not necessary to the sputtered thin film, and the light beam can be easily fed into the film. Therefore, an rf sputtering technique is used to fabricate the KLN thin-film grown on a sapphire substrate. The respective values of the principal refractive indices n_o and n_e are 2.277 and 2.163 at 632.8 nm, respectively [9]. The corresponding values for sapphire, used as the substrates, are 1.766 and 1.758, respectively [10].

In this chapter, growth of KLN film on sapphire substrates by an rf sputtering method is described. Further, the optical propagation loss in the KLN film is also described.

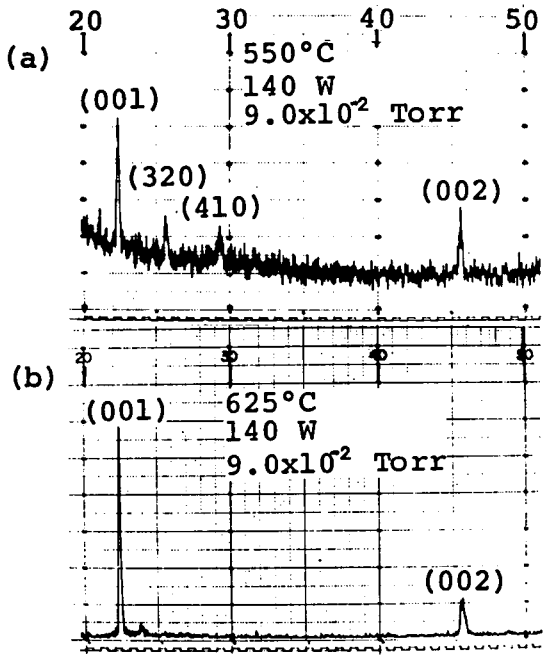

Fig. 8.1 X-ray diffraction patterns for KLN films sputtered on $(01\bar{1}2)$ sapphire substrates. 550 °C (a) and 625 °C (b) substrate temperature.

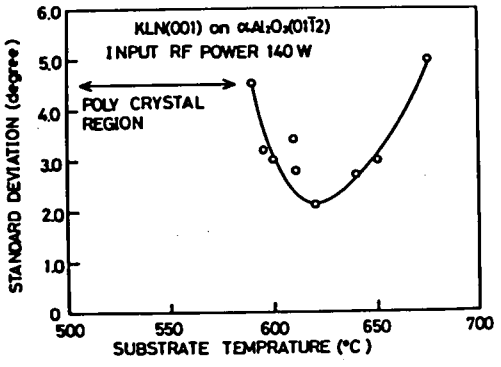

Fig. 8.2 The substrate temperature dependence of the standard deviation angle σ in KLN films.

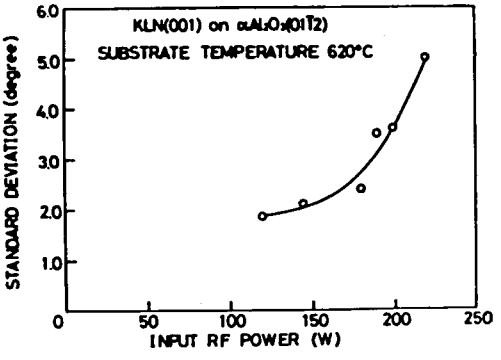

Fig. 8.3 Input rf power versus the standard deviation angle σ in KLN films.

8.2 EXPERIMENTAL PROCEDURE

An rf diode sputtering equipment (ANELVA FP-21) was used to fabricate the KLN film. The target used in the present experiment was prepared by sintering a compressed powder with a potassium- and lithium-enriched composition of 33 mole % K_2CO_3, 22 mole % Li_2CO_3, and 45 mole % Nb_2O_5. (0001) and $(01\bar{1}2)$ sapphire plates were used as substrates. The optimum growth conditions for KLN films deposited on sapphire substrates were Ar (50 %) + O_2(50 %) atmosphere, 9.0×10^{-2} Torr, about 140 W rf power, and 600 to 650 °C substrate temperature. The deposition rate under these conditions was about 1400 Å/h.

8.3 EXPERIMENTAL RESULTS AND DISCUSSION

8.3.1 Evaluation of KLN Films from X-ray Diffraction Patterns

Figure 8.1 shows typical X-ray diffraction patterns for KLN thin films sputtered on $(01\bar{1}2)$ sapphire substrates at substrate temperatures of 550 and 625 °C. KLN polycrystalline thin films were obtained at substrate temperatures below 580 °C, as shown in Fig. 8.1 (a), but (001)-oriented films were obtained above 600 °C, as shown in Fig. 8.1 (b). Optimum growth conditions evaluated from the standard deviation angle σ of the X-ray rocking curves for the thin films of KLN on the $(01\bar{1}2)$ sapphire substrates were substrate temperatures of 600 to 650 °C and rf input power below 150 W, as shown in Figs. 8.2 and 8.3, respectively. On the other hand, (001)-oriented KLN films sputtered on (0001) sapphire substrates were obtained at film-thicknesses greater than 10 μm under the above conditions as

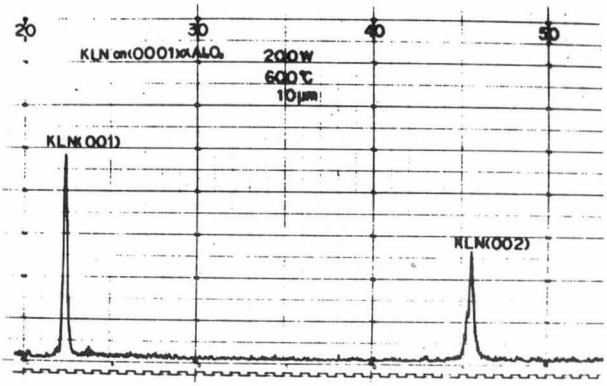

Fig. 8.4 An X-ray diffraction pattern of a KLN film sputtered on an (0001) sapphire substrate.

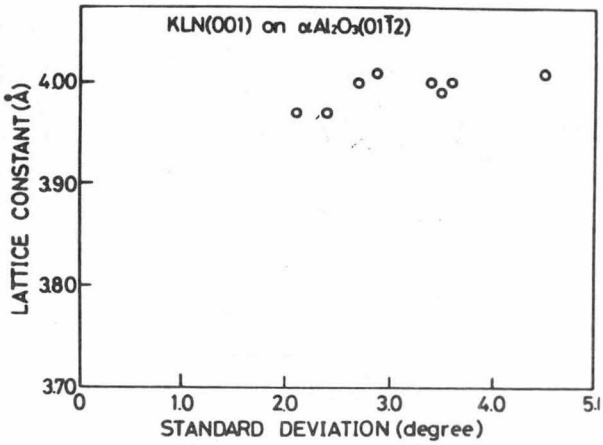

Fig. 8.5 The lattice constant of KLN films evaluated from the standard deviation angle σ .

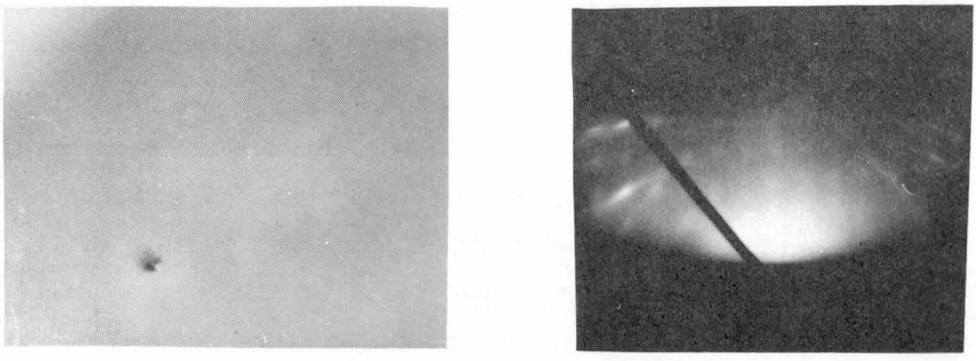

(a) (b)

Fig. 8.6 SEM photograph (a) and RED pattern (b) in the (001) KLN film on the (01$\bar{1}$2) sapphire substrate.

shown in Fig. 8.4. The lattice constant c in the KLN films was 3.97 Å for both $(01\bar{1}2)$ and (0001) sapphire substrates in average as shown in Fig. 8.5. This value agrees fairly well with that of the KLN single crystal [11].

8.3.2 Evaluation of KLN Films by SEM and RED

The (001)-oriented KLN films on sapphire substrates were examined by SEM and RED. Figure 8.6 (a) is an SEM photograph for an (001) KLN film surface on an $(01\bar{1}2)$ sapphire substrate. An RED pattern for an (001) KLN film on an $(01\bar{1}2)$ sapphire substrate is shown in Fig. 8.6 (b), where clear diffraction spots and Kikuchi lines are observed, indicating that the film is of single crystal with considerably good quality. The (001) KLN films sputtered on $(01\bar{1}2)$ sapphire substrates were transparent, and their surfaces were smooth. These X-ray and electron diffraction results showed that an (001) KLN single-crystal film is grown epitaxially on an $(01\bar{1}2)$ sapphire substrate by the rf sputtering method. On the other hand, the (001) KLN films sputtered on (0001) sapphire substrates were seen to be polycrystalline from the RED measurement and their surfaces were relatively rough as shown in Fig. 8.7, because the surface-normal axes of the (001) KLN and the (0001) sapphire possess 4-fold (tetragonal) and 3-fold (trigonal) properties, respectively.

8.3.3 Optical Properties of KLN Films

A 632.8 nm He-Ne laser beam was successfully fed into

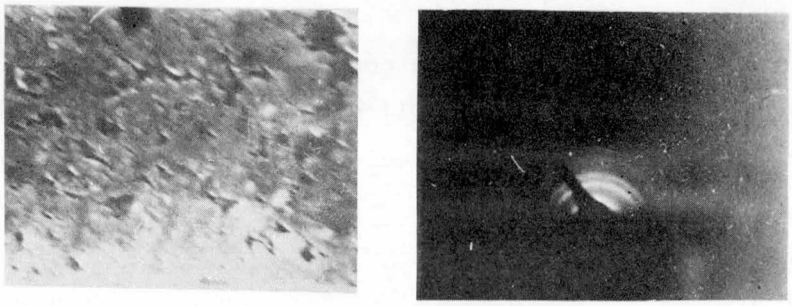

(a) (b)

Fig. 8.7 SEM photograph (a) and RED pattern (b) in the (001) oriented KLN film on the (0001) sapphire substrate.

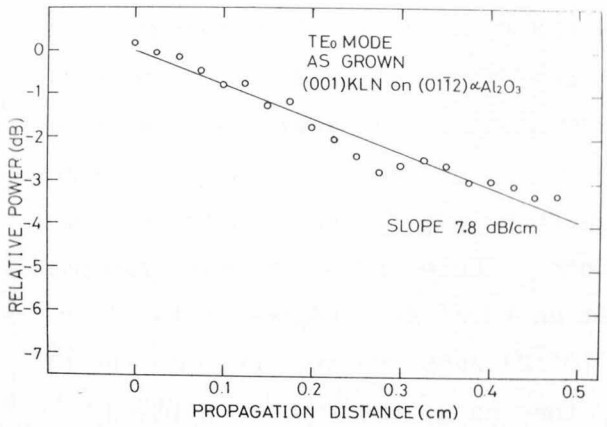

Fig. 8.8 Scattered-light intensity versus propagation distance for a KLN film on an (01$\bar{1}$2) sapphire substrate.

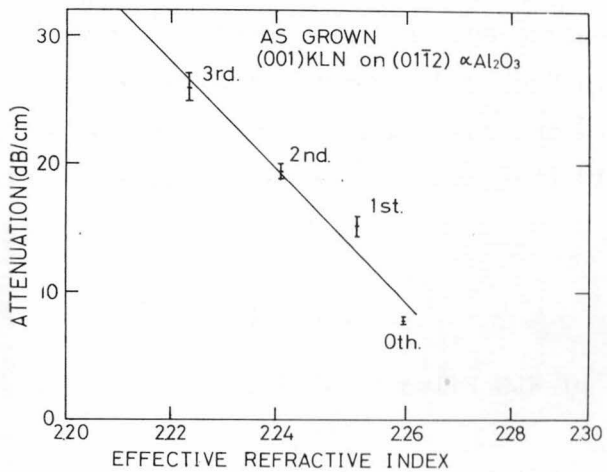

Fig. 8.9 Attenuation versus effective refractive index for a KLN film on an (01$\bar{1}$2) sapphire substrate.

the KLN films deposited on the $(01\bar{1}2)$ sapphire substrates by sputtering, using a prism coupler and without polishing the surface. The optical loss was measured using the scattered light, which is collected by a 0.13-mm-diametr optical-glass fiber and is probed by placing the end of the fiber about 0.025 mm away from the waveguide and scanning it across the streak of guided light perpendicular to the propagation direction. Figure 8.8 shows the TE_0 optical attenuation in a KLN film about 2.7 μm thick. The value, 7.8 dB/cm, is less than those of $LiNbO_3$ films grown by the rf-sputtering [4] or LPE method [2,12]. Figure 8.9 shows optical attenuation which was measured for several different modes. The refractive index n_o in this KLN film was determined as 2.27 by measuring the coupling angles for 11 TE modes. This value is close to that of the bulk KLN crystal.

8.4 SUMMARY

The X-ray and electron diffraction results showed that an (001) KLN single-crystal film is epitaxially grown on an $(01\bar{1}2)$ sapphire substrate at substrate temperatures above 600 °C by rf sputtering, and also that the KLN film obtained is single-crystal with considerably good quality. Further, the optical propagation losses in the KLN film were less than those of $LiNbO_3$ films grown by rf sputtering or LPE methods, though they were one order magnitude higher than those of $LiNbO_3$ films grown by the EGM method. Therefore, the KLN film is a promising material for optical IC devices.

References

[1] S. Miyazawa: Appl. Phys. Letters 23 (1973) 198.

[2] S. Kondo, S. Miyazawa, S. Fushimi and K. Sugii: Appl. Phys. Letters 26 (1975) 489.

[3] T. Fukuda and H. Hirano: Appl. Phys. Letters 28 (1976) 575.

[4] S. Takada, M. Ohnishi, H. Hayakawa and N. Mikoshiba: Appl. Phys. Letters 24 (1974) 490.

[5] Y. Higuma, K. Tanaka, T. Nakagawa, T. Kariya and Y. Hamakawa: Jpn. J. Appl.Phys. 16 (1977) 1707.

[6] A. Ishitani and M. Kimura: Appl. Phys. Letters 29 (1976) 289.

[7] M. Adachi, M. Hori, T. Shiosaki and A Kawabata: Jpn. J. Appl. Phys. 17 (1978) 2053.

[8] M. Adachi, T. Shiosaki and A. Kawabata: Jpn. J. Appl. Phys. 18 (1979) 193.

[9] L. G. Van Uitert, S. Singh, H. J. Levinstein, J. E. Geusic and W. A. Bonner: Appl. Phys. Letters 11 (1967) 161.

[10] M. A. Jeppesen: J. Opt. Soc. Am. 48 (1958) 629.

[11] M. Adachi and A. Kawabata: Jpn. J. Appl. Phys. 17 (1978) 1969.

[12] S. Miyazawa, S. Fushimi and S. Kondo: Appl. Phys. Letters 26 (1975) 8.

CHAPTER 9 $K_3Li_2Nb_5O_{15}$ AND $Pb_2KNb_5O_{15}$ TUNGSTEN-BRONZE FILMS FOR SAW DEVICES

9.1 INTRODUCTION

A ferroelectric crystal may be a useful material for surface acoustic wave (SAW) devices, since it has moderately strong electromechanical coupling. Among various ferroelectric crystals, tungsten-bronze ferroelectrics with a general chemical formula $(A_1)(A_2)_2C_2(B_1)(B_2)_4O_{15}$ (where A = Pb, Ba, Na, K, etc. and B = Nb or Ta) have attracted much attentions for SAW device applications [1-4]. High electromechanical coupling has been observed in ferroelectric phases of a number of tungsten-bronze oxides. For example, electromechanical coupling factors in $K_3Li_2Nb_5O_{15}$ crystal are k_{15} = 0.34, k_{31} = 0.18, k_t = 0.53 and k_{33} = 0.52 [5], and also those in $Pb_2KNb_5O_{15}$ (PKN) are k_{15} = 0.69 and k_{24} = 0.73 [6]. Furthermore, both ferroelectrics have zero temperature coefficients of delay (ZTCD) cut for SAW's [1,7]. Therefore, these materials are found to be very attractive for high piezoelectric coupling, temperature compensated SAW devices.

However, it has been very difficult to obtain high-quality and large-size single crystals of these materials [5,8]. An approach for the solution of this serious problem is to grow epitaxial films of these crystals. A single-crystal film of KLN can be grown on a $K_2BiNb_5O_{15}$ substrate by epitaxial growth of melting (EGM) and/or sputtering method as described in the previous Chapts. 6 and 7.

In this chapter, SAW characteristics of a layered-structure consisting of KLN or PKN film on an appropriate substrate are

Table 9-I Material constants of KLN, PKN, KBN and Al_2O_3.

		KLN	PKN	KBN	Al_2O_3 [11]
Symmetry		Tetragonal	Orthorhombic	Orthorhombic	Trigonal
Lattice constants (Å)		a=12.58 c= 4.01	a=17.84 b=18.05 c=3.917	a=17.85 c= 7.84	a_H=4.758 c_H=12.991
Melting temperature (°C)		1050	1300	1313	2050
Density ($\times 10^3 kg/m^3$)		4.26	6.14	5.24	3.986
Dielectric constants					
	$\varepsilon_{11}^S/\varepsilon_0$	271	810	430	9.34
	$\varepsilon_{22}/\varepsilon_0$	271	680	430	9.34
	$\varepsilon_{33}/\varepsilon_0$	83	81	500	11.6
Stiffness coefficient ($\times 10^{11}/m^2$)	C_{11}^E	2.20	1.66	1.61	4.97
	C_{12}	0.74	0.37	-0.371	1.64
	C_{13}	0.59	0.45	-0.387	1.11
	C_{22}	2.20	1.61	1.62	4.97
	C_{23}	0.59	0.41	-0.387	1.11
	C_{33}	1.09	1.24	1.50	4.98
	C_{44}	0.68	0.31	0.621	1.47
	C_{55}	0.68	0.30	0.619	1.47
	C_{66}	0.70	0.63	0.634	1.665
Piezoelectric coefficient (c/m^2)	e_{15}	4.6	14	——	
	e_{24}	4.6	15	——	
	e_{31}	-0.6	0.4	——	0
	e_{32}	-0.6	1.4	——	
	e_{33}	5.5	6.9	——	

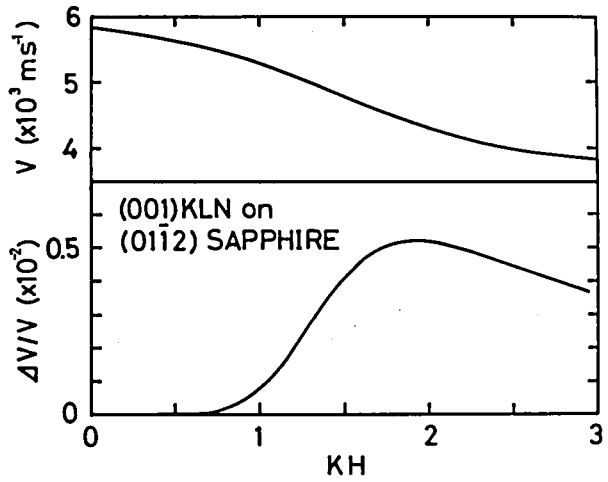

Fig. 9.1 The phase-velocity and electro-mechanical coupling factor of SAW's on an (001) KLN / (01$\bar{1}$2) sapphire combination propagating along the [100] direction on a KLN film.

calculated. In addition, preliminary experimental results on SAW properties of the layered structure of the KLN film deposited on a sapphire substrate is also described.

9.2 CALCULATION OF SAW CHARACTERISTICS

In order to investigate the SAW properties of the layered structures of (KLN film)/(substrate) and (PKN film)/(substrate), a similar theoretical method to that proposed by Farnell and Adler [9] was used, on conjunction with the experimental data listed in Table 9-I, to calculate the SAW velocity, electromechanical power flow angle (PFA) and electromechanical coupling factor ($\Delta v/v = k^2/2$).

Although, four different arrangements of the interdigital transducer (IDT) and the short electrode can be considered in the case of the layered structure, an arrangement where the IDT's are formed on the surface of the layer without the short electrode, has been considered in this chapter, because only this arrangement can easily be realized by sputtering method.

In this section, the SAW characteristics are calculated for the layered structures in the following (film)/(substrate) combinations, i.e., (1) ((001) KLN film)/((01$\bar{1}$2) sapphire), (2) ((001) PKN)/((001) KBN), (3) ((001) PKN)/((001) KLN) and (4) ((001) PKN)/((01$\bar{1}$2) sapphire).

Figure 9.1 shows the relationship of the theoretical results on the phase velocity v and the electromechanical coupling factor $\Delta v/v$ versus the quantity KH, where K is the wavenumber and H is the film thickness. In Fig. 9.1, the SAW propagates along the [100] direction on the KLN thin layer. As KH increases, the v decreases monotonically from 5830 to

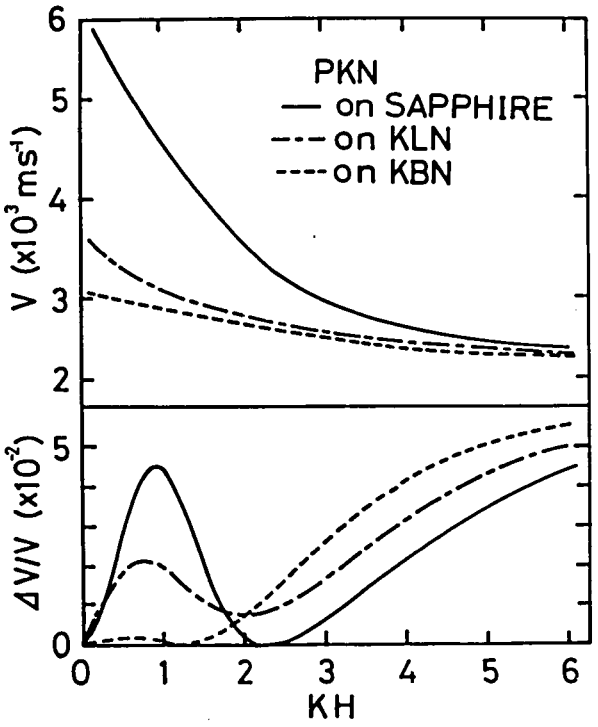

Fig. 9.2 The phase-velocities and electro-mechanical coupling factors of SAW's on (PKN)/(substrate) layered structures. The SAW propagates along the [010] direction on PKN films.

3670 m/s, which corresponds to the values of the Rayleigh wave velocity on the sapphire substrate and on the semi-infinite bulk of KLN, respectively. The $\Delta v/v$ shows a broad peak at KH = 1.9 and the maximum attainable value for the $\Delta v/v$ is 0.0052. The value obtained here is 10 times larger than that of ST cut quartz.

Figure 9.2 shows the calculated results for the v and the $\Delta v/v$ versus KH for the (001) PKN films on the $(01\bar{1}2)$ sapphire, (001) KLN and (001) KBN substrates, where the SAW propagates along the [010] direction on the PKN film. From this calculation for the (PKN)/(substrate) structures, the following features are obtained.

i) Each curve for the v decreases monotonically from the value of the Rayleigh wave velocity on each substrate to that of the semi-infinite bulk of PKN, i.e., 2340 m/s.

ii) The dispersion for the v is small in the layered struture of (PKN)/(KBN) combination.

iii) For $0 \leq KH \leq 2$, the curves for the $\Delta v/v$ have maximum. The magnitudes of maximum attainable values for the layered structures of (PKN)/(sapphire), (PKN)/(KLN) and (PKN)/(KBN) combinations are 0.045 at KH = 0.9, 0.021 at KH = 0.8, and $0.0\overset{v}{\underset{0}{}}15$ at KH = 0.5, respectively. It is noted that the maximum values of these lst peaks depend on the values of the dielectric constants of the substrates, that is, they increase with decreasing the dielectric constant of the substrate.

iv) For $2 < KH \leq 6$, curves for the $\Delta v/v$ increase with increasing KH.

v) For $6 < KH$, curves for the $\Delta v/v$ and the v are almost close to 0.057 and 2340 m/s respectively, for sufficiently large values of KH.

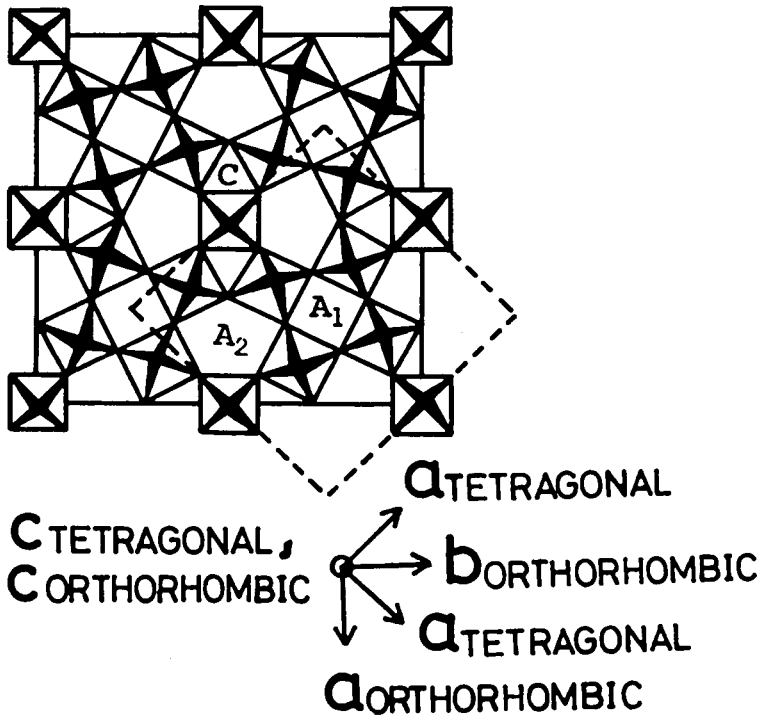

Fig. 9.3 Tungsten-bronze structure and reference axes. The (001) projection of both $Pb_2KNb_5O_{15}$ and $K_2BiNb_5O_{15}$ lattice is shown by dashed square. The dark crosses represent NbO_6 octahedra with Nb ions at their centers in the plane of the paper. The polar axes of KLN and PKN are $c_{tetragonal}$ and $b_{orthorhombic}$ axes, respectively.

It should be noted that the maximum value of the 1st peak for the $\Delta v/v$ in the layered structure of (PKN)/(sapphire) combination is about twice as large as that of Y-cut, Z-prop., $LiNbO_3$, whose maximum value for the $\Delta v/v$ is 0.0246.

9.3 EXPERIMENTAL PROCEDURE

The typical crystallographic properties of KLN, PKN, KBN and sapphire crystals are listed in Table 9-I. KLN, PKN and KBN crystals belong to tungsten-bronze structures. The KLN crystal is a tetragonal ferroelectrics with a point group 4mm [5]. On the other hand, PKN [8] and KBN [10] crystals are both orthorhombic materials with mm2. These tungsten-bronze structures and their reference axes are shown in Fig. 9.3. The lattice mismatches between the KLN film and the KBN substrate, and between the PKN film and the KBN substrate are about 0.33, 0.33 and 2.3 %, and about 0.06, 1.1 and 0.08 %, respectively, for the a, b and c axes in the orthorhombic coordinate system as shown in Fig. 9.3. Among three different ferroelectric materials described above, it has been reported to be very easy to obtain large pale-yellow KBN single crystals up to about 40 mm in diameter [5]. As a result, it would be expected that, by using the KBN as a substrate material, good-quality KLN or PKN epitaxial films can be grown onto KBN substrates. The same rf diode sputtering equipment described in the previous Chapts. 7 and 8, was used to prepare the KLN films in this study. Sapphire plates were used as substrate materials.

9.4 EXPERIMENTAL RESULTS ON SAW CHARACTERISTICS OF THE LAYERED STRUCTURE OF (KLN FILM)/(SAPPHIRE)

The preliminary experiments on SAW properties of the layered structure of (KLN)/(sapphire) were carried out. The sample used in this study was a 9 μm thick KLN film sputtered on an $(01\bar{1}2)$ sapphire substrate at a substrate temperature of 520 °C The IDT's are normal electrodes with 25 finger pairs and a 100 μm spatial period, which were evaporated on the film surface. The center to center propagation path length was 12.5 mm. Accordingly, the value of KH for this sample was 0.6. A synchroscope trace of the SAW output signal excited by the IDT's is shown in Fig. 9.4. Since the delay time of the SAW propagation was 2.3 μs, the SAW velocity on this KLN film was determined to be 5430 m/s, which is in good agreement with the calculated value, 5500 m/s at KH = 0.6, as shown in Fig. 9.1. However, the measurement on the $\Delta v/v$ has not been attempted because the calculated value for the $\Delta v/v$ is of as small as about 8×10^{-6} at KH = 0.6.

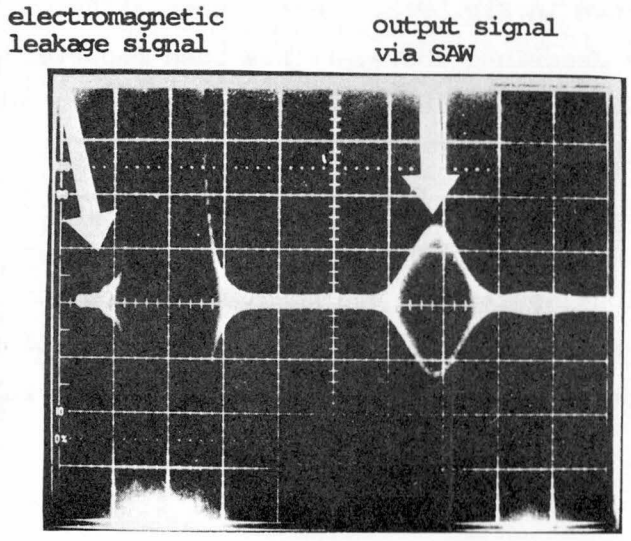

Fig. 9.4 A synchroscope trace of the SAW output signal excited by the IDT's on a KLN film/ sapphire layered structure.
x: 0.5 μs/div.,
y: 2 mV/ div..

9.5 SUMMARY

Characteristics of SAW properties of the layered structures consisting of (KLN film)/(substrate) and (PKN film)/(substrate) combinations have been calculated. For the layered structure of a KLN film formed on a sapphire substrate, the electromechanical coupling factor $\Delta v/v$ showed a broad band with a peak at KH = 1.9 and its maximum attainable value for the $\Delta v/v$ was 0.0052. This value is 10 times larger than that of ST cut quartz. Meanwhile, for the layered structures of (PKN)/(sapphire), (PKN)/(KLN) and (PKN)/(KBN) combinations, each $\Delta v/v$ had maximum at KH = 0.9, 0.8 and 0.6, respectively, whose magnitudes of maximum attainable values were equal to 0.045, 0.021 and 0.015, respectively. The maximum value 0.045 of the 1st peak for the $\Delta v/v$ in the layered structure of (PKN)/(sapphire) is about twice as large as that of Y-cut, Z-prop., $LiNbO_3$. The theoretical results of SAW characteristics on the layered structures of (PKN)/(substrate) are the most superior as a SAW device material.

Although a study on the epitaxial growth of PKN film on various substrates is now in progress, it would be expected that higher-quality epitaxial film of PKN can successfully be grown on KBN substrates compared with KLN films on KBN substrates, because the lattice mismatch between PKN and KBN is much smaller than that between KLN and KBN, as shown in Table 9-I. In addition, the theoretical results of SAW characteristics on (PKN)/(substrate) layered structures , as mentioned in the previous section, showed that PKN is more superior than KLN as a SAW device material. Therefore,the studies on the hetero-epitaxial growth of PKN films onto various substrates are now in progress in order to realize the SAW devices with high coupling.

Therefore, it is concluded that the layered structures of (KLN)/(substrate) and (PKN)/(substrate) combinations are the most suitable for SAW applications.

References

[1] R. M. O'connel: J. Appl. Phys. 49 (1978) 3324.

[2] H. Yamauchi: Appl. Phys. Letters 32 (1978) 599.

[3] W. P. Robbins and S. T. Liu: Ferroelectrics 27 (1980) 157.

[4] R. W. Whatmore: J. Cryst. Growth 48 (1980) 530.

[5] M. Adachi and A. Kawabata: Jpn. J. Appl. Phys. 17 (1978) 1969.

[6] T. Yamada: J. Appl. Phys. 46 (1975) 2894.

[7] K. Yamashita and H. Takeuchi: The 40th Annual Meeting of Japan Soc. Appl. Phys. No. 2a-Q-5 (1979) [in Japan.].

[8] J. Nakano and T. Yamada: J. Appl. Phys. 46 (1975) 2361.

[9] G. W. Farnell and E. L. Adler: *Properties of elastic surface waves in Physical Acoustics*, edited by W. P. Mason and R. N. Thurston (Academic Press, New York, 1970) Vol. 6, p.109.

[10] T. Sugai and M. Wada: Jpn. J. Appl. Phys. 11 (1972) 1863.

[11] A. J. Slobodnik, Jr., E. D. Conway and R. T. Delmonico: USAF Cambridge Research Laboratory Report No. AFCRL-TR-73-0597, (1973).

CHAPTER 10 CONCLUSION

In this thesis, growth and properties of tungsten-bronze crystals and films (mainly $K_3Li_2Nb_5O_{15}$) are studied and discussed in detail from an applicational point of view.
The results and conclusions obtained in this study are summarized as follows.

Chapter 2:

(1) Crystals of KLN have been grown by the Czochralski method from a melt using a KLN or KBN crystal as the seed. The starting composition with excess K_2O and Li_2O has been mainly used, which is necessary to obtain crystals of good quality. Pale-yellow single crystals up to about 8 to 10 mm in diameter and 30 mm in length have been obtained. The composition of the grown-crystals was analyzed chemically to be $K_{2.89}Li_{1.55}Nb_{5.11}O_{15}$.

(2) X-ray, dielectric and chemical etching measurements have been carried out. The lattice constants a and c were determined as 12.58 and 4.01 Å, respectively. The dielectric constants $\varepsilon_{11}^T/\varepsilon_0$ and $\varepsilon_{33}^T/\varepsilon_0$ at room temperature were 306 and 115, respectively. The constant $\varepsilon_{33}^T/\varepsilon_0$ showed a marked anomaly at the transition point of 405 °C. On the other hand, the $\varepsilon_{11}^T/\varepsilon_0$ did not show any anomaly, and decreased gradually with increasing temperature.

(3) It has been very difficult to obtain higher-quality large-size single crystals of KLN because the KLN is not congruently melting composition. It will therefore be necessary to find an appropriate solution for this problem

for device applications.

Chapter 3:

(1) All the elastic and piezoelectric constants of KLN have been measured from room temperature to about 120 ^{o}C by observing resonant and antiresonant frequencies. The electro-mechanical coupling factors k_{15}, k_{31}, k_{33} and k_t were 0.34, 0.18, 0.52 and 0.53, respectively. The temperature coefficients of elastic compliances Ts_{33}^{E}, Ts_{44}^{E} and Ts_{66}^{E} were -0.98, -1.2 and 0.075 x $10^{-4}/^{o}$C, respectively.

(2) It is concluded that the KLN crystal can be a suitable material for applications to the electro-mechanical transducers in thickness shear or longitudinal mode and also SAW devices.

Chapter 4:

(1) Crystals of $K_{3(1-x)}Na_{3x}Li_2Nb_5O_{15}$ (KNLN) have been grown by the Czochralski method. The attempted values for x were 0, 0.1, 0.2, 0.25 and 0.3. However it was not very successful to grow reasonably large and crackless crystals, when x value increased.

(2) The analyses on the crystallographic and dielectric properties showed that the structural phase change from the tungsten-bronze to the perovskite structures occurred at x between 0.2 and 0.25.

(3) It was found that the crystals with x value larger than 0.2 can not be effectively poled because the composition approaches the limits of stability of the tungsten-bronze structure, and presumably the material is no longer ferroelectric in the vicinity of x = 0.2.

(4) The electro-optical half-wave voltage (v_π) relating to

the electro-optic constant r_c for KNLN could be reduced to such an extent as much smaller than that for KLN, by adjusting the Na concentration to x = 0.1.

(5) On the other hand, one of the nonlinear-optic coefficients, d_{31}, of KNLN (x = 0.1) was somewhat larger than that of KLN (x = 0) and was determined as $d_{31}^{KNLN(x = 0.1)} = 1.6\ d_{31}^{KLN}$.

(6) It is therefore concluded that although piezoelectricity in KNLN crystals becomes weaker as Na concentration increases, the addition of small amount of Na to KLN as a whole results in more preferable linear-optic and nonlinear optic behaviors than pure KLN.

Chapter 5:

(1) Tungsten-bronze KBN crystals have been grown by an rf heating Czochralski method. Since the vapor pressure of K_2O and Bi_2O_3 was high at the melting point of KBN (1310 °C), the starting composition with excess K_2O and Bi_2O_3 was used, which is necessary to obtain large crystals of good quality. Large pale-yellow transparent single-crystals of KBN up to about 35 mmϕ x 40 mm in size have been easily grown.

(2) From the experimental results obtained by the X-ray measurements, it is concluded that KBN belongs to an orthorhombic system with lattice constants a = 17.878, b = 17.888 and c = 7.853 Å, respectively, but its spontaneous deformation b/a is nearly equal to 1.

(3) The dielectric constants $\varepsilon_{11}^T/\varepsilon_0$ ($\simeq\varepsilon_{22}^T/\varepsilon_0$) and $\varepsilon_{33}^T/\varepsilon_0$ at room temperature were 530 and 560, respectively. Both the dielectric constants exhibited anomalies at the Curie temperature of about 380 °C. It is to be noted that inhomo-

geneities in the crystals are clearly improved by the crucible rotation.

(4) Based on the results obtained from the poling and chemical etching treatments, it was found that KBN is a ferroelectric material with the polar axis parallel to the [001] axis.

(5) All the elastic constants at room temperature have been determined from the ultrasonic velocity measurements. It was found that the velocities propagated in KBN are somewhat smaller than those of $LiNbO_3$. This result is expected from the fact that KBN contains the heavy metal such as Bi.

(6) Four of the twelve independent photoelastic tensor elements were measured for applications to acousto-optic devices. It was found that the photoelastic constants p_{11} and p_{33} of KBN are greater than those of $LiNbO_3$ and $LiTaO_3$.

Chapter 6:

(1) KLN single-crystal films have been successfully grown with good epitaxy on KBN substrates by the EGM method.

(2) The results obtained by X-ray, SEM and RED analyses showed that a single-crystal film of (001) KLN is epitaxially grown on an (001) KBN substrate, and also that of (110) KLN is grown on a (100) KBN substrate.

(3) The KLN films obtained were single-crystals of high quality and also were transparent. However the top surfaces of the as-grown films were relatively rough. Therefore, optical polishing will be needed for the purpose of optical waveguides.

Chapter 7:

(1) KLN single-crystal films have been sputtered on the KBN substrates. The KLN target was prepared by sintering the pressed powder with potassium and lithium enriched composition.

(2) Optimum growth conditions for the high-quality single crystal KLN films were Ar (50 %) + O_2 (50 %) atmosphere, 9 x 10^{-2} Torr, rf power input below 150 W, and substrate temperatures of 580 to 630 ^{o}C.

(3) The crystallographic identifications of the KLN films were made by X-ray, SEM and RED measurements. It was found that single-crystal films have been epitaxially grown on KBN substrates. Lattice constants a and c of the KLN film were 12.7 and 3.96 $\mathring{A}$, respectively.

(4) The laser beam has been successfully fed into the KLN film sputtered on the (001) KBN substrate. The ordinary refractive index n_o in the KLN film has been determined as 2.27.

Chapter 8:

(1) An rf diode sputtering equipment was used to prepare KLN films on sapphire substrates. The optimum growth conditions were Ar (50 %) + O_2 (50 %) atmosphere, 9 x 10^{-2} Torr, about 140 W rf input power and 600 to 650 ^{o}C substrate temperature.

(2) The X-ray and RED results showed that an (001) KLN single-crystal film has been epitaxially grown on an $(01\bar{1}2)$ sapphire substrate at substrate temperatures above 600 ^{o}C and also that the KLN film obtained is of a single-crystal with considerably good quality. On the other hand, an

(001)-oriented KLN film sputtered on an (0001) sapphire substrate was seen to be polycrystalline, and its surface was relatively rough, because the surface-normal axes of (001) KLN and (0001) sapphire possess 4-fold (tetragonal) and 3- fold (trigonal) properties, respectively.

(3) The TE_0 mode optical propagation loss in the KLN film was relatively small as 7.8 dB/cm, which is less than that of the $LiNbO_3$ film grown by the rf sputtering or LPE methods. Accordingly, the KLN film is a suitable material for optical waveguides.

Chapter 9:

(1) Characteristics of SAW properties of tungsten-bronze layered structures of (KLN film)/(substrate) and (PKN film)/(substrate) combinations have been calculated. For the layered structure of a KLN film formed on a sapphire substrate, the SAW electro-mechanical coupling factor $\Delta v/v$ showed a broad band with a peak at KH (wave number times film thickness) = 1.9 and its maximum attainable value for the $\Delta v/v$ was 0.0052 at KH = 1.9. This value is 10 times larger than that of ST cut quartz.

(2) For the layered structures of (PKN)/(sapphire), (PKN)/(KLN) and (PKN)/(KBN) combinations, each $\Delta v/v$ had maximum at KH = 0.9, 0.8 and 0.6, respectively, whose magnitudes of maximum attainable values were 0.045, 0.021 and 0.015, respectively. The maximum value, 0.045, of the 1st peak for the $\Delta v/v$ in the layered structure of (PKN)/(sapphire) is twice as large as that of Y-cut, Z-prop., $LiNbO_3$.

(3) KLN single-crystal films have been successfully grown

with good epitaxy on sapphire substrates. By using this KLN film, the preliminary experiments on the SAW properties have been carried out. The SAW propagation on the KLN film has been observed for the first time. The SAW velocity was determined to be 5430 m/s, which is in good agreement with the calculated value, 5500 m/s at KH = 0.6. However, the measurement on the $\Delta v/v$ has not been attempted because the calculated value for the $\Delta v/v$ are of as small as about 8×10^{-6} at KH = 0.6.

(4) Although a study on the epitaxial growth of PKN film on various substrates is now in progress, it would be expected that higher-quality epitaxial films of PKN can successfully be grown on KBN substrates compared with KLN films on KBN substrates.

(5) It is concluded that the layered structures of (KLN)/(substrate) and (PKN)/(substrate) combinations are suitable for SAW applications.

ADDENDUM

I. LIST OF PUBLICATIONS

1) "Piezoelectric Properties of Potassium Tantalate-Niobate Single Crystal,"
M. Adachi, and A. Kawabata,
Jpn. J. Appl. Phys., 11 (1972) p. 1855.

2) "Elastic and Piezoelectric Properties of Potassium Lithium Niobate (KLN) Crystals,"
M. Adachi, and A. Kawabata,
Jpn. J. Appl. Phys., 17 (1978) pp. 1969-1973.

3) "Epitaxial Growth of Potassium Lithium Niobate Single-Crystal Films on Potassium Bismuth Niobate Single Crystals by Sputtering,"
M. Adachi, M. Hori, T. Shiosaki, and A. Kawabata,
Jpn. J. Appl. Phys., 17 (1978) pp. 2053-2054.

4) "Epitaxial Growth of Potassium Lithium Niobate Single-Crystal Films on Potassium Bismuth Niobate Single Crystals by the EGM Technique,"
M. Adachi, T. Shiosaki, and A. Kawabata,
Jpn. J. Appl. Phys., 18 (1979) pp. 193-194.

5) "$K_3Li_2Nb_5O_{15}$ Optical Waveguides Fabricated on Sapphire by RF Sputtering,"
M. Adachi, M. Hori, T. Shiosaki, and A. Kawabata,
Jpn. J. Appl. Phys., 18 (1979) pp. 1637-1638.

6) "Epitaxial Growth of $K_3Li_2Nb_5O_{15}$ (KLN) Single-Crystal Films on $K_2BiNb_5O_{15}$ (KBN) by RF Sputtering,"
M. Adachi, M. Hori, T. Shiosaki, and A. Kawabata,
Proc. of the 2nd Meeting on Ferroelectric Materials and Their Applications, Kyoto, 1979, (1979) pp. 173-178.

7) "Epitaxial Growth of Potassium Lithium Niobate Single-Crystal Films for Optical-Waveguides,"
M. Adachi, T. Shiosaki, and A. Kawabata,
Ferroelectrics, 27 (1980) pp. 89-92.

8) "$K_3Li_2Nb_5O_{15}$ and $Pb_2KNb_5O_{15}$ Tungsten-Bronze Films for SAW Devices,"
M. Adachi, K. Kumagawa, T. Shiosaki, and A. Kawabata,
Proc. of the 3rd Meeting on Ferroelectric Materials and Their Applications, Kyoto, 1981, and Supplement to Jpn. J. Appl. Phys., Suppl. 20-4 (1981) pp. 17-22.

9) "Sputtering and Chemical Vapor Deposition of ZnO, AlN, and $K_3Li_2Nb_5O_{15}$ for Optical Waveguide and Surface Acoustic Wave Devices,"
T. Shiosaki, M. Adachi, and A. Kawabata,
to be published in Thin Solid Films, (1982).

II. LIST OF TECHNICAL REPORTS

1) "Single-Crystal Growth of $KTaO_3$-$KNbO_3$ Solid Solutions and Their Electrical Properties,"
M. Adachi, T. Shiosaki, and A. Kawabata,
Annual Report of Study Group on Applied Ferroelectrics in Japan, 20 (1971) pp. 35-39.

2) "Crystal Growth of $K_2BiNb_5O_{15}$ and Its Elastic Properties,"
M. Adachi, M. Miyake, M. Oku, and A. Kawabata,
the Annual Meeting of the Institute of Electronics and Electrical Communication Engineers of Japan, No. 164, p. 166, July (1974).Hokkaido Univ.

3) "Measurements on Piezoelectric and Elastic Constants of Ferroelectric $K_3Li_2Nb_5O_{15}$ Crystals,"
M. Adachi, M. Miyake, and A. Kawabata,
the Annual Meeting of Phys. Soc. of Japan, No. 4p-P-4, p. 98, April (1975) Kyoto Univ.

4) "Single- Crystal Growth of $K_3Li_2Nb_5O_{15}$ and $K_{3(1-x)}Na_{3x}Li_2Nb_5O_{15}$ and Their Properties,"
M. Adachi, M. Miyake, and A. Kawabata,
Annual Report of Study Group on Applied Ferroelectrics in Japan, 23 (1975) pp. 130-136.

5) "Dielectric and Piezoelectric Properties of Sodium Modified KLN Crystals,"
M. Adachi, M. Miyake, and A. Kawabata,
the Fall Meeting of Phys. Soc. of Japan, No. 11p-K-4, p. 109, October (1975) Nippon Univ.

6) "Crystal Growth of KLN and Its Electro-Optic Properties,"
M. Adachi, M. Miyake, and A. Kawabata,
the Kansai Meeting of the Institute of Electrical Engineers of Japan, No. S3-1, p. S14, November (1975) Kobe Univ.

7) "Fabrication of Transparent Ceramics in the $KNbO_3$-$LiNbO_3$-$NaNbO_3$ Ternary System,"
T. Toyama, K. Hagihara, M. Adachi, T. Shiosaki, and A. Kawabata,
the Annual Meeting of Phys. Soc. of Japan, No. 5a-N-4, p. 22, April (1976) Nagoya Univ.

8) "Ferroelectricity of $K_2BiNb_5O_{15}$ Single Crystal,"
M. Adachi, and A. Kawabata,
the Annual Meeting of Phys. Soc. of Japan, No. 5a-N-10, p. 25, April (1976) Nagoya Univ.

9) "Electrical Properties of (Na, K, Li)NbO_3 Piezoelectric Ceramics and Their Surface Acoustic Wave (SAW) Applications,"
T. Kozu, M. Adachi, T. Shiosaki, and A. Kawabata,
the Fall Meeting of Japn. Soc. Appl. Phys.,No. 1p-N-4, p. 187, October (1976) Tohoku Univ.

10) "Ferroelectricity of $K_2BiNb_5O_{15}$ Single Crystals : II,"
M. Adachi, and A. Kawabata,
the Fall Meeting of Phys. Soc. of Japan, No. 8p-K-7, p. 175, October (1976) Tohoku Univ.

11) "Ferroelectricity (Ferroelasticity) of $K_2BiNb_5O_{15}$ Single Crystals : III,"
M. Adachi, and A. Kawabata,
the Annual Meeting of Phys. Soc. of Japan, No. 4a-J-4, p. 97, April (1977) Yamaguchi Univ.

12) "Epitaxial Growth of $K_3Li_2Nb_5O_{15}$ Single-Crystal Films on $K_2BiNb_5O_{15}$ Single-Crystal Substrates,"
M. Adachi, T. Shiosaki, and A. Kawabata,
Annual Report of Study Group on Applied Ferroelectrics in Japan, 26 (1977) pp. 8-13.

13) "Optical Properties of KBN Single Crystal,"
M. Adachi, M. Hori, and A. Kawabata,
the Annual Meeting of Phys. Soc. of Japan, No. 9a-N-5,

p. 3, October (1977) Science Univ. of Tokyo.

14) "Single-Crystal Growth of $KNbO_3$-$LiNbO_3$-$NaNbO_3$ Solid Solutions and Their Electrical Properties,"
M. Adachi, and A. Kawabata,
the Annual Meeting of Phys. Soc. of Japan, No. 2a-BD-4
p. 94, March (1978) Tohoku Univ.

15) "Epitaxial Growth of $K_3Li_2Nb_5O_{15}$ Deposited on $K_2BiNb_5O_{15}$ by RF Sputtering,"
M. Hori, M. Adachi, T. Shiosaki, and A. Kawabata,
the Fall Meeting of Japan. Soc. Appl. Phys.,No. 4a-B-6,
p. 41, November (1978) Kinki Univ.

16) "Fabrication of $K_3Li_2Nb_5O_{15}$ Thin Films by RF Sputtering and Their Optical Waveguide Applications,"
M. Hori, M. Adachi, T. Shiosaki, and A. Kawabata,
the Annual Meeting of Japan. Soc. Appl. Phys.,No. 27p-H-5,
p. 555, March (1979) Gakushuin Univ.

17) "Epitaxial Growth of Potassium Lithium Niobate Single-Crystal Films for Optical-Waveguides,"
M. Adachi, T. Shiosaki, and A. Kawabata,
International IEEE 1979 Symposium on Applications of Ferroelectrics, Symposium Digest, p. 37, June (1979) Minneapolis.

18) "Thermal Expansion of Tungsten-Bronze Type $K_2BiNb_5O_{15}$ Single Crystal,"
M. Adachi, and A. Kawabata,
the Annual Meeting of Phys. Soc. of Japan, No. 27a-W-10,
p. 53, March (1980) Waseda Univ.

19) "Fabrication of Sputtered-Ferroelectric $K_3Li_2Nb_5O_{15}$ Thin Film and Its Electrical Property,"
M. Adachi, J. Kiyose, A. Kawakatzu, T. Shiosaki, and A. Kawabata,
the Annual Meeting of Japan. Soc. Appl. Phys., No. 3p-M-5,

p. 694, April (1980) Yamanashi Univ.

20) "Surface Acoustic Wave (SAW) Properties of Tungsten-Bronze $K_3Li_2Nb_5O_{15}$ Thin Films,"
M. Adachi, A. Kawakatzu, T. Shiosaki, and A. Kawabata,
the Fall Meeting of Japan. Soc. Appl. Phys., No. 19p-N-4,
p. 659, October (1980) Nagoya Institute of Technology.

21) "Fabrication of Tungsten-Bronze $K_3Li_2Nb_5O_{15}$ Thin Films and Its C-Axis Orientation,"
M. Adachi, T. Shiosaki, and A. Kawabata,
the Annual Meeting of Japan. Soc. Appl. Phys., No. 31a-B-6,
p. 724, March (1981) Musashi Institute of Technology.

22) "Fabrication of Tungsten-Bronze $Pb_2KNb_5O_{15}$ Films and their Applications to SAW Devices : I,"
M. Adachi, K. Kumagawa, T. Shiosaki, and A. Kawabata,
the Fall Meeting of Japan. Soc. Appl. Phys., No. 8a-W-9,
p. 778, October (1981) Fukui Univ.